

**SYNTHESIS, CHARACTERISATION AND
ELECTROCHEMICAL APPLICATIONS OF NANOMATERIALS**

By

MANOJ KUMAR SHARMA

CHEM01200604032

Bhabha Atomic Research Centre, Mumbai, INDIA

A thesis submitted to the

Board of Studies in Chemical Sciences

In partial fulfillment of requirements

For the Degree of

DOCTOR OF PHILOSOPHY

of

HOMI BHABHA NATIONAL INSTITUTE

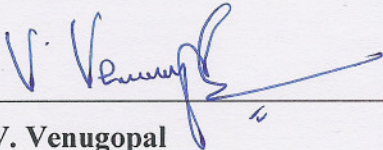


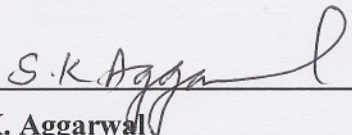
September 2012

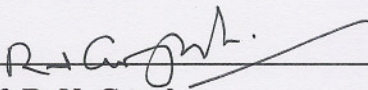
Homi Bhabha National Institute

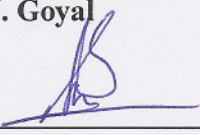
Recommendations of the Viva Voce Board

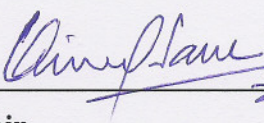
As members of the Viva Voce Board, we certify that we have read the dissertation prepared by Manoj Kumar Sharma entitled "*Synthesis, Characterisation and Electrochemical Application of Nanomaterials*" and recommend that it may be accepted as fulfilling the dissertation requirement for the Degree of Doctor of Philosophy.

 Date: 22/2/13
Chairman – Prof. V. Venugopal

 Date: 22/2/13
Guide/Convener – Prof. S. K. Aggarwal

 Date: 22/2/13
External Examiner – Prof. R. N. Goyal

 Date: 22/2/13
Member 1 – Prof. S. K. Mukerjee

 Date: 22/2/2013
Member 2 – Prof. V. K. Jain

Final approval and acceptance of this dissertation is contingent upon the candidate's submission of the final copies of the dissertation to HBNI.

I hereby certify that I have read this dissertation prepared under my direction and recommend that it may be accepted as fulfilling the dissertation requirement.

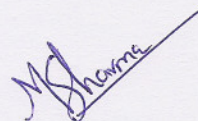
Date:

Place: RLG, BARC, Mumbai

STATEMENT BY AUTHOR

This dissertation has been submitted in partial fulfillment of requirements for an advanced degree at Homi Bhabha National Institute (HBNI) and is deposited in the Library to be made available to borrowers under rules of the HBNI.

Brief quotations from this dissertation are allowable without special permission, provided that accurate acknowledgement of source is made. Requests for permission for extended quotation from or reproduction of this manuscript in whole or in part may be granted by the Competent Authority of HBNI when in his or her judgment the proposed use of the material is in the interests of scholarship. In all other instances, however, permission must be obtained from the author.



Manoj Kumar Sharma

DECLARATION

I, hereby declare that the investigation presented in the thesis has been carried out by me. The work is original and has not been submitted earlier as a whole or in part for a degree / diploma at this or any other Institution / University.



Manoj Kumar Sharma

DEDICATED

To

My NANAJI

(Maternal Grandfather)

Late. Shri Pt. Chintamani Joshi

(a great soul who taught me the ultimate
purpose of life)

&

MY PARENTS

(a constant source of endless love and
unconditional support in my life)

ACKNOWLEDGEMENTS

Some feats cannot be accomplished alone

First, I would like to express my sincere appreciation and gratitude to my guide, Prof. S. K. Aggarwal, for giving me the chance to register for PhD under him, and for all the support, trust, encouragement and guidance over the last five years of this work. I acknowledge his excellent input and insightful comments during the preparation of this thesis.

I am also grateful to Prof. V. Venugopal, Chairman, Doctoral Committee, Ex-Director, Radiochemistry & Isotope Group, for his encouragement and enthusiasm. I also thank the Doctoral Committee members, Prof. S. K. Mukerjee (Head, Process Chemistry Section, Fuel Chemistry Division) and Prof. V. K. Jain (Head, Chemistry Division) for the helpful advices and discussions.

A large number of people have helped me during my PhD work through technical discussions and experimental techniques. I acknowledge them for their support.

I acknowledge Shri N. Gopinath for the stimulating discussions on electrochemical techniques and solution chemistry of U & Pu, and I am also grateful to Dr. A. K. Pandey for helpful and enriching technical discussions on nanoparticles' preparation, characterisation and applications.

I thank Dr. R. Tiwari (BARC), Mr. B. T. Naidu Babu and Mr. L. S. Mombasawala (SAIF, IIT Bombay) for help in TEM experiments. I acknowledge the great help of Dr. K. Krishnan and Shri S. Sanjay Shastri in XRD and EDXRF characterizations, respectively.

I must thanks Arvind Ambolika for helping me in carrying out the electrochemical experiments.

I express gratitude to all my colleagues in Electrochemistry Section and Chemical Analysis Section for their wholehearted support, encouragement and co-operation. This work could not have been done without the support provided by the workshop staff and office staff, so I wholeheartedly acknowledge their support.

I express special thanks to my parents (Shri Krishna Nand Sharma and Smt. Radha Sharma), my brother, Ashok, and my sister, Meena, for endless love and support, for being the inspiration of my life, and for teaching me that “no adversity and setback is forever”. Last but not the least, I acknowledge and admire Reena, my wife and best friend, for being supportive and compassionate, for believing in me and for all the good things in my life.

MANOJ

CONTENTS

SYNOPSIS	i
LIST OF FIGURES	xiv
Chapter 1: Introduction	1
1.1. Introduction	2
1.2. Synthesis Techniques	6
1.3. Characterisation Techniques	9
1.4. Properties and Applications	15
1.5. Electrochemistry and Nanomaterials	17
1.6. An Overview of the Work Carried out	19
Chapter 2: In-situ Synthesis of Gold-Polyaniline Composite in Nanopores of Polycarbonate Membrane	24
2.1. Introduction	25
2.2. Experimental	29
2.3. Result and Discussion	30
2.4. Conclusion	40
Chapter 3: Electrochemical Synthesis of Gold Nanorods in Track-Etched Polycarbonate Membrane using Removable Mercury Cathode	41

3.1. Introduction	42
3.2. Experimental	46
3.3. Result and Discussion	48
3.4. Conclusion	57
Chapter 4: Investigation on Redox Behaviour of Pu(IV)/Pu(III) in H₂SO₄ on Pt Nanoparticles-Modified Glassy Carbon and Pt Electrodes	58
4.1. Introduction	59
4.2. Experimental	62
4.3. Result and Discussion	63
4.4. Conclusion	73
Chapter 5: Investigations on Electrochemical Behaviour of U(VI) at Nanomaterials-Modified Electrode Surface	74
5.1. Electrochemical Studies of U(VI)/U(V) in Saturated Na₂CO₃ Solution at Gold Nanoparticles Embedded CTA-Modified Electrode	78
5.1.1. Introduction	79
5.1.2. Experimental	81
5.1.3. Result and Discussion	83
5.1.4. Conclusion	93
5.2. Electrochemical Reduction of U(VI) in H₂SO₄ at Gold Nanoporous	94

Film Electrode	
5.2.1. Introduction	95
5.2.2. Experimental	98
5.2.3. Result and Discussion	99
5.2.4. Conclusion	107
REFERENCES	108
List of Publications	127

SYNOPSIS

Nanomaterials have at least one dimension in the size range of 1-100 nm and are of great interest to research community because of their unique chemical and physical properties that are distinct from the bulk materials and individual atoms or molecules. Nanomaterials have found a wide range of applications in many disciplines of science and technology e.g. electronics, catalysis, sensors, medicines, advanced functional materials etc. Nanoscience and nanotechnology have emerged as true interdisciplinary research and have brought physicists, chemists, biologists, material scientists and even mathematicians at a common platform to understand the fundamental aspects and put them for variety of applications for the benefit of human race. The interest in nanomaterials research and its benefits can be easily appreciated by the massive funding allotted to this particular branch of science and the large number of publications reported every year in the last two decades. The properties of nanomaterials are so much dependent on size and shape that at nanoscale dimensions, a single material can show a wide range of physical and chemical properties, and it can be used for different applications by tuning the shape and size of the material. Therefore, the synthesis of shape and size controlled nanomaterials is a subject of great interest to researchers.

Templates are used to tune the size and the shape of the nanomaterials. Porous anodized alumina and track-etched polycarbonate (PC) membranes are commercially available templates for synthesizing one-dimensional (1D) nanomaterials - nanowires, nanorods and nanotubules of metals, semiconductors and conducting polymers. The electrochemical template synthesis of nanowires, nanorods and nanotubules involves coating of one surface of the template membrane with a metal film, usually done by sputtering technique, and then using this metal film as cathode for electrodeposition of metal nanowires within the pores of the membrane. The nanowires can be freed from the template membrane by dissolving it in a suitable solvent. The nanowires are attached to the coated metal film and protrude from its surface like bristles of a brush. The free-standing nanowire can be obtained by detaching it from coated metal film. It is impossible to obtain free-standing malleable template membranes with nanowires in its pores due to the metal coating on one surface. In the present thesis, the electrochemical synthesis of gold nanorods within the pores of track-etched PC membrane using a removable mercury cathode is reported and this new approach does not require the metal film coating of one surface of the template membrane. A free-standing malleable track-etched PC membrane with gold nanorods in its pore

was obtained. The free-standing Au nanorods were obtained by dissolving Au-deposited PC membrane in the dichloromethane.

Polymers are promising hosts for nanoparticles. Composites of metal nanoparticles with polymers have superior hybrid properties compared to metal nanoparticles alone. Composites of electrically conducting polymer like polyaniline and gold nanoparticles have potential applications in molecular electronic devices, gas sensors, biosensors, capacitors and catalysts. For putting these polymer/metal composites in real world applications, it is desirable to immobilize them on some support/substrate. Chemically synthesized gold–polyaniline composite is in the form of either powder or precipitate in solution. In the present thesis, an in situ chemical synthesis route for the preparation of a gold–polyaniline composite within the pores of track-etched PC membrane is reported. Track-etched PC membrane was used as a supporting matrix for the immobilization of gold–polyaniline composite synthesized. The gold nanorods within the pores can be chemically or biochemically functionalized with desired chemical or biochemical species and the functionalized track-etched PC membrane can be used to develop sensors.

Nanomaterials of noble metals and their composites, especially Pt and Au, are the most studied. Nanoparticles of noble metals have been utilised by electrochemists to modify the surface of conventional electrodes to obtain better electrochemical response due to their large effective surface area, increased mass transport, and better electronic interaction between the analyte and the electrode. All these advantages of nanoparticles lead to higher catalytic activity, better sensitivity and selectivity. Electrochemical deposition techniques are promising to synthesise and immobilise the metal nanoparticles onto the electrode surface with easy control of particle shape and size. The modification of conventional electrodes by noble metal nanoparticles reduces the loading of noble metals. A very few electrochemical studies of actinides, especially uranium and plutonium, are reported using either nanoparticles or nanocomposite-modified electrodes. In the present work, the Pt nanoparticles were prepared on Pt and glassy carbon electrodes' surfaces by electrochemical deposition, and modified electrodes were found to significantly improve the redox kinetics of Pu(IV)/Pu(III) couple in 1 M H₂SO₄. The gold nanoparticles (AuNPs) were prepared in the matrix of cellulose triacetate (CTA) containing Aliquat-336 via anion exchange transfer of AuCl₄⁻ ions in the CTA followed by chemical reduction with NaBH₄. The AuNPs-CTA modified electrode showed improved

electrochemical reversibility with very large current density for the reduction of UO_2^{2+} to UO_2^+ in saturated Na_2CO_3 solution.

Present work is focused on the synthesis, characterisation and electrochemical applications of noble metals nanoparticles and nanocomposites. The thesis comprises five chapters.

Chapter 1 briefly reviews the properties, synthesis and applications of nanomaterials. Chapter 2 describes an in situ one-step chemical synthesis route for the preparation of gold-polyaniline nanocomposite in the pores of track-etched PC membrane and its characterisation. Chapter 3 highlights the development of a new and novel method for the electrochemical template synthesis of gold nanorods within the pores of track-etched PC membrane using a removable mercury cathode. The characterisation of gold nanorod and the gold-deposited track-etched PC membrane is discussed. Chapter 4 and Chapter 5 deal with the electrochemical applications of platinum and gold nanoparticles modified electrodes in studying the redox behaviour of Pu(IV)/Pu(III) in H_2SO_4 and U(VI)/U(V) in saturated Na_2CO_2 , respectively.

Chapter 1

Introduction

Nanomaterials have received a great attention in the last two decades because of their unique properties that find potential applications in many fields of science and technology. The unique chemical and physical properties of nanomaterials are compared with their bulk counterpart, and shape and size-dependent properties of nanomaterials are discussed. A brief description of various methods available for synthesis and characterisation of nanomaterials is given. The applications of nanomaterials in catalysis, sensors development, magnetic, electronic and optical devices, etc. are discussed. The applications of nanomaterials in electrochemistry and electrochemical techniques for the preparation of nanomaterials are highlighted.

Chapter 2

In situ synthesis of gold-polyaniline (Au-PANI) nanocomposite in the pores of track-etched polycarbonate (PC) membrane

Gold-polyaniline composite was synthesized within the pores of commercially available track-etched PC membrane by an in situ one step chemical method. Track-etched PC membrane acts as a supporting matrix for chemically synthesized gold-polyaniline nanocomposite. A two-

compartment cell was designed and fabricated for this experiment. Nucleopore track-etched PC membrane with a pore diameter of 200 nm and thickness of 10 μm was used. The PC membrane placed between the two compartments separated the aqueous solution of 10 mM HAuCl_4 from 0.5 M aniline in 1 M HCl. Concentration gradient across the membrane caused the movement of AuCl_4^- and anilinium ions in the pores, which act as reaction vessels of nano-dimensions. The redox reaction between anilinium and AuCl_4^- led to the formation of gold-polyaniline nanocomposite by simultaneous oxidation of aniline to polyaniline and reduction of AuCl_4^- to Au. The formation of gold-polyaniline nanocomposite within the pores of PC membrane was confirmed by EDXRF, XRD, UV-Visible absorbance spectroscopy, FTIR and TEM studies. The EDXRF spectrum showed the $L_{\alpha 1}$ and $L_{\beta 1}$ lines of gold at 9.76 and 11.52 keV, respectively. The broadened peaks at 2θ equal to 38.22, 44.46 and 64.68 correspond to the 111, 200 and 220 planes of the face-centered cubic phase of the Au. The Au particles formed within the pores of PC membrane are nanocrystallites. The broadening of the diffraction peak width of the (111) Bragg reflection was analyzed to estimate the size of Au nanocrystallites within the pores of PC membrane using Scherrer equation. The average size of the Au nanocrystallites in gold-polyaniline composite was calculated to be 24 ± 4 nm. The UV-visible absorbance spectrum of gold-polyaniline composite was recorded in both transmission and reflectance mode. The transmission mode spectrum showed characteristic absorption bands at 340 nm and 750 nm due to the π - π^* transition of the benzenoid rings and benzenoid to quinoid excitonic transition, respectively, in polyaniline. A small shoulder at 430 nm was observed resulting from polaron/bipolaron transition in polyaniline. The surface plasmon resonance peak of gold nanoparticles at ~ 520 nm was superimposed by broad absorption band at $\lambda_{\text{max}} \sim 750$ nm. The reflectance mode spectra of the surfaces of the PC membrane exposed to the HAuCl_4 and aniline solutions showed broad band with λ_{max} at 495 nm (SPR of Au) and 595 nm (benzenoid to quinoid excitonic transition), respectively. The FTIR spectrum also confirmed the formation of polyaniline within the pores of PC membrane. The TEM studies suggested that clusters of polyaniline were formed and gold particles (size < 50 nm) were randomly dispersed in these polyaniline clusters. The selected area electron diffraction (SAED) pattern corresponded to a characteristic polycrystalline ring pattern for a face-centered cubic structure. These characterisation results suggested that the surfaces of the PC membrane exposed to the HAuCl_4 and aniline solutions had significantly higher concentration of Au nanoparticles and polyaniline,

respectively. Experiments were repeated to prepare gold-polyaniline composite in PC membrane with different preparation times (2, 4 and 8 hours).

Chapter 3

Electrochemical synthesis of gold nanorods in the pores of track-etched polycarbonate (PC) membrane using removable mercury cathode

A novel method for the electrochemical template synthesis of gold nanorods within the pores of track-etched PC membrane using a removable mercury cathode was developed and this new approach does not require the coating of one surface of the template membrane with a metal film. A free-standing malleable track-etched PC membrane with gold nanorods in its pores was obtained. The electrochemical template synthesis of nanowires, nanorods and nanotubules involves coating of one surface of the template membrane with a metal film, usually done by sputtering technique, and then this metal film is used as a cathode for the electrodeposition of metal nanowires within the pores of the membrane. In some reports, sputtering was followed by the electrochemical deposition of metal to further increase the metallic layer thickness so that the coated metallic layer completely covers the pores that may not be blocked during sputtering. In the present work, a two-compartment electrochemical cell was designed and used. The PC membrane placed between the two compartments separated the aqueous solution of HAuCl_4 from mercury, which was the cathode for the electrodeposition of gold within the pores of PC membrane. The electrochemical deposition of gold in the pores of PC membrane was carried out by applying a constant potential of -0.2 V on mercury for 1000 s and 3000 s. The new approach is simple, cost-effective and saves time because it does not require the sputtering of the metal film coating. The free-standing Au nanorods were obtained by dissolving Au-deposited PC membrane in dichloromethane. The Au-deposited PC membrane and free-standing Au nanorods were characterized by EDXRF, XRD, UV-Visible spectroscopy, AFM and FEG-TEM. The EDXRF spectrum of the gold-deposited PC membrane showed the $L_{\alpha 1}$ and $L_{\beta 1}$ lines of Au at 9.76 keV and 11.52 keV, respectively. The XRD pattern had the broad peaks at the scattering angles (2θ) equal to 38.16° , 44.34° and 64.52° corresponding to 111, 200 and 220 planes, respectively, of the face-centered cubic phase of Au within the pores of PC membrane. A single red-shifted very broad peak was observed at around 636 nm in the visible absorbance spectrum of the gold-deposited gold PC membrane. The TEM studies showed the formation of cigar-shaped gold nanorods within the pores of the PC membrane. The diffraction spots in SAED

pattern were indexed to (111), (200) and (220) diffraction planes of the face-centered cubic structure of gold in agreement with the XRD pattern. AFM studies revealed that the gold-deposited PC membrane having shorter deposition time (1000 s) had open pores on both the surfaces of the template membrane. The gold-deposited PC membrane with longer deposition time (3000 s) showed blocked pores on one surface and open pores on the other surface of the template membrane. The deposition of gold in PC membrane was also carried out by galvanic reaction between HAuCl_4 and mercury for 1000 s in a similar two-compartment cell as discussed above, without applying the cathodic potential. The EDXRF spectrum of the gold-deposited in PC membrane by the galvanic reaction showed the $L_{\alpha 1}$ and $L_{\beta 1}$ lines of Hg at 10.02 keV and 11.88 keV, respectively along with the $L_{\alpha 1}$ and $L_{\beta 1}$ lines of Au at 9.76 keV and 11.52 keV, respectively. These observations lead to a conclusion that the spontaneous galvanic reaction between HAuCl_4 and Hg was forbidden on applying the cathodic potential of -0.2 V vs. Ag/AgCl on Hg. The gold nanorods within the pores can be chemically or biochemically functionalized with the desired chemical or biochemical species and the functionalized track-etched PC membrane can be used to develop sensors. The new and novel aspect of this work can be applied more generally for the preparation of nanorods/nanowires of other metals, semiconductors, conducting polymers etc.

Chapter 4

Investigations on redox behaviour of Pu(IV)/Pu(III) in H_2SO_4 on Pt nanoparticles-modified glassy carbon and platinum electrodes

The redox behaviour of Pu(IV)/Pu(III) couple has been studied on various electrodes (Pt, Au, carbonaceous materials such as graphite, glassy carbon) in different supporting electrolytes. In the present work, the redox behaviour of Pu(IV)/Pu(III) couple in 1 M H_2SO_4 on platinum nanoparticles-modified glassy carbon and Pt electrodes was investigated. PtNPs-modified electrodes were prepared by electrochemical deposition of Pt from 10 mM K_2PtCl_4 + 0.1 M H_2SO_4 solution by applying a constant potential of -0.2 V for 10 s. The reversible hydrogen adsorption-desorption voltammogram showed the presence of adsorption states associated with (110) and (100) sites of Pt at -0.28 V and -0.13 V vs. Ag/AgCl electrode, respectively. The electrochemically active surface area of the Pt and PtNPs/Pt were compared with the amount of charge passed for the anodic desorption of the adsorbed hydrogen. The electrochemically active surface area of PtNPs/Pt was higher than that of the bare Pt. The cyclic voltammetry (CV) and

differential pulse voltammetry (DPV) studies showed that the redox kinetics of Pu(IV)/Pu(III) couple improved significantly for both the oxidation and the reduction processes after electrodeposition of PtNPs in comparison to the bare electrodes. The peak potential separation (ΔE_p) on bare Pt was 157 mV which decreased to 79 mV on PtNPs/Pt electrode. The Pu(IV) reduction and Pu(III) oxidation waves were better defined in case of PtNPs/Pt than the bare Pt electrode. However, significant improvement was seen for the reduction of Pu(IV) to Pu(III) on PtNPs deposited glassy carbon (PtNPs/GC) electrode compared to bare GC electrode. The SEM image of the PtNPs electrodeposited on GC surface showed well dispersed PtNPs with a good surface coverage, and particles size ranging from 160 to 200 nm. In the potential range of 0 to 0.7 V, a small anodic peak corresponding to the oxidation of Pu(III) to Pu(IV) was observed, but no peak corresponding to reduction of Pu(IV) to Pu(III) was observed on the bare GC electrode. The electrocatalytic activity of PtNPs/GC electrode towards the Pu(IV)/Pu(III) redox couple was clearly established by the appearance of well defined cathodic and anodic peaks. The redox process was diffusion-controlled for PtNPs-modified electrode. The electrochemical impedance spectra (Nyquist plots) showed that the electrodeposition of PtNPs on GC electrode decreased the interfacial electron-transfer resistance. These studies are of great relevance to develop new electroanalytical methodologies using nanoparticles modified electrodes for Pu determination.

Chapter 5

Part 1

Electrochemical studies of U(VI)/U(V) in saturated Na₂CO₃ solution at gold nanoparticles embedded CTA-modified electrode

Gold nanoparticles (AuNPs) were prepared in the matrix of cellulose triacetate (CTA) membrane containing a liquid anion exchanger trioctylmethylammonium chloride (Aliquat-336). The AuCl₄⁻ ions were transferred in the membrane matrix by anion-exchange process, and then subsequently reduced with NaBH₄ to form AuNPs in the membrane. The AuNPs-embedded CTA (AuNPs-CTA) membrane was characterized by the UV-Visible spectroscopy, XRD and AFM. The strong absorption band at 542 nm in the visible absorbance spectrum was attributed to the surface plasmon resonance of Au nanoparticles. The XRD pattern showed the broadened peaks at 2θ equal to 38.18° and 44.32° corresponding to the 111 and 200 planes, respectively, of the face-centered cubic phase of the Au. The Au particles formed in the membrane are nanocrystallites. The size of the Au nanoparticles embedded in the membrane was calculated to

be ~ 5 nm using the Scherrer equation. Three-dimensional noncontact AFM image indicated a node-grid type structure having egg-basket like external appearance and the gold nanoparticles were embedded in the membrane. The AuNPs-CTA composite membrane was coated on the bare Au electrode to modify the electrochemical interface, and the electrochemical properties of the AuNPs-CTA modified electrode were evaluated by studying the redox behaviour of $\text{UO}_2^{2+}/\text{UO}_2^+$ couple in saturated Na_2CO_3 solution using voltammetric techniques. In carbonate solution, the predominant species of UO_2^{2+} is $[\text{UO}_2(\text{CO}_3)_3]^{4-}$, and a stable $\text{UO}_2(\text{CO}_3)_3^{5-}$ complex is formed by one-electron reduction of $\text{UO}_2(\text{CO}_3)_3^{4-}$. Previous reports show that the $\text{UO}_2^{2+}/\text{UO}_2^+$ couple, which is electrochemically reversible in less complexing media, becomes electrochemically irreversible in aqueous CO_3^{2-} solution (a strong complexing medium). In this study, an electrocatalytic reduction of UO_2^{2+} to UO_2^+ in saturated Na_2CO_3 solution was observed at AuNPs-CTA-modified electrode with higher current density and faster heterogeneous electron-transfer kinetics than that at bare Au electrode. The peak potential separation (ΔE_p) on bare Au was 163 mV and it decreased to 54 mV on AuNPs-CTA modified electrode, thus showing increasing electrochemical reversibility of the redox process. The standard heterogeneous rate constant, k^0 , for the reduction process at AuNPs-CTA modified electrode was about 25 times higher than that at bare Au electrode. The diffusion-controlled redox process was observed on bare Au electrode. On AuNPs-CTA modified electrode, the redox process was predominantly diffusion-controlled at lower scan rates, but at higher scan rates the current due to the reduction of weakly adsorbed $\text{UO}_2(\text{CO}_3)_3^{4-}$ contributed significantly to the total current. It was concluded that AuNPs-CTA membrane has improved the interfacial electron-transfer properties of electrode, resulting in a better electrochemical response than bare Au electrode.

Part 2

Electrochemical reduction of U(VI) in H_2SO_4 at gold nanoporous film electrode

Gold nanoporous film (AuNPF) was grown on gold substrate by electrochemical oxidation at 5 V (vs. Ag/AgCl reference electrode) for 180 s in 0.1 M phosphate buffer solution (pH 7.4) and then the oxidized gold film was reduced with freshly prepared 1 M ascorbic acid aqueous solution. The AuNPF was characterized by the UV-Visible spectroscopy and AFM. The surface roughness of bare Au electrode increased many folds on formation of nanoporous film. The cyclic voltammograms of the AuNPF and bare gold electrode in 0.5 M H_2SO_4 showed that the electrochemically active surface of the AuNPF electrode was about 12 times more than that

of the bare gold electrode. The UV-visible spectra of the AuNPF showed two peaks maxima at 565 nm and 700 nm. The peak potential for U(VI) reduction at bare gold electrode is -0.478 V which shifted to -0.337 V on AuNPF. The anodic shift of 0.141 V in cathodic peak potential shows that the AuNPF electrode exhibited high electrochemical activity toward U(VI) reduction in 0.5 M H₂SO₄. The impedance spectra (Nyquist plot), however, showed that the charge transfer resistance (R_{ct}) is almost equal for both bare gold and the AuNPF electrodes. Therefore, the decrease in U(VI) reduction potential cannot be attributed to the catalytic properties of nanoporous gold film, and the thin-layer mass transport regime within the nanoporous gold film is the most possible cause for the anodic shift in the cathodic peak potential.

Highlights of the present work:

1. In situ one-step chemical synthesis route for the preparation of gold-polyaniline nanocomposite in the pores of track-etched PC membrane is reported. Pores in PC membranes were used as the nano-dimension reaction vessels where the redox reaction between aniline and HAuCl_4 led to the synthesis of gold-polyaniline nanocomposite. Track-etched PC membrane acts as a supporting matrix for chemically synthesized gold-polyaniline nanocomposite. The characterisation results showed that the surfaces of the PC membrane exposed to HAuCl_4 and aniline have significantly higher concentration of gold nanoparticles and polyaniline, respectively. These pores, filled with gold-polyaniline composite, are promising host to immobilize enzymes for developing biosensors.
2. A novel method for the electrochemical template synthesis of gold nanorods within the pores of track-etched PC membrane using a removable mercury cathode was developed and this new approach does not require the coating of one surface of the template membrane with a metal film. A free-standing malleable track-etched PC membrane with gold nanorods in its pores was obtained. The new approach is simple, cost-effective and saves time because it does not require the sputtering of the metal film coating. The gold nanorods within the pores can be chemically or biochemically functionalized with the desired chemical or biochemical species and the functionalized track-etched PC membrane can be used to develop sensors.
3. The redox behaviour of Pu(IV)/Pu(III) couple in $1\text{M H}_2\text{SO}_4$ was investigated on platinum nanoparticles-modified glassy carbon (GC) and Pt electrodes. The platinum nanoparticles were prepared by electrochemical deposition. A significant improvement in the redox kinetics of Pu(IV)/Pu(III) couple at Pt nanoparticles-modified electrode was observed compared to bare Pt and GC electrodes. These studies are of great relevance for the development of nanoparticles modified electrodes for quantitative determination of plutonium by coulometry and voltammetry.
4. Gold nanoparticles were prepared in cellulose triacetate membrane containing a liquid anion exchanger trioctylmethylammonium chloride (Aliquat-336). The gold nanoparticles embedded CTA membrane was coated on the bare Au electrode to tailor its interfacial properties. An electrocatalytic reduction of UO_2^{2+} to UO_2^+ in saturated Na_2CO_3 solution was observed at AuNPs-CTA modified electrode with higher current density and faster heterogeneous electron transfer rate (about 25 times higher) than that at bare Au electrode.

5. Gold nanoporous film (AuNPF) was grown on gold substrate by electrochemical methods and was characterized by AFM, UV-Visible spectroscopy and electrochemical techniques. The cyclic voltammograms in 5 mM U(VI) in 0.5 M H₂SO₄ showed the peak potential for U(VI) reduction at AuNPF electrode ($E_{pc} = -0.478$ V) has decreased by 0.141 V compared to bare gold electrode ($E_{pc} = -0.337$ V). The impedance spectra (Nyquist plot), however, showed that the charge transfer resistance (R_{ct}) is almost equal for both bare gold and the AuNPF electrodes indicating similar heterogeneous electron-transfer rate at bare Au and the AuNPF electrodes. Therefore, the thin-layer mass transport regime within the nanoporous gold film, compared to semi-infinite mass transport at bare gold electrode, is the most possible cause for the anodic shift in cathodic peak potential.

Part of the work being submitted for the award of the degree of Doctor of Philosophy has been published / communicated in following International Journals.

1. In-situ synthesis of gold-polyaniline composite in nanopores of polycarbonate membrane
Manoj K. Sharma, Arvind S. Ambolika and Suresh K. Aggarwal
Journal of Material Science, 46 (2011) 5715-5722.
2. Investigation on redox behaviour of Pu(IV)/Pu(III) in H₂SO₄ on platinum nanoparticles-modified glassy carbon and platinum electrode
Manoj K. Sharma, Arvind S. Ambolika and Suresh K. Aggarwal
Radiochimica Acta, 99 (2011) 17-21.
3. Electrochemical studies of U(VI)/U(V) in saturated Na₂CO₃ solution at gold nanoparticles embedded CTA-modified electrode
Manoj K. Sharma, Arvind S. Ambolika and Suresh K. Aggarwal
Radiochimica Acta, 99 (2011) 555-561.
4. Electrochemical synthesis of gold nanorods in track-etched polycarbonate membrane using removable mercury cathode
Manoj K. Sharma, Arvind S. Ambolika and Suresh K. Aggarwal
Journal of Nanoparticle Research (Communicated).

In addition to these journal publications, five contributed papers in various Symposia were presented.

List of Figures

Figure No.	Figure Caption	Page No.
Figure 2.1	Schematic of two-compartment cell. Porous PC membrane separates the two compartments.	29
Figure 2.2	SEM image of the porous polycarbonate membrane (36 μm X 27 μm)	31
Figure 2.3	AFM image of the porous polycarbonate membrane	31
Figure 2.4	Photo of the PC membrane containing gold-polyaniline composite	31
Figure 2.5	EDXRF spectra of PC membrane containing gold-polyaniline composite with preparation time of overnight	32
Figure 2.6	EDXRF spectra of PC membranes containing gold-polyaniline composite with preparation times of 2 and 4 hours	33
Figure 2.7	X-ray diffraction pattern of PC membrane containing gold-polyaniline composite with preparation time of overnight	34
Figure 2.8	X-ray diffraction pattern of PC membrane and PC membranes containing gold-polyaniline composite with preparation times of 2, 4 hours and overnight	35
Figure 2.9	UV-Vis spectrum of PC membrane containing gold-polyaniline composite in transmission mode	36
Figure 2.10	UV-Vis spectrum of PC membrane containing gold-polyaniline composite in reflectance mode	37
Figure 2.11	FTIR spectrum of PC membrane containing gold-polyaniline	38

	composite in ATR mode	
Figure 2.12	TEM images of gold-polyaniline composite prepared in PC membrane and corresponding SAED pattern	39
Figure 3.1	Schematic of electrochemical synthesis in insulating template membrane using sputter deposited metallic layer as cathode	43
Figure 3.2	Schematic of the two-compartment electrochemical cell (W.E. – working electrode; C.E. – counter electrode)	44
Figure 3.3	Schematic of electrochemical template synthesis in insulating template membrane using removable mercury cathode	45
Figure 3.4	AFM images of the track-etched PC membrane surface before electrochemical deposition of gold	48
Figure 3.5	Gold-deposited track-etched PC membrane	48
Figure 3.6	EDXRF spectrum of Au-deposited PC membrane prepared by electrochemical deposition	49
Figure 3.7	XRD pattern of Au-deposited PC membrane prepared by electrochemical deposition	50
Figure 3.8	Visible absorbance spectrum of Au-deposited PC membrane prepared by electrochemical deposition (A, $t_d = 1000$ s & B, $t_d = 3000$ s)	51
Figure 3.9	FEG-TEM images of the gold nanorods after dissolution of the PC membrane (a) $t_d = 1000$ s (b) $t_d = 3000$ s (c) 2 nm resolution image showing lattice distances (d) SAED pattern	52
Figure 3.10	AFM images of both the surfaces of the track-etched PC membrane after electrochemical deposition of gold ($t_d = 1000$ s). Side 1: (a) and	54

	side 2: (b)	
Figure 3.11	AFM images of both the surfaces of the track-etched PC membrane after electrochemical deposition of gold ($t_d = 3000$ s). Side 1: (a) and side 2: (b)	54
Figure 3.12	Schematic of the growth of gold nanorods in the PC membrane using the removable mercury cathode in two-compartment electrochemical cell for shorter deposition time, $t_d = 1000$ s, (a, b) and longer deposition time, $t_d = 3000$ s, (c, d). Gold-deposited membrane after removing the mercury and HAuCl_4 from the cell compartments and washing it with deionized water: (b, d)	55
Figure 3.13	EDXRF spectrum of Au-deposited PC membrane prepared by galvanic reaction	56
Figure 4.1	Cyclic voltammograms obtained at a scan rate of 100 mV/s in 0.5 M H_2SO_4 for bare Pt and PtNPs coated Pt (PtNPs/Pt) electrodes	63
Figure 4.2	Cyclic voltammograms of 0.84 mM Pu(IV) in 1 M H_2SO_4 on (a) Pt and (b) PtNPs/Pt (The potential scanning rate was 20 mV/s)	64
Figure 4.3	DPV of 0.84 mM Pu(IV) in 1 M H_2SO_4 on (a) Pt and (b) PtNPs/Pt	65
Figure 4.4	Cyclic voltammograms of 0.34 mM Pu(IV) in 1 m H_2SO_4 on Pt electrode at scan rate from 20 to 120 mV/s in intervals of 20 mV/s	66
Figure 4.5	Cyclic voltammograms of 0.34 mM Pu(IV) in 1 m H_2SO_4 on PtNPs/Pt electrode at scan rate from 20 to 120 mV/s in intervals of 20 mV/s	66
Figure 4.6	Plot of peak current (I_p) vs. square root of scan rate for bare Pt and PtNPs/Pt electrodes	67

Figure 4.7	DPV of Pu(IV) in 1 M H ₂ SO ₄ at PtNPs/Pt electrode at different concentrations of Pu(IV)	68
Figure 4.8	Cyclic voltammogram obtained at a scan rate of 100 mV/s in 0.5 M H ₂ SO ₄ for PtNPs coated GC (PtNPs/GC) electrode	69
Figure 4.9	SEM image of PtNPs coated GC electrode	69
Figure 4.10	Cyclic voltammogram of 0.84 mM Pu(IV) in 1 M H ₂ SO ₄ on (a) GC and (b) PtNPs/GC. The potential scanning rate was 20 mV/s	70
Figure 4.11	DPV of 0.84 mM Pu(IV) in 1 M H ₂ SO ₄ on (a) GC and (b) PtNPs/GC	71
Figure 4.12	Impedance spectra (Nyquist plots) of (a) GC and (b) PtNPs/GC. Data were recorded in the presence of 0.84 mM Pu(IV)/Pu(III) at E = 0.314 V with an a.c. potential modulation amplitude of 10 mV and for frequencies ranging between 200 kHz to 0.05 Hz	72
Figure 5.1.1	UV-Visible spectrum of AuNPs-CTA membrane	83
Figure 5.1.2	XRD spectrum of AuNPs-CTA membrane	84
Figure 5.1.3	Noncontact AFM images (2D, 3D and profilogram) of AuNPs-CTA membrane	85
Figure 5.1.4	Cyclic voltammograms of the AuNPs-CTA modified electrode and bare gold electrode in 1 M H ₂ SO ₄ solution. Scan rate = 100 mV/s	86
Figure 5.1.5	Cyclic voltammograms of 5 mM UO ₂ ²⁺ in saturated Na ₂ CO ₃ at bare gold and AuNPs-CTA modified electrodes. Scan rate = 50 mV/s	87
Figure 5.1.6	Chronoamperometric transients of 5 mM UO ₂ ²⁺ in saturated Na ₂ CO ₃ at bare gold and AuNPs-CTA modified electrodes upon the application of a reductive potential step from -0.6 V to -1.2 V	88

Figure 5.1.7	Plot of i_{pc} vs. $v^{1/2}$ on (A) bare gold and (B) AuNPs-CTA modified electrodes at scan rate from 20 to 400 mV/s in intervals of 20 mV/s. (C) Plot of E_{pc} vs. $\log v$ at higher scan rates. Solution: 5 mM UO_2^{2+} in saturated Na_2CO_3	89-90
Figure 5.1.8	Impedance spectra (Nyquist plots) of bare gold and AuNPs-CTA modified electrodes. Data were recorded in the presence of 2.5 mM $[Fe(CN)_6]^{3-/4-}$ with an a.c. potential modulation amplitude of 10 mV and for frequencies ranging between 100 kHz to 0.1 Hz	92
Figure 5.2.1	AFM images of (a) bare gold (b) gold nanoporous film (AuNPF) surface	99
Figure 5.2.2	CVs of a bare gold (Au) and a gold nanoporous film (AuNPF) electrodes in 0.5 M H_2SO_4 at a scan rate of 50 mV/s	100
Figure 5.2.3	UV-Visible reflectance spectrum of the gold nanoporous film (AuNPF) electrode	101
Figure 5.2.4	CVs of a bare gold (Au) and a gold nanoporous film (AuNPF) electrodes in 5 mM UO_2^{2+} in 0.5 M H_2SO_4 at a scan rate of 50 mV/s	102
Figure 5.2.5	Cathodic peak current (i_{pc}) vs. $v^{1/2}$ (square root of scan rate) of a bare Au and a AuNPF electrodes for the reduction of 5 mM UO_2^{2+} in 0.5 M H_2SO_4	103
Figure 5.2.6	Chronoamperometric transient of 5 mM UO_2^{2+} in 0.5 M H_2SO_4 at bare Au and AuNPF electrodes to a potential step from 0.1 V to -0.38 V	104
Figure 5.2.7	Impedance spectra (Nyquist plots) of the bare Au and AuNPF electrodes. Data were recorded in the presence of 1 mM $[Fe(CN)_6]^{3-/4-}$	105

with an a.c. potential modulation amplitude of 10 mV and for frequency ranging between 100 kHz to 0.5 Hz

Figure 5.2.8 Cottrell plots for bare Au and AuNPF electrodes

106

CHAPTER 1

Introduction

1.1. Introduction

The word 'nano' is derived from the Greek word 'nanos' or the Latin word 'nanus' which mean dwarf. Nanoparticles are sized between 1 nm and 100 nm. The reduction in size of material not only leads to its miniaturization but at a certain size scale, usually in nanometer-size, a drastic and dramatic change in the bulk properties of the material takes place. For example, an inert and noble bulk gold metal shows a size-dependent catalytic activity for CO oxidation at size < 5 nm. A drastic change in physical, chemical, optical, electrical, catalytic, magnetic properties of materials is observed at a size-scale of less than 100 nm. In general, the size at which nanomaterial displays properties different from that of the bulk is material dependent as well as property dependent i.e., different properties of a nanomaterial show transition from the bulk at different size scales. This size can be larger than 100 nm in case of some materials. For example, though one-dimensional (1D) nanomaterials like nanowires, nanorods and nanotubules have diameters in the range of a few nanometers but have lengths in the range of tens of microns. These 1D nanomaterials have many new properties and functionalities that are different from the bulk materials, e.g. carbon nanotubes have properties, different from other allotropes of carbon, with a large number of promising applications in sensors, catalysis etc. Therefore, a nanoparticle is defined as a particle with at least one dimension in the size range of 1 nm to 100 nm.

Depending on the number of dimensions which are reduced to nanometer size range, nanomaterials can be defined as zero-dimensional (quantum dots), one-dimensional (nanowires, nanorods, and nanotubules) and two-dimensional (quantum well, nanosheet, graphene). In zero-dimensional nanomaterials, all the three dimensions are reduced to nanometer range. In one-dimensional nanomaterials, two dimensions are in the nanometer range and one can remain

large. In two-dimensional nanomaterials, one dimension is reduced to nanometer range and the other two dimensions remain large.

The origin of unique physical, chemical, optical, electrical, catalytic, magnetic properties of nanoparticles, that are neither similar to bulk nor to individual atoms or molecules, can be explained either in terms of surface effect or quantum-size effect owing to quantum-mechanical rule.

Surface effect:

For bulk materials, usually greater than one micron, the percentage of atoms at the surface is infinitesimally small compared to the total number of atoms of the material. As the size of the material is reduced, the ratio of surface atoms to inner atoms (or total atoms) starts increasing. Atoms on the surface of a bulk crystalline solid are principally located on basal planes, but they transform almost completely in edge and corner atoms with a decrease in size. Because of the low coordination number, edge and corner atoms are highly chemically reactive, catalytically active, highly polarizable, and so on, in comparison with the atoms on basal planes. As a result, in the nanometer size range, the role of surface atoms starts becoming predominant in determining the properties of the material (surface effect) instead of the inner atoms. Therefore, higher proportion of the surface atoms results in some of the interesting and unexpected properties of nanoparticles that are different from the bulk properties. For example, bulk gold is an inert noble metal, but gold nanoparticles are excellent catalyst with size-dependent catalytic ability. Nanoparticles of noble metals such as gold and silver have various colors in the visible region based on surface plasmon resonance, which is due to the collective oscillations of the conduction electrons at the surface of the nanoparticles on interaction with the electric-field of the incident light photon. The very high surface area to volume ratio provides a

tremendous driving force for diffusion, especially at elevated temperatures. Sintering can take place at lower temperatures, over shorter time scales than for bigger particles. This theoretically does not affect the density of the final product, though flow difficulties and the tendency of nanoparticles to agglomerate complicates matters. The large surface area to volume ratio also reduces the incipient melting temperature of nanoparticles. Gold nanoparticles melt at much lower temperatures (~300 °C for 2.5 nm size) than the gold slabs (1064 °C). Absorption of solar radiation in photovoltaic cells is much higher in materials composed of nanoparticles compared to that in thin films of continuous sheets of material, i.e. the smaller the particles, the greater the solar absorption.

Quantum-size effect:

The processes of diminishing the macroscopic size to nanometer range in one, two or all the three dimensions lead to the confinement of movement of conduction electrons in a very small space, which is comparable to their De Broglie wavelength. This leads to the formation of discrete energy levels in nanomaterials similar to atoms, unlike the continuous energy levels in the bulk materials. In case of semiconductor nanoparticles, the band gap energy increases when exciton (a bound electron-hole pair produced by a photon) is confined to a length scale comparable or smaller to its Bohr radius. The optical absorption (and thus the nanoparticle color) and the emission spectra shifts toward the shorter wavelength (higher energy) and become sensitive to the size and shape of the particles.

Why nanoparticles are so interesting?

Nanomaterials show size, shape and composition-dependent properties. Therefore, a single material can show a wide range of properties and applications depending on the size in the world of nano. Because of their size-dependent properties, they are considered as an intermediate

state of matter lying between an individual atom and bulk matter. Nanoscience and nanotechnology have emerged as an interdisciplinary subject in true sense because of widespread interest among the chemists, physicists, biologists and technologists working in different research domains. In recent times, nanomaterial research has found a huge interest, and nanomaterials are finding a large numbers of applications in every aspect of human life, ranging from electronics industry to health care. For example, the reduction in the dimension of electronic circuits has led to the development of smaller, faster and smarter electronic devices with very large data storage capacity. Studies have confirmed that tunable surface plasmon resonance properties of nanostructures of gold (nanoshells and nanorods) are promising for early detection and treatment of cancer. Scientists and technologists are trying to exploit a wide range of nanomaterials properties by carefully tuning the shape, size, and composition of the material. The interesting properties of nanomaterials have been extolled with many great promising applications in near future. A lot of research activities have been focused on various applications of nanomaterials - catalysis, sensors, electronics, optical, magnetic, diagnostic, therapeutic etc. A large numbers of original research articles and reviews are available on the subject.

Changes in properties are not always desirable at nanoscale:

The changes in properties are not always desirable as we usually expect from nanomaterials. Ferroelectric materials smaller than 10 nm can switch their magnetization direction using room temperature thermal energy, thus making them useless for memory storage. Nanoparticles exhibit a number of special properties that are very different from the bulk material. For example, bulk copper is malleable because the bending of bulk copper (wire, ribbon, etc.) occurs with movement of copper atoms/clusters at about 50 nm scale. Copper

nanoparticles smaller than 50 nm are considered super hard materials that do not exhibit the same malleability and ductility as bulk copper.

1.2. Synthesis Techniques

Size, shape and composition-controlled monodisperse nanomaterials of metals, semiconductors, organic polymers, conducting polymers, inorganic materials, and their composites have been synthesized by different routes. Controlled synthesis of monodisperse nanomaterials with desired tunable properties is still a subject of great interest among the research communities and efforts are being continuously made to scale up the production for various applications. There are two principal approaches for the preparation of nanomaterials called the “top-down” approach and the “bottom-up” approach.

Top-down approach

The top-down approach involves reducing the dimension(s) of the large macroscopic materials to very small-sized particles by the systematic breakdown of bulk material. The top-down method involves some form of grinding (ball-milling), lithographic or laser ablation-condensation techniques. The advantage of grinding mechanism is its simplicity and there is no requirement of various organic and inorganic compounds (sometimes volatile and toxic) during the preparation process. However, the quality of the nanoparticles produced by grinding is known to be poor in comparison with the materials produced by the bottom up methods. The main drawbacks include contamination problems from grinding equipment, low particle surface areas, irregular shape and size distributions and high energy requirements needed to produce relatively small particles. However, nano-material produced by top-down approach still finds use for catalytic, magnetic and structural purposes.

Bottom-up approach

In bottom-up approach, the nanoparticles are prepared by assembling the individual atoms or molecules in the presence of stabilizer or protecting agent e.g. reduction of metal ions to form metal nanoparticles. Stabilizer or protecting agents prevent the agglomeration of nanoparticles by either steric repulsion or electrostatic repulsion among nanoparticles. A number of chemical, electrochemical and physical methods have been reported for the synthesis of nanomaterials via bottom-up approach. In the past few years, research articles on the microbial/biological synthesis of nanomaterials have also been published. The shape and size controlled nanoparticles are prepared by using either templates or controlling the ratio of metal ion to stabilizer. The template can be either hard (track-etched polymeric membranes, porous anodized alumina etc.) or soft (micelles of surfactant or block copolymers, proteins, DNA etc.)

Metal Nanoparticles and its nanocomposites

Metal nanoparticles are usually prepared by the reduction of metal ions. The modes of reduction are chemical, electrochemical, microbial, radiation-assisted (UV light, electron beam, γ -radiation) etc. The medium for metal nanoparticles synthesis may be either aqueous or non-aqueous or sometimes both. Metal nanoparticles supported on solid substrate like metal oxide, organic and inorganic polymers etc. have also been synthesized, and are known to have very good catalytic activity. Metal nanoparticles of various shapes, sizes and composition have been prepared either by using templates or without templates. One-dimensional metal nanoparticles like nanowires, nanotubes are usually prepared using templates like track-etched polycarbonate or porous anodized alumina membranes. Metal alloy (Au-Ag, Au-Pt etc.) nanoparticles are also prepared by simultaneous reduction of two different metals, and have properties superior to individual metals, for example, lowered barrier for a specific chemical reaction, an increased

selectivity and an enhanced resistance against contamination and poisoning. The core-shell metal nanoparticles are synthesized by depositing one metal on the surface of other metal. Physical methods like molecular beam epitaxy (MBE), chemical vapor deposition (CVD), physical vapor deposition (PVD) etc. are widely used to prepare supported metal nanoparticles. Thermolysis of organometallic precursor in presence of stabilizer is another method of producing metal nanoparticles. Nanocomposites of metals with polymer are prepared by incorporating metal nanoparticles into the polymer matrix. Nanocomposites of noble metal (Au, Pt) with conducting polymer (polyaniline, polypyrrole) are prepared in-situ and ex-situ by chemical and electrochemical routes.

Semiconductor nanoparticles

Nanoparticles of semiconductors (CdS, PbS etc.) are either prepared in suspension by chemical route (mixing of metal and chalcogenide ions) or can be directly synthesized on support using techniques like MBE, CVD etc. The chemical mixing of metal ions and chalcogenide ions produces precipitate of nanoparticles with very high polydispersity. The technological applications of tunable and size-dependent physical and optical properties have aroused interest in the synthesis of size-selective, monodisperse semiconductor nanoparticles. A simpler hybrid electrochemical/chemical route for the synthesis of supported semiconductor nanoparticles with size selectivity is also reported. The kinetics of reaction between metal- and chalcogenide-containing covalent compounds is tuned, by controlling the amount of heat supplied, to prepare monodisperse nanoparticles. The highly crystalline nanoparticles with very narrow size distribution are prepared by rapid addition of a room-temperature mixture of both precursors into the preheated (340-360 °C) solvent, which results in rapid nucleation, and then temperature of the solvent is lowered (280-300 °C) to slow down the growth of the nanocrystals.

Conducting polymer nanoparticles

Nanoparticles of conducting polymers are prepared by controlled oxidation of monomers using chemical and electrochemical methods. One-dimensional nanostructures of conducting polymers are prepared via electrochemical template synthesis using track-etched polymer membranes, porous anodized alumina etc. Some recent reports mention the preparation of conducting polymer nanowires without using templates. The nanoparticles of conducting polymers prepared by chemical methods are usually in the form of precipitate in solution, but electrochemical method produces supported conducting polymer nanoparticles.

1.3. Characterisation Techniques

Characterization is necessary to establish understanding and control of nanoparticles synthesis and their applications. Characterization is done by using a variety of different techniques. Some of the characterisation techniques which are used on regular basis are ultraviolet-visible spectroscopy, electron microscopy (TEM, SEM), atomic force microscopy (AFM), powder X-ray diffraction (XRD) etc.

UV-visible spectroscopy

The optical properties of metal nanoparticles differ substantially from the optical properties of the bulk metals. Under the influence of an electrical field of an incident light photons, there is a plasmon excitation of the conduction electron at the nanoparticles' surface. This resonance, which take place at a certain energy of the incident light photon, results in an optical absorption, the so-called surface plasmon absorption or surface plasmon resonance (SPR) absorption. The spectral position (λ_{max}), full-width at half-maximum (FWHM) and relative intensity (I_r) depend on various physical parameters e.g. dielectric function of the metal, particle

size and shape distribution, dielectric constant of the surrounding medium, interparticle interactions etc. The spherical metal nanoparticles give only a single peak in absorption spectrum, but metal nanorods show two peaks corresponding to transversal and longitudinal oscillations. However, the exact determination of the size and shape of the nanoparticles is a prerequisite for description of the optical properties.

X-ray diffraction (XRD)

To determine the structure of a crystal, and thereby ascertain the position of its atoms in the lattice, a collimated beam of X-rays is directed at the crystal, and the angles at which the beam is diffracted are measured. Each diffracted X-ray signal corresponds to a coherent reflection, called Bragg reflection, from successive planes of the crystal for which Bragg's Law is satisfied

$$2d\sin\theta = n\lambda$$

The analysis of X-ray diffraction pattern provides variety of information. This includes qualitative (phase identification) and quantitative (lattice parameter determination and phase fraction analysis). The peak positions contain information about crystal system, space group symmetry, translational symmetry, unit cell dimension and qualitative phase identification. The information contained in peak intensities is unit cell contents, point symmetry and quantitative phase identification. The analysis of peak shape and width (full-width at half maximum) of the Bragg peaks of the X-ray diffraction pattern provide information on the crystallite size and strain. A perfect crystal would extend in all directions to infinity, so one can say that no crystal is perfect due to its finite size. This deviation from perfect crystallinity leads to a broadening of the diffraction peaks. However, above a certain size (100-500 nm), this type of broadening is negligible. Peak broadening arises from several sources: instrumental effects, finite crystallite

size (< 100-500 nm), strain (atoms deformed from ideal positions in a non-uniform manner), extended defects (terminate “crystal” and lead to size broadening). Since the peak broadening arises from a combination or convolution of crystallite size, microcrystalline strain and instrumental broadening effects, it is necessary to correct for the instrumental broadening and to sort out the strain components to determine the average crystallite size.

There are various methods for obtaining crystallite size and strain information. Scherrer formula provides average crystallite size if strains and instrumental broadening are corrected. Scherrer (1918) first observed that small crystallite size could give rise to line broadening. He derived a well known equation for relating the crystallite size to the broadening, which is called the Scherrer Formula.

$$D_v = \frac{K \lambda}{\beta \cos \theta}$$

D_v = Volume weighted crystallite size

K = Scherrer constant, somewhat arbitrary value that falls in the range 0.87-1.0.

λ = Wavelength of the radiation

β = Full-width at half maximum (in radians) at 2θ .

Integral breadth methods provide average values of size and strain. Peak shape methods provide size and strain distributions. To do an accurate analysis for size and/or strain effects, one must accurately account for instrumental broadening. The method of doing this differs depending upon the peak shape.

Crystallite size is a measure of the size of a coherently diffracting domain. Due to the presence of polycrystalline aggregates, crystallite size is generally not the same thing as the

particle size. Other techniques for measuring size (electron microscopy, dynamic light scattering, X-ray or neutron scattering, atomic force microscopy etc.) measure the particle size rather than the crystallite size.

Scanning electron microscopy

Electron microscopy (scanning electron microscopy, SEM and transmission electron microscopy, TEM) is the most powerful method to determine size and shape distributions of the nanoparticle assemblies. Electron microscopes were developed due to the limitations of light microscopes which are limited by the physics of light. Electron microscopes use a beam of energetic electrons to examine objects on a very small scale.

The basic instrumentation of SEM includes an electron source (thermal or field emission gun), aperture (condenser and objective) to eliminate some high-angle electrons, electromagnetic lenses (condenser and objective) to focus the electron beam on the sample, sample holder, and various types of detectors to detect the signals (scattered electrons, X-rays etc.) generated when electron beam strikes the sample. The signal generated by the interaction of the incident electron beam with the sample can be broadly categorized as electron signal (back-scattered electron, secondary electron, Auger electron) or photon signal (X-rays). SEM provides the characteristic information on (1) Topography - the surface features of an object or "how it looks", its texture (2) Morphology - the shape and size of the particles making up the object, (3) Composition - the elements and compounds that the object is composed of and the relative amounts of them, and (4) Crystallographic - information about the arrangement of atoms in the object.

Transmission electron microscopy

In TEM, electron beam of very high energy (about hundreds of KeV) is focused on an ultra thin sample and it interacts with the sample while transmitting through the sample. An image is formed from the interaction of the electrons transmitted through the specimen; the image is magnified and focused onto an imaging device, such as a fluorescent screen, on a layer of photographic film, or is detected by a sensor such as a CCD camera. TEMs are capable of imaging at a significantly higher resolution (sub-nanometer) than light microscopes, owing to the small de Broglie wavelength of electrons. This enables to examine the particles in nanometer size range, which is tens of thousands times smaller than the smallest resolvable object in a light microscope. The most common mode of operation for a TEM is the bright field imaging mode. In this mode, the contrast is formed directly by occlusion and absorption of electrons in the sample. Thicker regions of the sample or regions with a higher atomic number will appear dark, whilst regions with no sample in the beam path will appear bright – hence the term "bright field". Crystal structure can be investigated by high-resolution transmission electron microscopy (HRTEM), also known as phase contrast. TEM forms a major analysis method in nanoscience and nanotechnology. However, extensive sample preparation is often required and can cause preparation effects, and thus the TEM micrographs sometimes are not representative of the whole nanoparticle-containing insulating materials.

Atomic force microscopy

Atomic force microscopy (AFM) is a very high-resolution type of scanning probe microscopy, with resolution of the order of fractions of a nanometer. The AFM is one of the foremost tools for imaging, measuring, and manipulating matter at the nanoscale. The information is gathered by scanning the surface with a mechanical probe. The AFM consists of a cantilever with a sharp tip (probe) at its end that is used to scan the specimen surface. The

cantilever is typically silicon or silicon nitride with radius of curvature of the tip of on the order of nanometers. When the tip is brought into proximity of a sample surface, forces between the tip and the sample lead to a deflection of the cantilever according to Hooke's law. Depending on the situation, forces that are measured in AFM include mechanical contact forces, van der Waals forces, capillary forces, chemical bonding, electrostatic forces, magnetic forces (magnetic force microscope, MFM), solvation forces, etc. The AFM can be operated in a number of modes, depending on the application. In general, possible imaging modes are divided into static (also called contact) modes and a variety of dynamic (non-contact or "tapping") modes where the cantilever is vibrated. In contact mode, the force between the tip and the surface is kept constant during scanning by maintaining a constant deflection. The contours of the surface are measured/mapped directly using the deflection of the cantilever. In the dynamic mode, the cantilever is externally oscillated at or close to its fundamental resonance frequency or a harmonic. The oscillation amplitude, phase and resonance frequency are modified by tip-sample interaction forces. These changes in oscillations with respect to the external reference oscillation provide information about the sample's morphology.

AFM has several advantages over the scanning electron microscope (SEM). Unlike the electron microscope which provides a two-dimensional projection or a two-dimensional image of a sample, the AFM provides a three-dimensional surface profile. Additionally, samples viewed by AFM do not require any special treatments (such as metal/carbon coatings) that would irreversibly change or damage the sample, and does not typically suffer from charging artifacts in the final image. While an electron microscope needs an expensive vacuum environment for proper operation, most AFM modes can work perfectly well in ambient air or even in a liquid environment.

Other techniques

Other characterisation techniques are X-ray photoelectron spectroscopy (XPS), scattering techniques (dynamic light scattering, small-angle X-ray or neutron scattering), Fourier transform infrared spectroscopy (FTIR), matrix-assisted laser desorption/ionization time-of-flight mass spectrometry (MALDI-TOF), nuclear magnetic resonance (NMR) etc.

1.4. Properties and Applications

Optical: Surface plasmon resonance

Some metal nanoparticles (Ag and Au) exhibit colors due to strong absorption bands in the visible region, and these colors are absent in the individual atoms as well as in the bulk. The basis of the light absorption by metal nanoparticles is the collective coherent oscillation of the conduction band electrons induced by the incident photon. The electric field of an incoming light wave induces a polarization of the (free) conduction electrons with respect to the much heavier ionic core of a spherical nanoparticle. The positive charges in the particle are assumed to be immobile and the negative charges, that is, the conduction electrons, move under the influence of external fields. Therefore, a displacement of the negative charges from the positive ones occurs when the metallic nanoparticle is placed in an electric field. This results in a net charge difference at the nanoparticle boundaries which in turn gives rise to a linear restoring force to the system. As a consequence, a dipolar oscillation of the electrons is created (with a particular time period), and this is known as the surface plasmon oscillation. For many metals, such as, Pb, In, Hg, Sn, and Cd, the plasmon frequency lies in the UV part of the spectrum and nanoparticles do not display strong color effects. Hence, surface plasmon experiments are most commonly carried out with Cu, Ag, and Au. The resonance frequency of this SPR is strongly dependent upon the

size, shape, composition, interparticle interactions, dielectric properties, and local environment of the nanoparticle. The unique surface plasmon absorbance features of metal nanoparticles have been exploited for a wide variety of applications - colorimetric sensor, early detection and treatment of tumors, photo and electrochromic switching.

Catalytic properties

Metal nanoparticles show enhanced catalytic activity compared to that of the bulk metal, and it is dependent on the size, shape, composition, nature of stabilizing agent, crystal orientation etc. An inert and noble bulk gold metal shows a size-dependent catalytic activity for CO oxidation at size < 5 nm. Catalytic activity of the supported metal nanoparticle depends on the nature and electronic properties of the support. Metal nanoparticles are fine tuners of interfacial properties at electrode-solution interface, and are widely used by electrochemists for decorating the surface of the conventional electrodes to produce electrocatalytic effect. Metal nanoparticles have been used for the immobilization of many redox enzymes, and bioelectrocatalysis of biomolecules (glucose, phenolic compounds, H₂O₂ etc.) has been observed. Metal nanoparticles, especially gold and platinum, find widespread electrochemical applications in electrocatalysis and electrochemical sensing.

Semiconductors

In a bulk semiconductor, a bound electron-hole pair (an exciton) is produced by exciting it with a photon having energy greater than the band gap energy. The band gap energy of the semiconductor is the energy difference between the top of the valence band and the bottom of the conduction band, and it is the minimum amount of energy required for the formation of the exciton. An electron and hole (the charge carriers) are separated by a distance known as the Bohr radius, and is on the nanometer length scale. When the size of the semiconductor is in the nano-

scale range, comparable to or smaller than the Bohr radius, the motion of the exciton is confined. Therefore, the energy of the band gap increases compared to that of the bulk semiconductor. The optical absorption (and thus the nanoparticle color) and the emission spectra shift towards the shorter wavelength (higher energy) and become sensitive to the size and shape of the particles. The size and shape-dependent optical and other physical and chemical (e.g. oxidation-reduction) properties of semiconductor nanoparticles are finding new technological applications – optoelectronics, photovoltaic, nanoelectronics, photocatalysis, photodegradation and detoxification of environmental pollutants etc.

Conducting polymers

One-dimensional nanomaterials like nanowires and nanotubules have enhanced molecular and supermolecular order. Enhanced molecular order means that the polymer contains fewer conjugation-interrupting defect sites. Enhanced supermolecular order means that the polymer chains are ordered through stretching, crystallization, or both. The enhanced ordering leads to very high conductivity which is one to two orders of magnitude higher than the bulk conducting polymer. The conducting polymer nanowires with higher surface area and higher conductivity have attractive properties as novel materials for electrochemical sensing, chemical sensing and biosensing. Single polypyrrole nanowire and polyaniline nanowires on Pt interdigitated microelectrode have been studied for NH_3 gas sensor application. Conducting polyaniline nanowire arrays have potential applications in supercapacitor electrode materials.

1.5. Electrochemistry and Nanomaterials

In electrochemical processes, electron transfer across the solid-liquid interface is the elementary step, and the interfacial properties such as conductivity, surface area, etc. have

significant influence on electron transfer. In classical voltammetry, the electrodes merely serve as a source or a sink for electrons, to transform electroactive species in solution. However, changes in the nature of the electrode surface can alter the efficiency of the electron-transfer process and/or mass-transport regime. Therefore, preparation of well-defined electrochemical interface with highly controllable properties is significant for both the fundamental and the applied studies in electrochemistry. Interest in obtaining the desired electrochemical properties/reaction at the interface between the electrode and the solution has motivated the electrochemists to modify the electrode surface. Nanoparticles are finding wide range of applications in electrocatalysis and electrochemical sensors because of their unique physical and chemical properties. Therefore, nanostructured-materials – carbon nanotubes, nanoparticles, nanoporous films – have been utilized to modify the surface of the bare electrodes to obtain better electrochemical responses resulting from larger effective surface area, increased mass transport, and better electronic interaction between the analyte and the electrode. All these advantages of nanoparticles coated electrodes lead to higher catalytic activity, better sensitivity and selectivity. The electrocatalytic behaviour (faster electrode kinetics) of nanostructured materials is amply documented in the literature and the commonly used diagnostic criteria are the smaller peak separations (or anodic shift in the reduction potentials in the case of irreversible processes) and the increased peak current. A few recent reports suggest that the above mentioned diagnostic criteria of electrocatalysis are valid if the mass transport regime for the unmodified and the modified electrodes are the same. In the case of carbon nanotubes modified electrode, porous structures/layers are formed, and the smaller peak separations and the increased peak current in the redox reaction of electroactive species can be described using thin-layer diffusion model. The metal nanoporous film on the bare metal electrode could result in faster electrode

kinetics, a change in the mass transport regime, or the combined effects leading to higher peak current and a smaller peak separation. Therefore, efforts are necessary to understand/determine the mass transport regime while extolling the electrocatalytic behaviour of nanoporous film modified electrode over the unmodified electrode.

Electrochemical deposition techniques are promising to synthesis and immobilize the metal nanoparticles onto the electrode surface with easy control of particle shape and size. Nanoparticles of noble metals like Au, Pt were electrodeposited on conducting substrates, like glassy carbon, graphite, indium tin oxide etc. The modification of carbonaceous electrodes by noble metals' nanoparticles also reduces the loading of noble metals. Semipermeable membranes embodying nanoparticles are widely prepared and used for the electrode surface modification because of great potential applications in catalysis and interface-electrochemistry.

1.6. An Overview of the Work Carried out

In the present thesis entitled “Synthesis, Characterisation and Electrochemical Applications of Nanomaterials”, nanomaterials of noble metal (Au and Pt) were prepared and the electrochemical behaviour of the actinides (uranium and plutonium) was studied on the nanomaterial-modified electrodes.

The incorporation of metal nanoparticles in the polymer matrix produces composites with properties and performance superior to polymer and metal nanoparticles alone. Gold-polyaniline composite, prepared by incorporation of gold nanoparticles into polyaniline matrix, has good stability, high conductivity and unique optical properties. Many reports show that incorporation of gold nanoparticles in the polyaniline matrix significantly enhances its electrocatalytic and sensing properties. Many chemical and electrochemical methods have been developed for the

synthesis of gold-polyaniline composite. In chemical synthesis, polyaniline and gold-polyaniline composite are prepared as powder or precipitate in solution. In electrochemical synthesis, polyaniline and gold-polyaniline composite have been prepared as film of varying thickness on various conducting substrates - gold, platinum, indium tin oxide, and various carbonaceous electrodes. For putting these polymer/metal composites in real world applications, it is desirable to have them immobilized on some support/substrate. Therefore, electrochemical synthesis is more favored than chemical synthesis in sensor and catalysis. In Chapter 2, an in situ one step chemical synthesis of gold-polyaniline composite in the nanopores of track-etched polycarbonate membrane and its characterisation are discussed. Nanopores in the polycarbonate membrane act as the reaction vessels of nano-dimension where aniline and HAuCl_4 were allowed to mix together and the redox reaction between aniline and HAuCl_4 led to the synthesis of gold-polyaniline composite. The nanopores also controlled the growth of gold-polyaniline composites by limiting the free volume available for the growth. Polycarbonate membrane with nanopores acted as a supporting matrix for immobilization of gold-polyaniline composites synthesized by chemical route.

Electrochemical template synthesis of one-dimensional (1D) nanomaterials - nanowires, nanorods and nanotubules of metals, semiconductors and conducting polymers are more frequently carried out in commercially available templates like porous anodized alumina and track-etched polycarbonate (PC) membranes. The previously reported method of electrochemical template synthesis in template membrane involves an indispensable and inevitable step of coating 500 nm to 1 μm thick metallic layer onto one surface of the insulating membrane by sputter deposition technique. The ensemble of the metal nanowires grown in the template membrane is attached to the coated metallic layer, and protrudes from its surface like the bristles

of brush after the dissolution of the template membrane. Therefore, the nanowires grown in the template membranes are not free-standing. In Chapter 3, the electrochemical synthesis of gold nanorods within the pores of track-etched PC membrane using a removable mercury cathode is discussed and this new approach eliminates the requirement of sputter deposition. A simple two-compartment electrochemical cell was used and the track-etched polycarbonate membrane was placed between the two compartments separating the aqueous solution of HAuCl_4 from mercury. Mercury, filled in one of the compartment, was in contact with one surface of the membrane (similar to sputter deposited metallic layer) and served as the conducting substrate/cathode. The ensemble of the metal nanowires grown in the template membrane was not attached to any conducting substrate, and gold nanorods could be easily freed from the template membrane after dissolution in dichloromethane. A malleable track-etched PC membrane embedded with free-standing cigar-shaped gold nanorods was prepared by the new method and was characterized by different techniques.

Electroanalytical chemistry of uranium and plutonium in various supporting electrolytes (acidic, basic, and non-aqueous) at different electrodes (Hg, Pt, Ag, Au, graphite, glassy carbon, and many chemically-modified electrodes) is well documented in literature. A limited number of publications dealing with the applications of nanomaterial modified electrodes for lanthanide and actinide electrochemistry are available. In Chapter 4, studies carried out to prepare platinum nanoparticles (PtNPs) electrochemically on the surface of glassy carbon and platinum electrodes by potentiostatic deposition technique are discussed. The electrochemical reduction and oxidation of Pu(IV)/Pu(III) couple in 1 M H_2SO_4 on the nanoparticles-modified electrodes was investigated by using voltammetric and impedance techniques. Redox kinetics was observed to improve in both the oxidation and the reduction processes after electrodeposition of PtNPs in

contrast to bare electrodes. However, significant improvement was seen for the reduction of Pu(IV) to Pu(III) in PtNPs coated GC electrode compared to the bare GC electrode. These studies are of great relevance to develop electroanalytical methodologies for Pu determination using nanoparticles modified electrodes.

In Chapter 5, the electrochemical behaviour of UO_2^{2+} ions at the nanostructured gold-modified electrodes is discussed. The nanostructured gold-modified electrodes were prepared by either physical entrapment of gold nanoparticles (AuNPs) in an anion-exchange membrane or by formation of gold nanoporous film (AuNPF) on bare Au electrode.

In Part 1 this Chapter, synthesis of gold nanoparticles (AuNPs) in an anion-exchange membrane, its characterisation, and preparation of AuNPs-embedded membrane modified electrode are discussed. Cyclic voltammetric and impedance studies were carried out to see the effect of nanoparticles modified electrode on the partial electrochemical irreversibility of the carbonato-complexes of U(VI)/U(V). Electrochemical studies showed the electrocatalytic reduction of UO_2^{2+} to UO_2^+ in saturated Na_2CO_3 solution at AuNPs-CTA modified electrode with higher current density and faster heterogeneous electron transfer kinetics than that using bare Au electrode. The standard heterogeneous rate constant, k^0 , for the reduction process at AuNPs-CTA modified electrode was about 25 times higher than that of bare Au electrode. Therefore, it was concluded that AuNPs-CTA membrane had improved the interfacial electron-transfer properties of the electrode, resulting in a better electrochemical response than bare Au electrode.

In Part 2 of this Chapter, the preparation of gold nanoporous film (AuNPF) electrode, its characterisation, and the electrochemical reduction of UO_2^{2+} in 0.5 M H_2SO_4 AuNPF electrode are discussed. The metal nanoporous film on the bare metal electrode could result in faster

electrode kinetics (electrocatalysis), change in the mass transport regime, or the combined effects leading to higher peak current and a smaller peak separation (or anodic shift in reduction potentials in case of irreversible processes). In cyclic voltammetric (CV) studies, anodic shift of 141 mV in the cathodic peak potential and an increase in the peak current for the reduction of UO_2^{2+} in 0.5 M H_2SO_4 was observed at the AuNPF electrode, showing evidence of its enhanced electrochemical activity as compared to that of the bare Au electrode. The interfacial charge transfer resistance values for the bare Au and the AuNPF electrodes obtained by electrochemical impedance spectroscopy were almost the same indicating similar rates of the heterogeneous electron-transfer kinetics at the bare Au and the AuNPF electrodes. The chronoamperometric studies indicated the thin-layer diffusion within the gold nanoporous film. Therefore, the observed anodic shift at the AuNPF electrode was attributed to the contribution from thin-layer diffusion within the gold nanoporous film.

CHAPTER 2

In-situ Synthesis of Gold-Polyaniline Composite in Nanopores of Polycarbonate Membrane

2.1. Introduction

The incorporation of nano-dimension metal particles into the polymer matrix leads to the formation of metal-polymer nanocomposite. The polymer matrix provides stability to nanoparticles against aggregation. Composites of electrically conducting polymers and metal nanoparticles are finding great interest not only because of scientific curiosity, but also for their potential applications in molecular electronic devices, gas sensors, biosensors, capacitors and catalysts [11-16]. Amongst the conducting polymers, polyaniline is of much interest because of its great environmental stability, controllable electrical conductivity and interesting electrochromic properties associated with different redox states [17-21]. Polyaniline nanowire has better electronic properties than polyaniline and thus has better gas sensing capability (higher sensitivity). The incorporation of metal nanoparticles in the polymer matrix produces composites with properties and performance superior to polymer and metal nanoparticles alone [16]. Incorporation of metal nanoparticles into polymer matrices improves their physical and chemical properties. Therefore, polymer/metal composites find widespread applications in catalysis, sensing, electronics etc. in comparison to either polymer or metal nanoparticles alone. Many times, a new set of properties arises due to blending of polymer with metal nanoparticles. Gold nanoparticles of different shapes and sizes have been extensively studied due to their unique electronic, optical, sensing and catalytic properties [22-33]. These nanoparticles are very stable and their surface can easily be functionalised by self-assembling of organic molecules through sulphur atom. Gold-polyaniline composite, prepared by incorporation of gold nanoparticles into polyaniline matrix, has good stability, high conductivity and unique optical properties [34-40]. Many reports show that incorporation of gold nanoparticles in the polyaniline matrix significantly enhances its electrocatalytic and sensing properties.

Many chemical and electrochemical methods have been developed for the synthesis of gold-polyaniline composite. Preformed polyaniline was used for the preparation of gold-polyaniline composite by exploiting multiple-oxidative states of polyaniline [40]. Completely reduced state of polyaniline (viz. leucoemeraldine) acts as a reductant for AuCl_4^- reduction to Au. Polyaniline is prepared by either chemical or electrochemical oxidation of aniline [41-42]. Chemical synthesis of polyaniline is carried out by oxidising aniline using ammonium persulphate as the oxidising agent. Polyaniline and gold-polyaniline composite are prepared as powder or precipitate in solution. Electrochemical oxidation of aniline is carried out by using any of the three methods viz. galvanostatic, potentiostatic or potentiodynamic. In electrochemical synthesis, polyaniline and gold-polyaniline composite has been prepared as film of varying thickness on various conducting substrates - gold, platinum, indium tin oxide, and various carbonaceous electrodes. Polyaniline nanowires have been electrochemically synthesized in various templates- polycarbonate membrane and porous alumina. For putting these polymer/metal composites in real world applications, it is desirable to have them immobilized on some support/substrate. Therefore, electrochemical synthesis is more favored than chemical synthesis in sensor and catalysis.

AuCl_4^- was used as an oxidant for the oxidative polymerisation of pyrrole [43-44], hexadecylaniline [45], o-anisidine [46], aniline [35] resulting in the formation of gold-polymer composite. Chemical synthesis of a gold-polyaniline composite is based on the oxidizing properties of auric acid. AuCl_4^- is reduced to Au^0 by aniline accompanying the simultaneous oxidation and polymerization of aniline to polyaniline at acidic pH. One-step chemical synthesis of gold-polyaniline composite involves mixing of aniline and gold salt (HAuCl_4), and the redox reaction between them leads to the formation of gold-polyaniline composite. Preparation of gold-

polyaniline composite using H_2O_2 [47], which acts as both oxidising and reducing agent, was reported. Preparation of gold-polyaniline composite using HBF_4 was reported [48]. Polyaniline nanoballs of a few microns size and decorated by gold nanoparticles (10-50 nm) were prepared in toluene solution by using a phase transfer catalyst [49]. Nanofiber shaped polyaniline was synthesised using HAuCl_4 but polymer and metal particle got completely phase separated [50]. Two-step synthesis of gold-polyaniline composite was carried out using 10-bromodecylperoxide, which acted as a stabiliser for the gold nanoparticles as well as the oxidant for aniline [51]. Electrochemical synthesis of gold-polyaniline composite was also reported [39,49]. For technological applications, it is desirable to have the gold-polyaniline composite of high surface area, high dispersion of gold nanoparticles into the polyaniline matrix, and an intimate contact between gold nanoparticles and polyaniline. Some of the preparation methods suffered from drawbacks, like poor dispersion of Au into polyaniline matrix or lack of intimate contact between gold and polyaniline that hamper the attainment of all the desired properties.

Mechanical properties such as miscibility, process ability, water resistance and transparency make polycarbonate (PC) an important matrix for dispersion of nanoparticles. Nanostructured composite film based on dispersion of thiol coated gold nanoparticles in PC was prepared by evaporating a solution of PC and thiol-coated Au nanoparticles in CHCl_3 [52]. This composite film was developed for applications as optical lenses. PC membrane was used as a template for the preparation of nanostructured materials [53]. Nanowires of metals and conducting polymer were electrodeposited in pores of PC membrane [54]. Synthesis of polypyrrole nanowires in PC membrane was reported using chemical method. PC membrane was placed between a two-compartment cell, pyrrole was added in one compartment and oxidant (FeCl_3) in the other compartment. Pyrrole got converted to polypyrrole through a polymerisation

reaction within each pore as oxidant diffused through these nanopores due to concentration gradient [55,56].

In this Chapter, an in-situ one-step chemical synthesis route developed for the preparation of a gold-polyaniline composite in nanopores of a PC membrane is presented. PC membrane with a pore diameter of 200 nm and 10 μm thickness was placed in a specially designed two-compartment cell, physically separating the aqueous solutions of aniline and HAuCl_4 (used as an oxidant). Aniline and HAuCl_4 molecules diffused towards each other under the concentration gradient in the nanopores of polycarbonate membrane. Nanopores in the polycarbonate membrane act as the reaction vessels of nano-dimension where aniline and HAuCl_4 were allowed to mix together and the redox reaction between aniline and HAuCl_4 led to the synthesis of gold-polyaniline composite. The gold-polyaniline composite in PC membrane was characterised by EDXRF, XRD, UV-Vis spectroscopy, FTIR and TEM. Peak broadening in XRD suggested that Au particles formed in the membrane were nanocrystallites with average crystallite size 24 ± 3.4 nm. TEM studies showed that gold nanoparticles were randomly dispersed in polyaniline clusters formed in the nanopores of PC membrane. Characterisation results showed that the surfaces of the PC membrane exposed to HAuCl_4 had significantly higher concentration of Au than the aniline-exposed surface.

These nanopores control the growth of gold-polyaniline composites by limiting the free volume available for the growth. Polycarbonate membrane with nanopores acted as a supporting matrix for immobilization of gold-polyaniline composites synthesized by chemical route. Enzymes or some other analyte-selective molecules can be immobilized on gold-polyaniline composite surface in the nanopores for various applications. Studies carried out for the characterisation of gold-polyaniline composite are also reported.

2.2. Experimental

Reagents

Nucleopore track-etched porous PC membrane with a pore diameter of 200 nm and 10 μm thickness was obtained from Whatman Ltd. Hydrochloric acid, aniline and HAuCl_4 used were of analytical grade. Deionised water (18 $\text{M}\Omega/\text{cm}$) purified by the MilliQ water purifier system from Millipore was used throughout the present studies.

Synthesis and characterisation of Au-PANI composite

The porous PC membrane (diameter = 1 cm) was sonicated in water for 5 minutes. It was placed in a specially designed two-compartment cell as shown in Fig. 2.1.

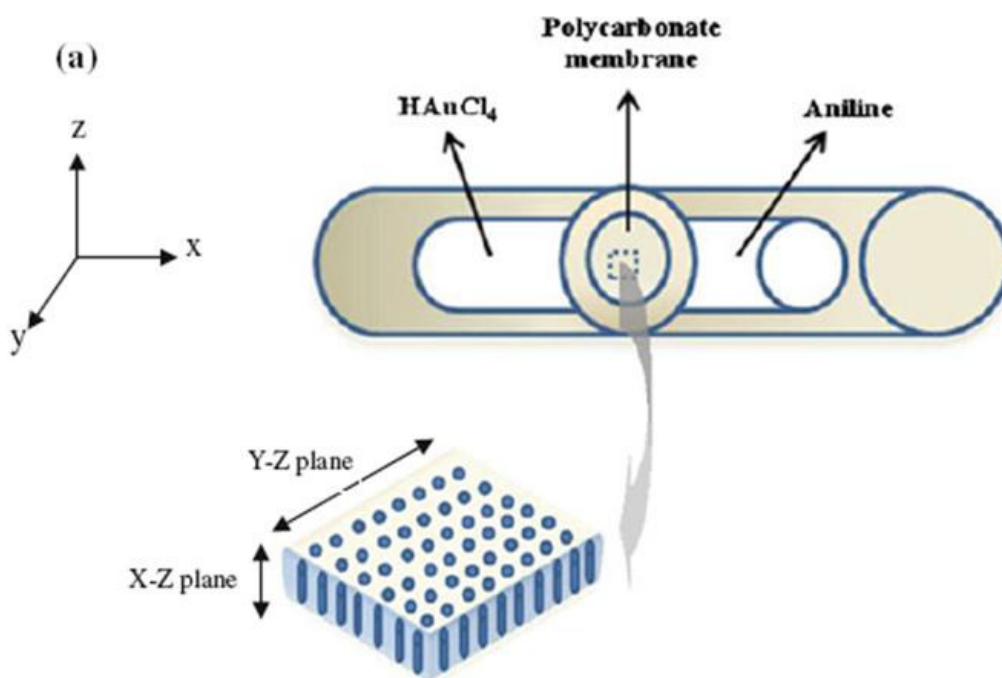


Figure 2.1: Schematic of two-compartment cell. Porous PC membrane separates the two compartments.

Solutions of 10 mM HAuCl_4 in water and 0.5 M aniline in 1 M HCl were filled in two compartments. The cell was kept undisturbed overnight to allow the redox reaction between aniline and HAuCl_4 to occur. The polycarbonate membrane has good chemical resistance in dilute acid solution. The membrane was then washed thoroughly in water and was allowed to dry in air. Similar experiments were repeated to prepare gold-polyaniline composite in PC membrane with different preparation time by keeping the cell undisturbed for time intervals of 2, 4 and 8 hours. Energy dispersive X-ray fluorescence measurement of membrane was carried out using Jordan Valley EX-3600 TEC EDXRF spectrometer having Rh target operated at voltage of 40 kV and current of 170 μA . XRD pattern were recorded on a STOE XRD unit using Cu target ($\text{Cu K}_\alpha = 1.5406 \text{ \AA}$) with graphite monochromator. Absorbance spectra of membrane were recorded using a UV-Vis spectrophotometer (QE65000, Ocean Optic Ltd.). The absorbance spectra were measured in air by placing the membrane in a quartz cell. FTIR spectra were recorded in ATR mode using JASCO FTIR 610 spectrophotometer with a resolution of 4 cm^{-1} . TEM was performed using a JEOL 2000 FX microscope. Sample preparation for TEM experiment was carried out by dissolving the PC membrane containing gold-polyaniline composite in dichloromethane and solution was pipetted onto carbon-coated copper grids.

2.3. Results and Discussion

Fig. 2.2 shows the SEM image ($36 \mu\text{m} \times 27 \mu\text{m}$) of the porous polycarbonate membrane. The black spots in the image were the nanopores present in the PC membrane. Pores were distributed randomly throughout the membrane surface. Fig 2.3 shows the 3-dimensional AFM image of the track-etched PC membrane surface before the synthesis of the gold-polyaniline nanocomposite. The pores were randomly distributed on the membrane surface, as shown in Fig. 2.3.

As measured from the AFM image, the pore diameter ranged from 145 to 238 nm and an average diameter of pore was about 194 nm. The overlapping of boundaries of two or more pores was observed at some places on the surface of the PC membrane. A number of pores in the membrane were not normal to the membrane surface, but instead made an angle with respect to the surface plane.

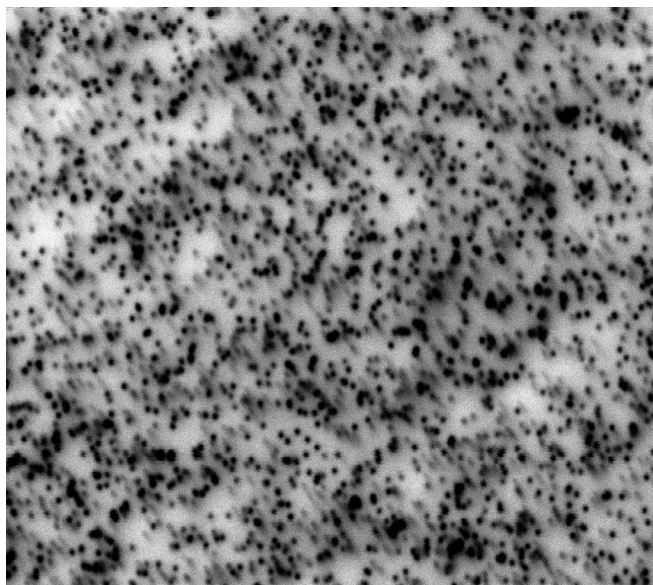


Fig. 2.2 SEM image of the porous polycarbonate membrane (36 μm X 27 μm)

Fig. 2.4 shows the photograph of gold-polyaniline composite loaded PC membrane. The dark-colored 10 mm diameter circle was the region where gold-polyaniline composite was immobilized into the thousands of nanopores in PC matrix.

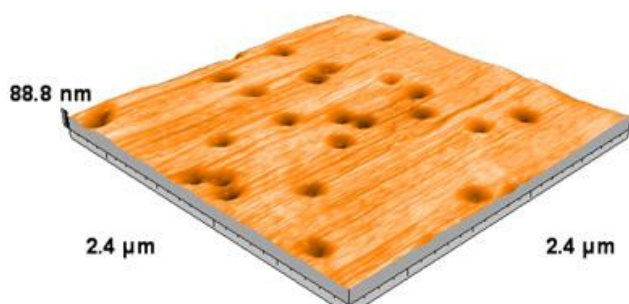


Figure 2.3: AFM image of the porous polycarbonate membrane

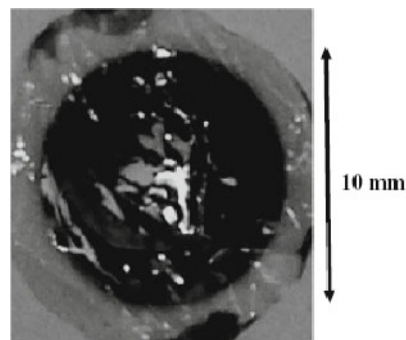


Figure 2.4: Photo of the PC membrane containing gold-polyaniline composite

The loading and reduction of AuCl_4^- by aniline in the pores of the 10 μm thick PC film was confirmed by EDXRF analyses. Significant difference in the concentration of Au was

observed on HAuCl_4 -exposed and aniline-exposed surfaces of the PC membrane. It is seen from Fig. 2.5 that the Au concentration was significantly higher on the side exposed to HAuCl_4 than the aniline-exposed side in PC membrane where redox reaction between aniline and HAuCl_4 was allowed overnight.

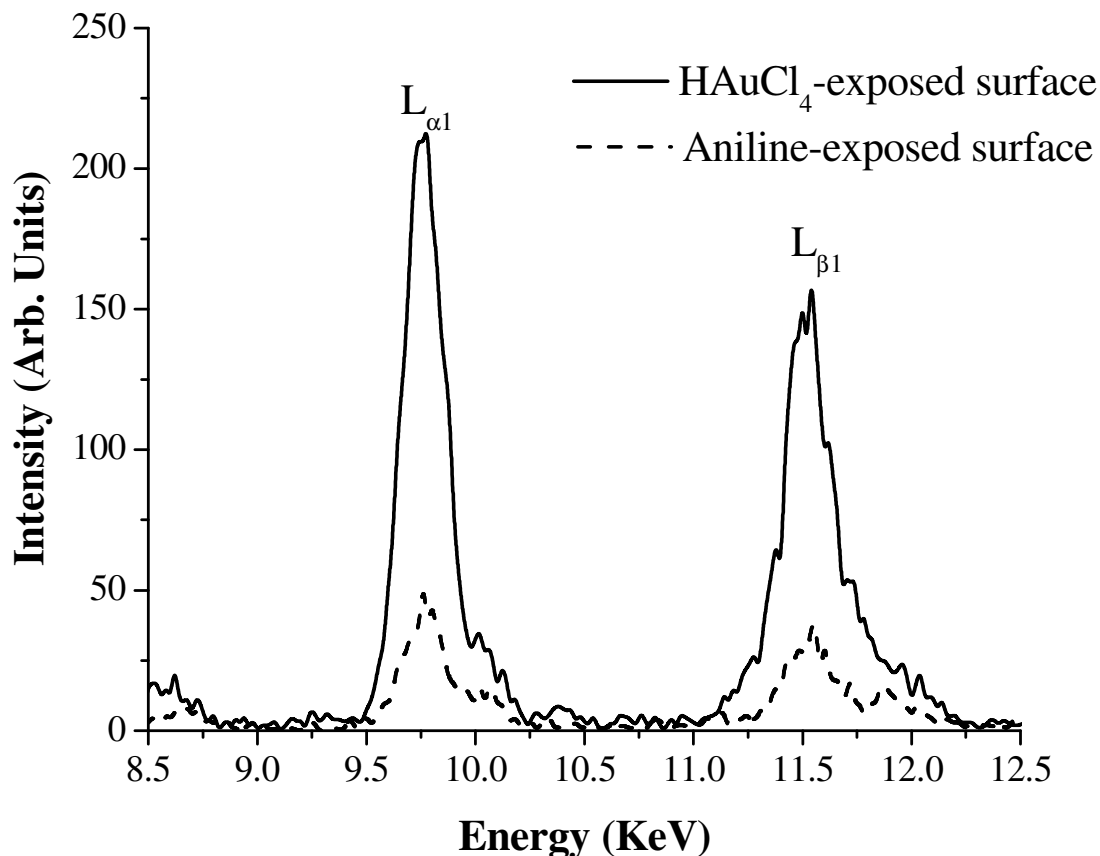


Figure 2.5: EDXRF spectra of PC membrane containing gold-polyaniline composite with preparation time of overnight

Fig 2.6 shows the EDXRF spectra of gold-polyaniline composite in PC membrane where redox reaction between aniline and HAuCl_4 was allowed for 2 and 4 hours. Similar difference in the concentration of Au was observed on HAuCl_4 -exposed and aniline-exposed surfaces of the PC membrane for time intervals of 4 and 8 hours. But for time interval of 2 hours, the concentration of Au was almost the same on HAuCl_4 -exposed and aniline-exposed surfaces of

the PC membrane. The presence of Au on both sides of the PC film suggested that the AuCl_4^- ions diffused throughout the length of the pores of PC membrane because of concentration gradient.

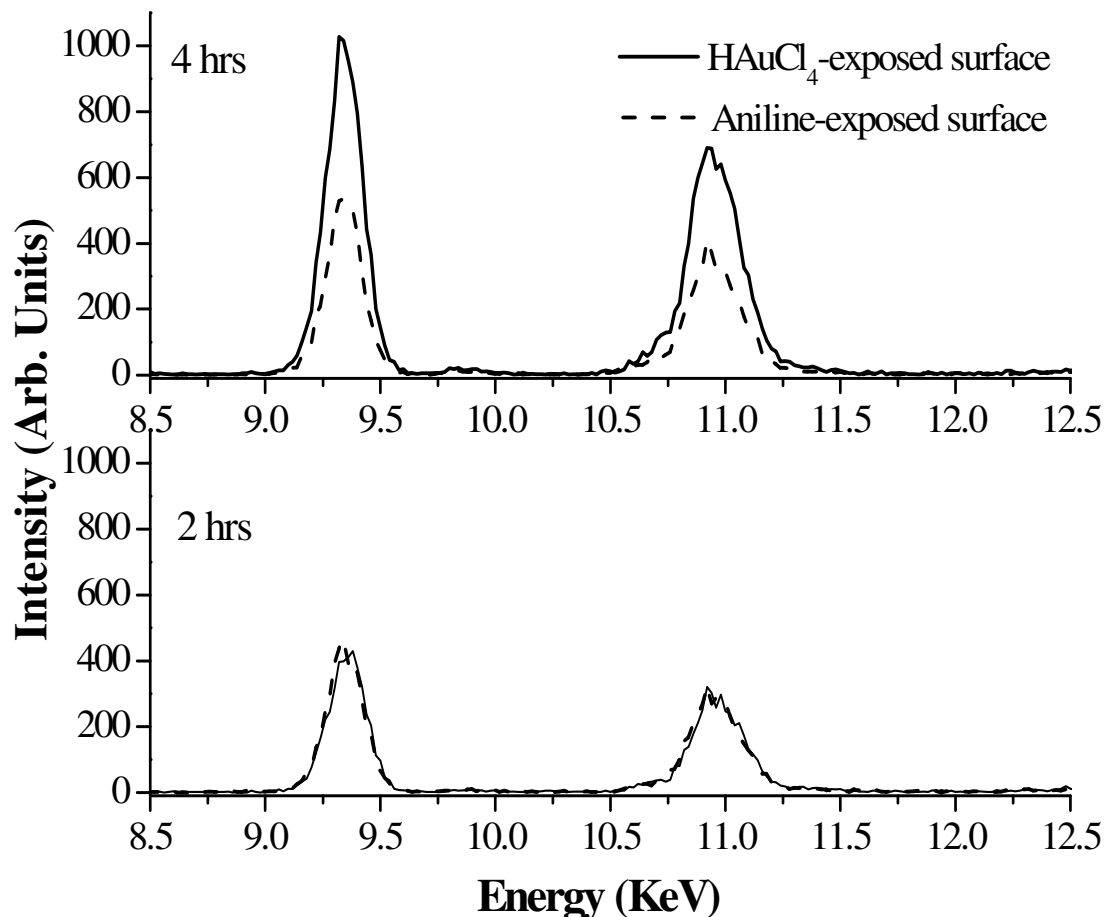


Figure 2.6: EDXRF spectra of PC membranes containing gold-polyaniline composite with preparation times of 2 and 4 hours

X-ray diffraction patterns of PC membrane and gold-polyaniline composites in PC membranes (with preparation times of 2, 4, 8 hours and overnight) were recorded. Fig. 2.7 shows the X-ray diffraction patterns of both the surfaces of Au-polyaniline embedded PC membrane where redox reaction between aniline and HAuCl_4 was allowed overnight. The XRD patterns showed broad peaks of the scattering angles (2θ) corresponding to the 111, 200, and 220 planes

of the face-centered cubic phase of Au. This indicated that Au particles formed in the membrane were nanocrystallites. Therefore, broadening of the diffraction peak width of the (111) Bragg reflection was analyzed to estimate the size of Au nanocrystallites embedded in the membrane using the Scherrer equation.

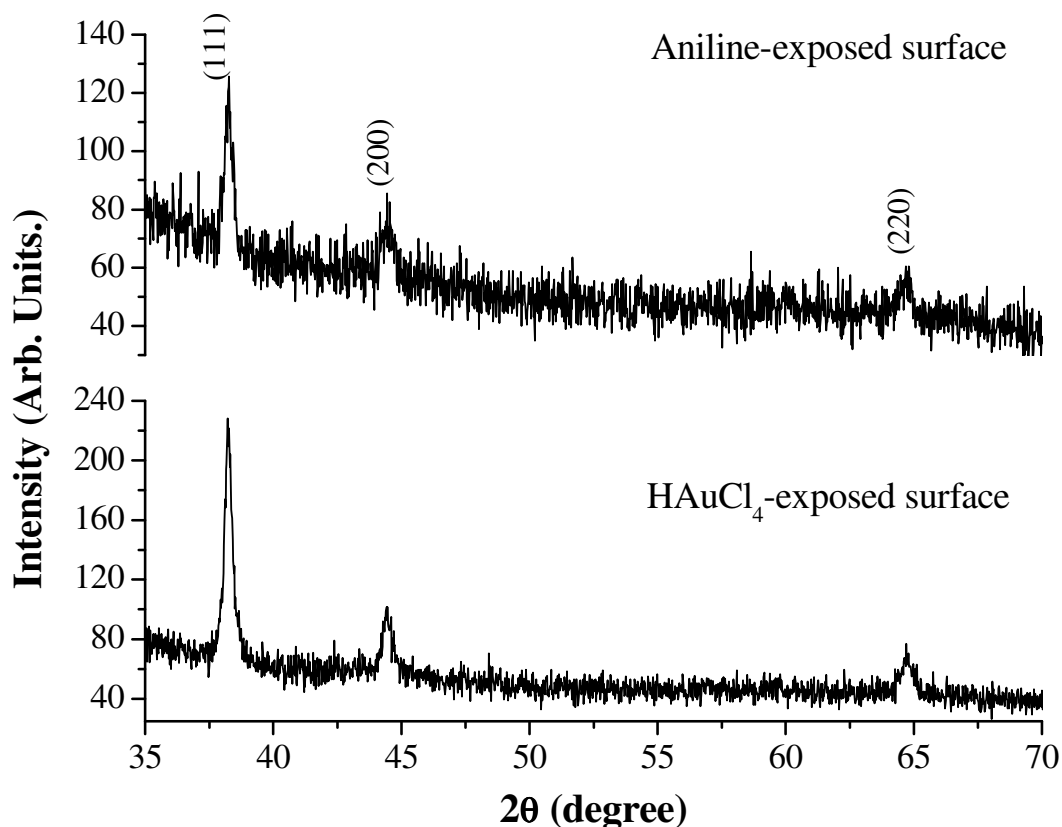


Figure 2.7: X-ray diffraction pattern of PC membrane containing gold-polyaniline composite with preparation time of overnight

Fig. 2.8 shows the XRD patterns of PC membrane and gold-polyaniline composites in PC membranes (with preparation times of 2, 4 hours and overnight). XRD pattern of the PC membrane showed a peak at 2θ of $\sim 17.3^\circ$. PC did not have any diffraction peak in the 2θ range where gold showed diffraction peaks. XRD patterns for gold-polyaniline composites in Fig. 2.8

showed broad peaks of the scattering angles (2θ) corresponding to the 111 and 200 planes of the face-centered cubic phase of Au.

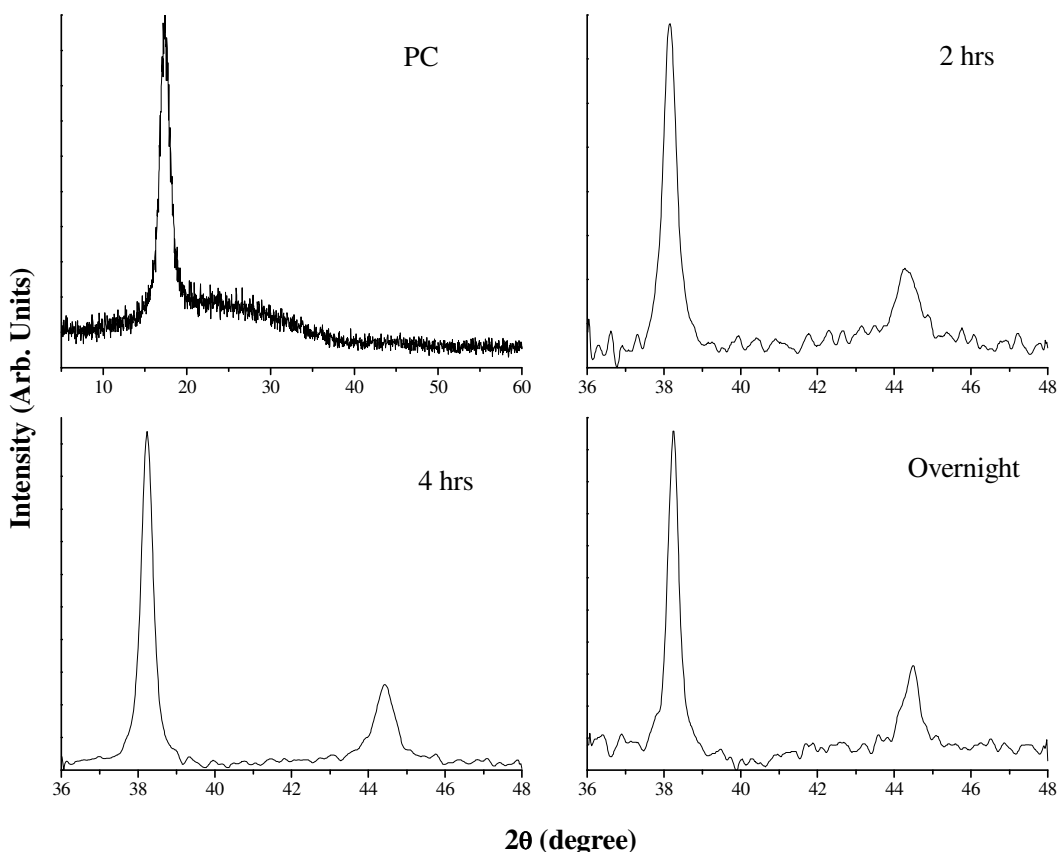


Figure 2.8: X-ray diffraction pattern of PC membrane and PC membranes containing gold-polyaniline composite with preparation times of 2, 4 hours and overnight

The average size of Au nanocrystallites in gold-polyaniline composites with different preparation times was calculated to be about 24 ± 3.4 nm. Intensities of the diffraction peaks were different at HAuCl_4 -exposed and aniline-exposed surfaces of the PC membrane. Intensity was higher on the surface exposed to HAuCl_4 than the aniline-exposed surface.

UV-Vis spectra of the gold-polyaniline composite in PC membranes were recorded in both the transmission and the reflectance mode. The UV-Vis spectrum in transmission mode (Fig. 2.9) showed characteristic absorption bands at 340 nm and 750 nm. A small shoulder at 430

nm was also observed resulting from polaron/bipolaron transition in polyaniline. The absorption band at 340 nm was due to the π - π^* transition of the benzenoid rings. The band at λ_{max} 750 nm was very broad and corresponded to the transition from a localized benzenoid HOMO to a quinoid LUMO, i.e., benzenoid to quinoid excitonic transition in polyaniline.

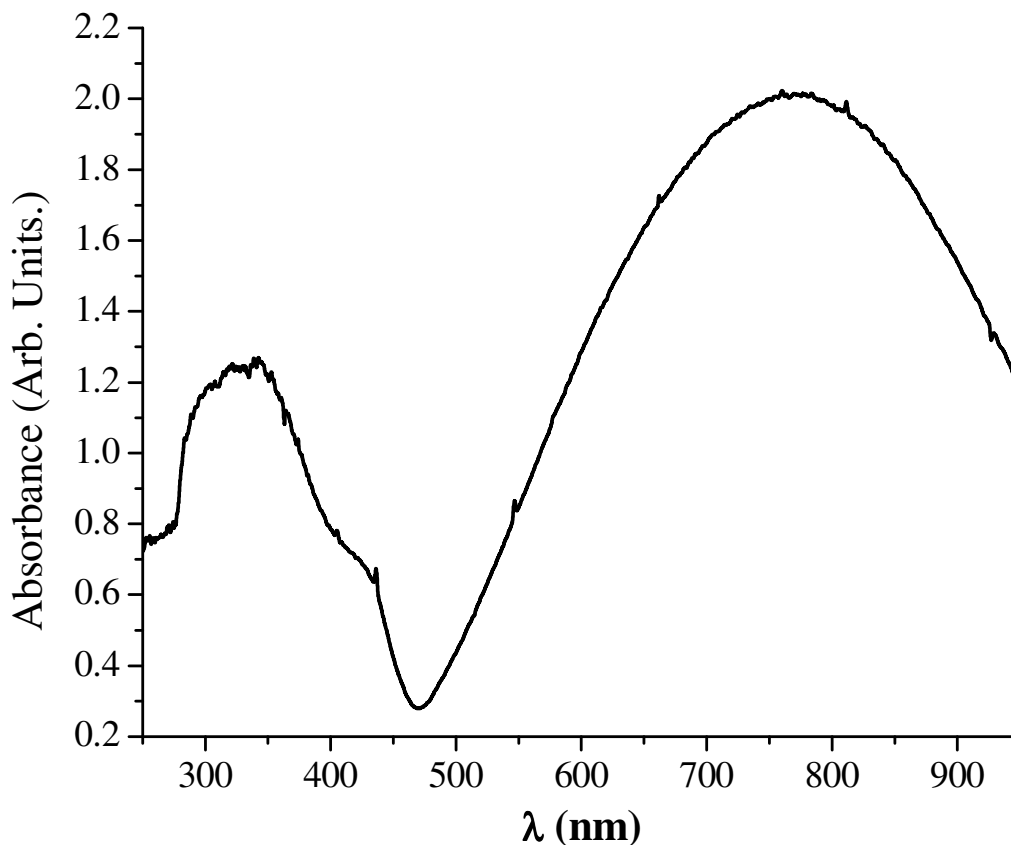


Figure 2.9: UV-Vis spectrum of PC membrane containing gold-polyaniline composite in transmission mode

The surface plasmon resonance (SPR) peak of gold nanoparticles was not observed in the transmission mode. In case of gold nanoparticles with spherical geometry, AuNPs show the maximum absorption at ~520 nm. Since it was a gold nanoparticle-polyaniline composite, the contribution of SPR of AuNPs at ~520 nm was superimposed by broad absorption band at λ_{max} ~750 nm.

The reflectance spectra were recorded on both the HAuCl_4 -exposed and the aniline-exposed surfaces, as shown in Fig. 2.10. The spectrum of HAuCl_4 -exposed surface showed a broad band with λ_{max} at 495 nm, which corresponded to λ_{max} of surface plasmon band of Au nanoparticles in gold-polyaniline composite in pores of PC membrane. It is well known that surface plasmon bands of metal nanoparticles are sensitive to their surrounding environment. The absorption peak and intensity can change drastically if the dielectric constant of the medium is changed. The spectrum of aniline-exposed surface showed a broad band with λ_{max} at 595 nm, which corresponded to benzenoid to quinoid excitonic transition. It was seen from the UV- Vis spectra that the surfaces of the PC membrane exposed to HAuCl_4 and aniline had significantly higher concentration of Au nanoparticles and polyaniline, respectively.

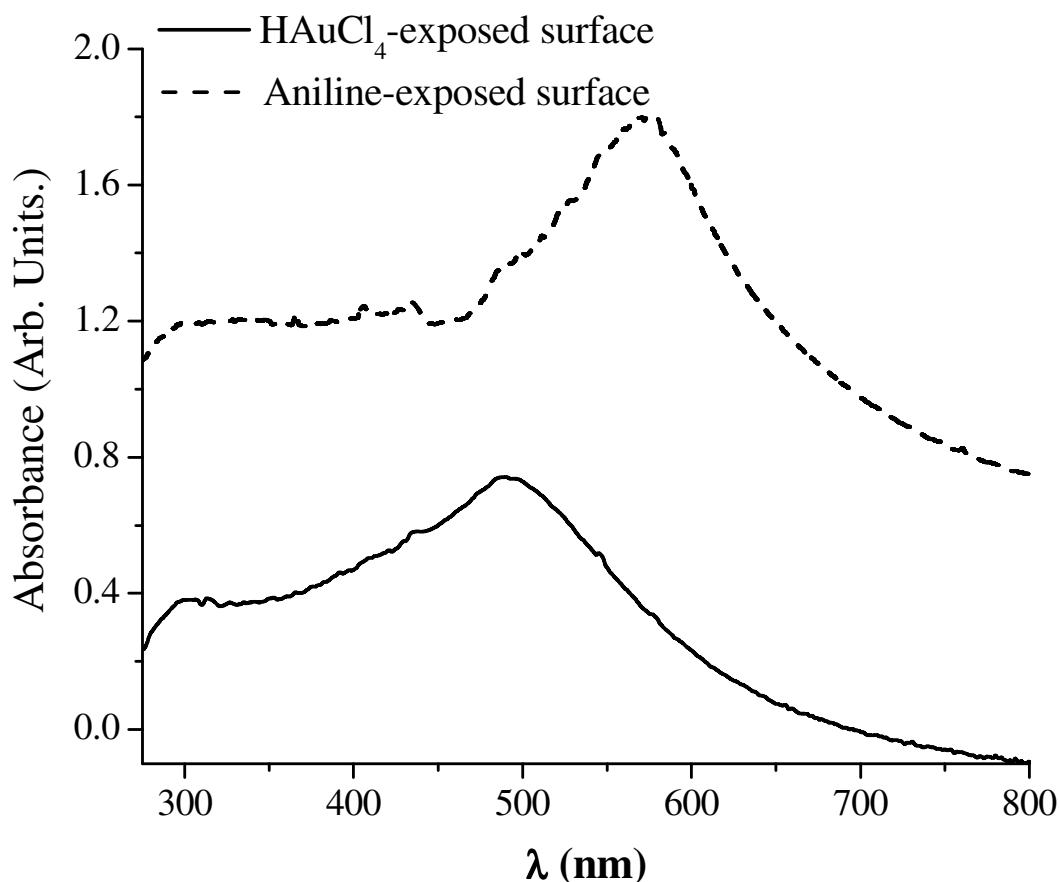


Figure 2.10: UV-Vis spectrum of PC membrane containing gold-polyaniline composite in reflectance mode

In the present experiment, UV-Vis measurements gave contribution both from polyaniline and surface plasmon band of gold nanoparticles (as shown in Fig. 2.9), it was difficult to interpret size of the gold nanoparticles. But from Fig. 2.10, it can be predicted that AuNPs were almost spherical and gold nanorods were not formed in the cylindrical pores of polycarbonate as there was only one peak at 495 nm. In case of gold nanoparticles with spherical geometry, the major axis and minor axis of the particles are same, and AuNPs show the maximum absorption at ~520 nm. When AuNPs deviate from spheroid and become elongated with increase in major axis, they show two plasmon absorption bands. One in the blue region near the original band position ~520 nm and other in the red region >600 nm.

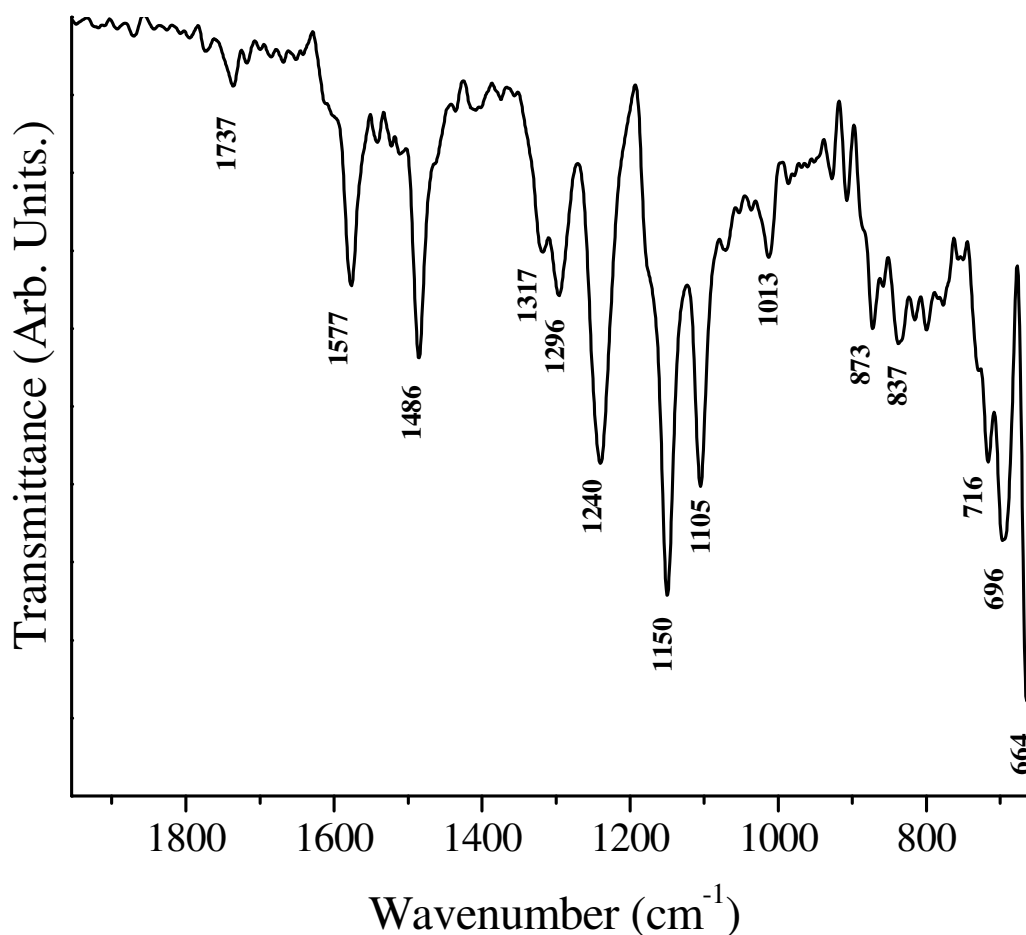


Figure 2.11: FTIR spectrum of PC membrane containing gold-polyaniline composite in ATR mode

Fig. 2.11 shows the FT-ATR-IR spectrum of the gold-polyaniline composite in the PC membrane. The peaks at 1577 cm^{-1} and 1486 cm^{-1} correspond to the stretching deformation of the $\text{N}=\text{Q}=\text{N}$ and $\text{N}-\text{B}-\text{N}$, respectively, where Q is quinoid and B is benzenoid ring. The bands at 1296 cm^{-1} and 1240 cm^{-1} correspond to the C-N stretching of the secondary aromatic amine and to the protonated C-N group, respectively.

Fig. 2.12 shows the TEM images of the gold-polyaniline composite prepared in the PC membrane and corresponding selected area electron diffraction (SAED) pattern.

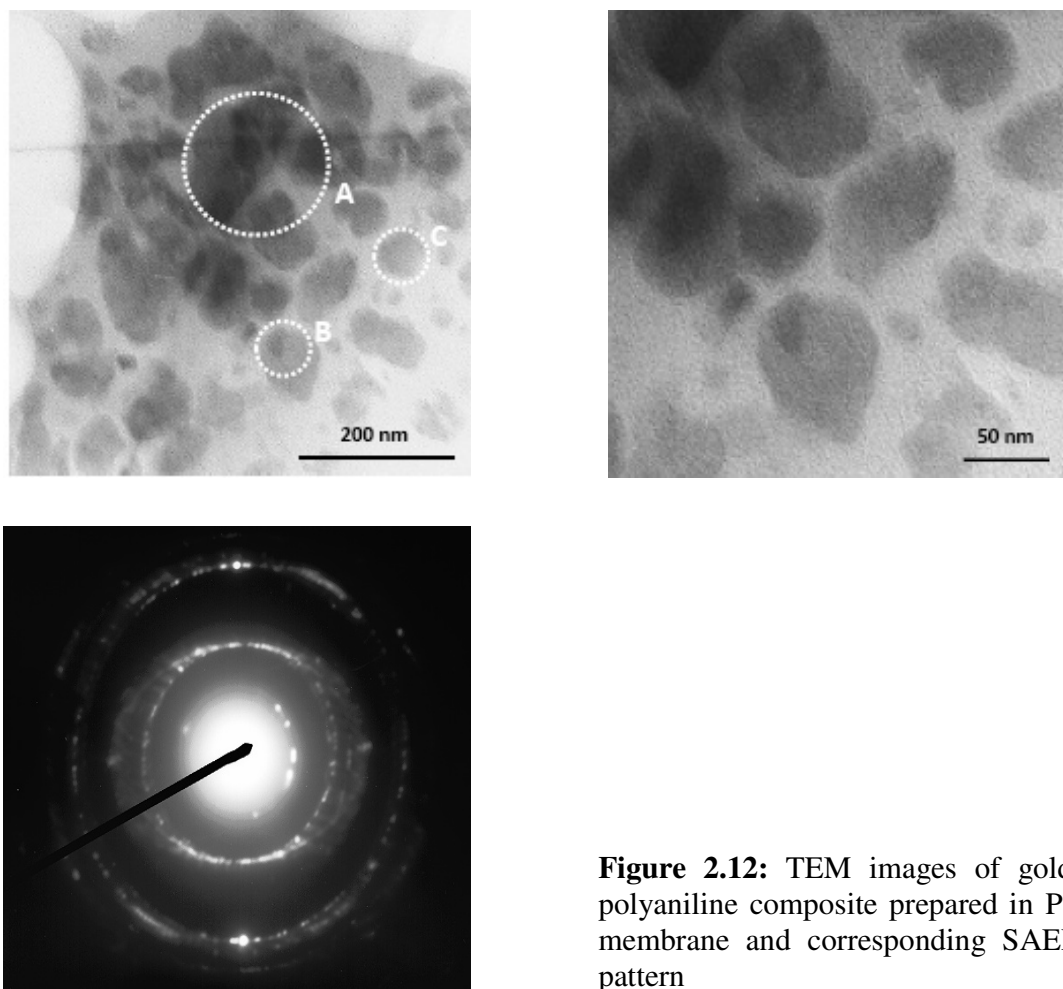


Figure 2.12: TEM images of gold-polyaniline composite prepared in PC membrane and corresponding SAED pattern

TEM images suggest that the clusters of polyaniline were formed and gold particles (size < 50 nm) were randomly dispersed in these polyaniline clusters. The three circles marked as A, B and C represent three different regions based on number density of gold particles in polyaniline clusters. The dark spots in region A have higher number density of gold particles compared to regions B and C. SAED pattern corresponded to a characteristic polycrystalline ring pattern for a face-centered-cubic structure.

2.4. Conclusion

In-situ one-step chemical synthesis of gold-polyaniline composite in nanopores of PC membrane was carried out. Nanopores in PC membrane acted as reaction vessels where aniline and HAuCl_4 were allowed to mix together, and the redox reaction between aniline and HAuCl_4 led to the formation of gold-polyaniline composite. TEM images suggested that the clusters of polyaniline were formed and gold particles were randomly encapsulated in these polyaniline clusters. Gold particles formed were nanocrystallites and average crystallite size was 24 ± 3.4 nm. EDXRF and other characterisation results showed that the surface of the PC membrane exposed to HAuCl_4 had significantly higher concentration of Au nanoparticles than aniline-exposed surface.

CHAPTER 3

Electrochemical Synthesis of Gold Nanorods in Track-Etched Polycarbonate Membrane using Removable Mercury Cathode

3.1. Introduction

Nanomaterials are of great interest to research community because of their unique chemical and physical properties that are distinct from the bulk [57-59]. Nanomaterials have found a wide range of applications in almost every discipline of science and technology. Nanomaterials are touching many aspects of human life in the form of advance materials for smart miniaturized devices, sensors, therapeutic agents etc. [60-62]. The properties of nanomaterials can be easily tuned by changing their shape and size [59, 63-66]. Therefore, the synthesis of shape and size controlled nanomaterials is still a subject of great interest to researchers [67]. Many template and non-template based methods for the synthesis of nanomaterials of various shapes and sizes are reported [68-73]. Aqueous colloidal suspension of gold nanorods was synthesized via an electrochemical method by introducing a shape-inducing reagent in solution [31]. Templates are more frequently used to tune the size and the shape of the nanomaterials. Porous anodized alumina and track-etched polycarbonate (PC) membranes are commercially available templates for chemical and electrochemical synthesis of one-dimensional (1D) nanomaterials - nanowires, nanorods and nanotubules of metals, semiconductors and conducting polymers [53, 54, 74]. Superior properties of 1D nanomaterial have been theoretically predicted and experimentally confirmed by the researchers.

The previously reported method of electrochemical template synthesis of nanowires, nanorods and nanotubules in template membrane involves an indispensable and inevitable step of coating an approximately 500 nm to 1 μm thick metallic layer onto one surface of the insulating membrane by sputter deposition technique. The schematic diagram in Fig. 3.1 shows the various experimental steps involved in the method. The coated metallic layer serves as a conducting substrate/cathode for the electrodeposition of metal nanowires within the pores of the membrane.

In some reports [75], sputter deposition was followed by the electrochemical deposition of metal to further increase the metallic layer thickness so that the coated metallic layer completely covers the pores that may not be blocked during sputter deposition method. The membrane is fixed on the conducting substrate (Au or Cu plate) with the cathodic metallic layer in contact with the substrate. The membrane fixed on the conducting substrate is mounted either as the working electrode in three-electrode electrochemical cell or as the cathode in two-electrode electrochemical cell.

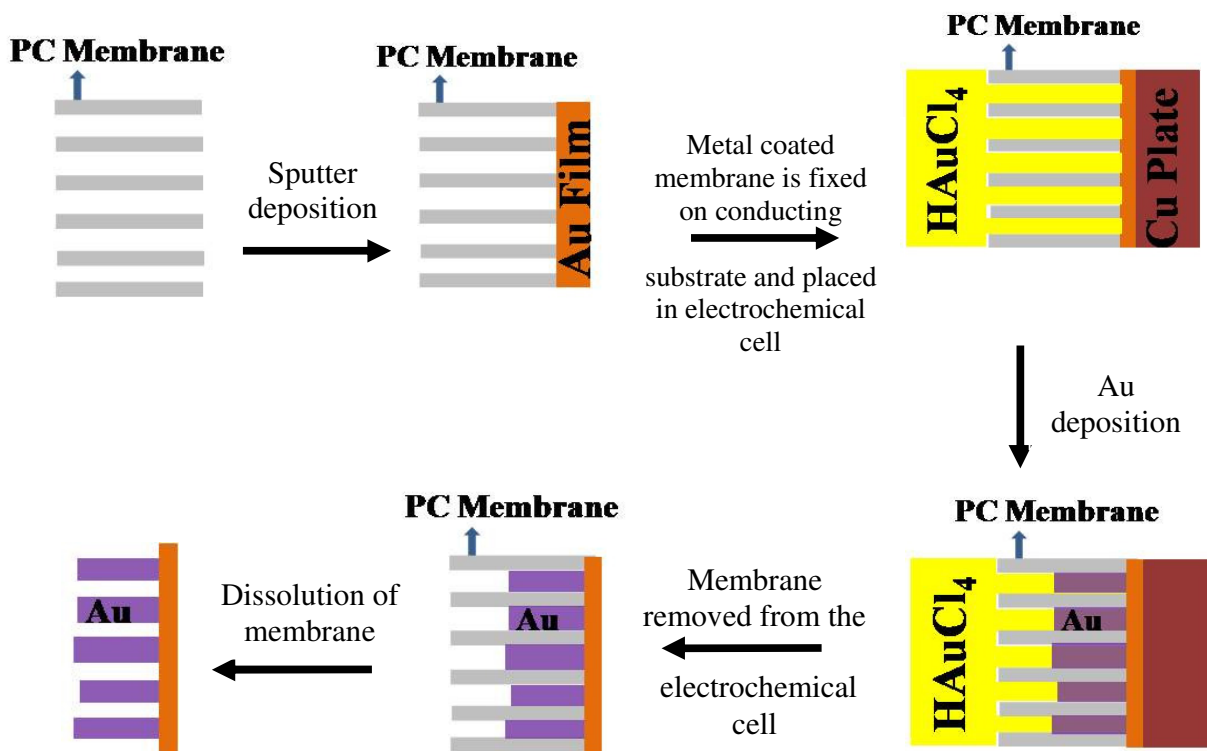


Figure 3.1: Schematic of electrochemical synthesis in insulating template membrane using sputter deposited metallic layer as cathode

The ensemble of the metal nanowires grown in the template membrane is attached to the coated metallic layer, and protrudes from its surface like the bristles of brush after the dissolution

of the template membrane. Therefore, the nanowires grown in the template membranes are not free-standing. The free-standing nanowire can be obtained by detaching it from the coated metal film. It is impossible to prepare a malleable track-etched membrane embedded with free-standing gold nanorods due to the sputter deposited metal coating on one surface. Sputter deposited metallic layer completely blocks the pores on one surface and the availability of unblocked pores on the other surface depends on electrodeposition time. If the deposition time is lesser than the time required for complete filling of pores, a large number of unblocked pores on one surface of the template membranes are available for encapsulation of the desired chemical or biochemical species by functionalizing the gold nanorods within the pores.

In this Chapter, the electrochemical synthesis of gold nanorods within the pores of track-etched PC membrane using a removable mercury cathode is discussed.

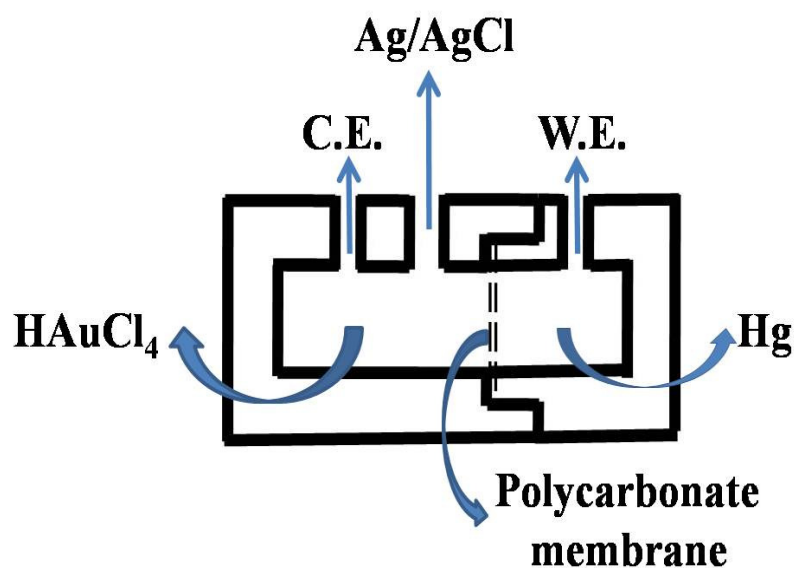


Figure 3.2: Schematic of the two-compartment electrochemical cell (W.E. – working electrode; C.E. – counter electrode)

This new approach eliminates the requirement of sputter deposition of a metallic layer coating onto one surface of the template membrane. A simple two-compartment electrochemical

cell was used and the track-etched polycarbonate membrane was placed between the two compartments separating the aqueous solution of HAuCl_4 from mercury, as shown in Fig. 3.2. Mercury, filled in one of the compartment, was in contact with one surface of the membrane (similar to sputter deposited metallic layer) and served as the conducting substrate/cathode for the electrochemical deposition of gold in the nanopores of track-etched PC membrane. Once the electrodeposition was completed, the mercury and the HAuCl_4 solution were removed from the compartments, and membrane was washed with ample amount of water. A malleable track-etched PC membrane embedded with free-standing gold nanorods was obtained. The ensemble of the metal nanowires grown in the template membrane was not attached to any conducting substrate, and gold nanorods could be easily freed from the template membrane after dissolution in dichloromethane.

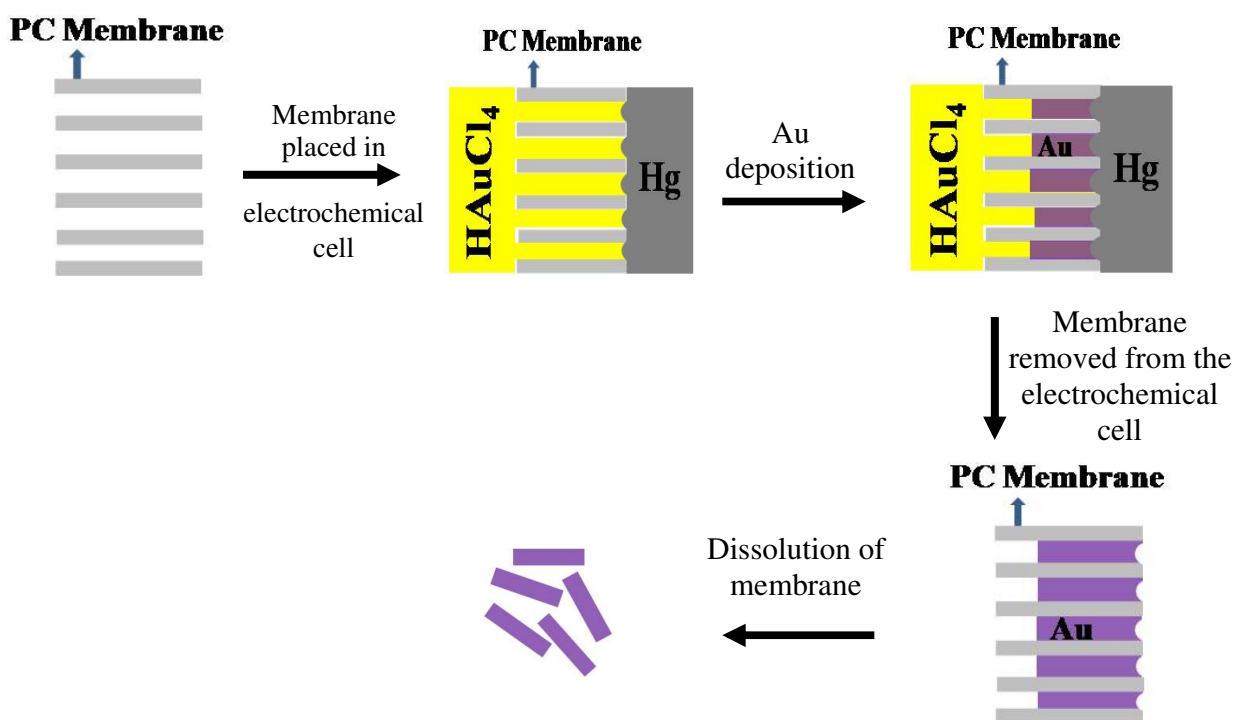


Figure 3.3: Schematic of electrochemical template synthesis in insulating template membrane using removable mercury cathode

The schematic diagram in Fig. 3.3 shows the various experimental steps involved in the method. The Au-deposited PC membrane and the gold nanorods obtained after the dissolution of PC membrane were characterized by EDXRF, XRD, UV-Visible spectroscopy, AFM and FEG-TEM. The TEM studies showed the formation of cigar-shaped gold nanorod in the pores of the PC membrane. If the deposition time is lesser than the time required for complete filling of pores, the gold nanorods embedded PC membrane has unblocked pores available onto both the surfaces (unlike the sputter deposited metal film coated template membrane). AFM studies showed that the PC membrane in which gold was deposited for short time had unblocked pores on the surface of both the sides of the membrane.

The new approach is simple, cost-effective and saves time. It can be used to prepare nanorods in other track-etched porous membranes without any change in the present experimental set-up. The internal architecture of the pores will be reflected in the shape of the electrodeposited nanorods. Therefore, the template porous membranes should have well-defined cylindrical pores to prepare good-quality nanorods within the membrane. The incomplete filled cylindrical pores with open mouth at the membrane surface can be used for encapsulation of desired chemical or biochemical species by functionalizing the gold nanorods within the pores and the functionalized track-etched PC membrane can be used to develop sensors based on the detection of analyte by Surface-Enhanced Raman Scattering (SERS) techniques [76]. These gold nanorods-containing track-etched membranes can also be used as smart surfaces/materials for catalytic and optical applications.

3.2. Experimental

All the reagents used were of analytical reagent (AR) grade. Nucleopore track-etched porous PC membrane with a pore diameter of 200 nm and thickness of 10 μm was obtained from

Whatman Ltd. Deionised water ($18 \text{ M}\Omega \text{ cm}^{-1}$) purified by the MilliQ water purifier system from Millipore was used throughout the present studies. The porous PC membrane (diameter = 2 cm) was sonicated in water for 5 min. It was placed in the two-compartment electrochemical cell. Mercury and aqueous solution of 10 mM HAuCl_4 were filled in two different compartments separated by the PC membrane. Mercury in contact with one side of the membrane served as the cathode. The electrochemical deposition of gold within the pores of the PC membrane was carried out by applying a constant cathodic potential of -0.2 V on mercury. The electrochemical deposition time (t_d) was 1000 s and 3000 s. Electrochemical experiments were performed using CHI 760D electrochemical workstation. The Ag/AgCl/3 M KCl aqueous and Pt wire were used as the reference electrode and the counter electrode, respectively. The membrane was then washed thoroughly in water and was allowed to dry in air. The deposition of gold in PC membrane was also carried out by galvanic reaction between HAuCl_4 and mercury for 1000 s in a similar two-compartment cell as discussed above, without applying the cathodic potential. Energy dispersive X-ray fluorescence (EDXRF) measurement of the membrane was carried out using Jordan Valley EX-3600 TEC EDXRF spectrometer having Rh target operated at a voltage of 40 kV and a current of 170 μA . Rh K_α was used as the excitation for L_α and L_β lines of gold. X-ray diffraction (XRD) patterns were recorded on a STOE XRD unit using Cu target ($\text{Cu } K_\alpha = 1.5406 \text{ \AA}$) with graphite monochromator. Absorbance spectra of the membrane were recorded in the transmittance mode using a UV–Vis spectrophotometer (QE65000, Ocean Optic Ltd.). The absorbance spectra were measured in air by placing the membrane in a quartz cell. For atomic force microscopy (AFM) studies of the PC membrane samples, tapping mode AFM measurements were performed in air at ambient temperature conditions using a Nanosurf easyScan 2 AFM (Nanosurf, Switzerland) with a 10 μm scanner head. The cantilevers used were

NCLR-10 (Nano World) with a resonance frequency of 190 kHz and force constant of 48 N m⁻¹. The scanned area was 2.4 μm × 2.4 μm. AFM data were analyzed using Nanosurf Report 4.1 software. FEG-TEM measurements were performed using a JEOL electron microscope (JEM 2100 F) operating at 200 kV. Sample preparation for TEM experiment was carried out by dissolving the Au-deposited PC membrane in dichloromethane and the solution was pipetted onto carbon-coated copper grids.

3.3. Results and Discussion

Atomic force microscopy (AFM) gives the surface morphology of the membrane with a nanometer or even atomic resolution by scanning the surface with a very sharp tip of atomic dimension. Fig. 3.4 shows the 3-dimensional AFM image of the track-etched PC membrane surface before the electrodeposition of gold. The pores were randomly distributed on the membrane surface, as shown in Fig. 3.4. As measured from the AFM image, the pore diameter ranged from 145 to 238 nm and an average diameter of pore was about 194 nm. The overlapping of boundaries of two or more pores was observed at some places on the surface of the PC membrane. A number of pores in membrane were not normal to the membrane surface, but instead made an angle with respect to the surface plane [69].

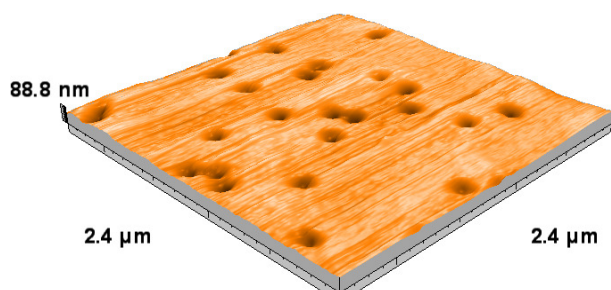


Figure 3.4: AFM images of the track-etched PC membrane surface before electrochemical deposition of gold

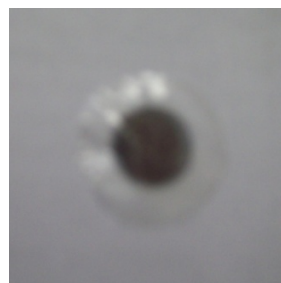


Figure 3.5: Gold-deposited track-etched PC membrane

The electrochemical deposition of gold within the pores of the PC membrane was carried out by applying a constant cathodic potential of -0.2 V on mercury. At -0.2 V, hydrogen evolution reaction (HER) was not observed at the mercury working electrode. There are many published literatures which describe the potentiostatic deposition/synthesis of gold nanostructures in the potential range of +0.5 to -0.5 V vs. Ag/AgCl/saturated KCl aqueous electrode [77, 29]. Fig. 3.5 shows the photograph of the track-etched PC membrane after electrochemical deposition of gold, and the dark colored circle of 1 cm diameter was the area in the PC membrane where gold was electrodeposited.

EDXRF analysis was carried out to confirm the electrochemical deposition of gold in the pores of the PC membrane.

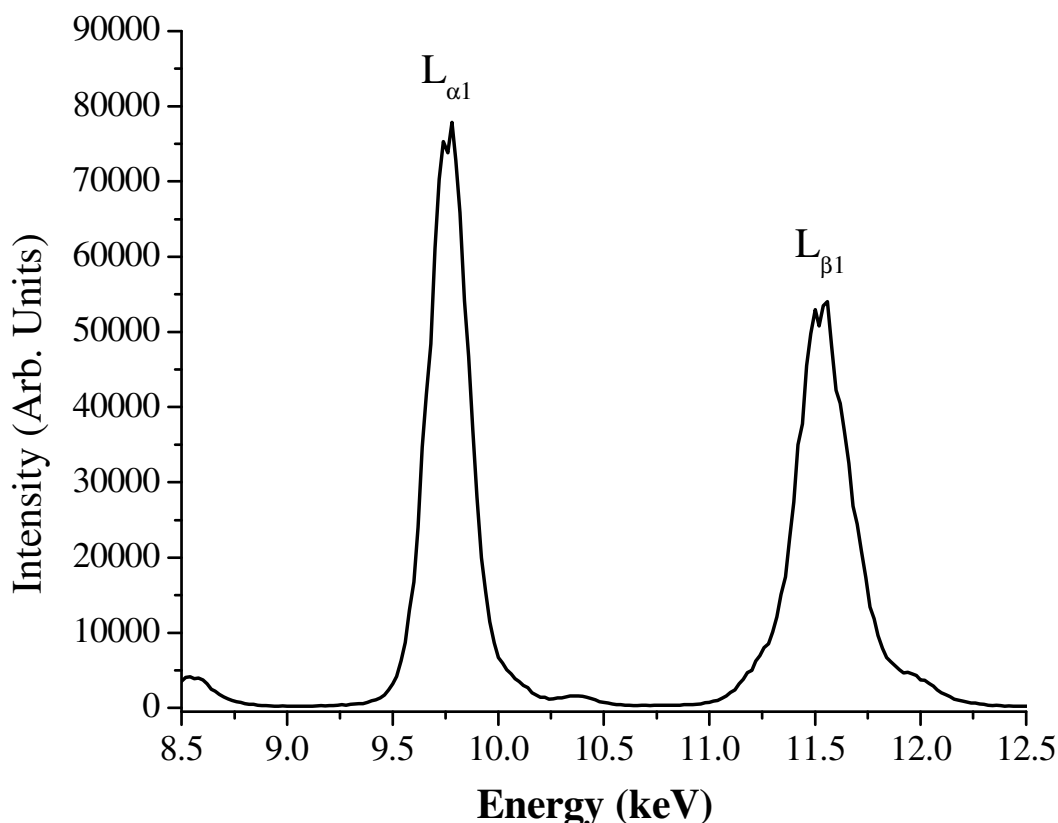


Figure 3.6: EDXRF spectrum of Au-deposited PC membrane prepared by electrochemical deposition

The EDXRF spectrum of the potentiostatically deposited gold in PC membrane (Fig. 3.6) showed the $L_{\alpha 1}$ and $L_{\beta 1}$ lines of the Au at 9.76 keV and 11.52 keV, respectively. The crystal structure of the electrochemically deposited gold in the pores of PC was investigated by XRD (Fig. 3.7). The broad peaks at the scattering angles (2θ) equal to 38.16° , 44.34° and 64.52° corresponded to the 111, 200 and 220 planes, respectively, of the face-centered cubic phase of Au. The broadened peaks indicated that Au particles deposited in the pores of PC membrane were nanocrystallites.

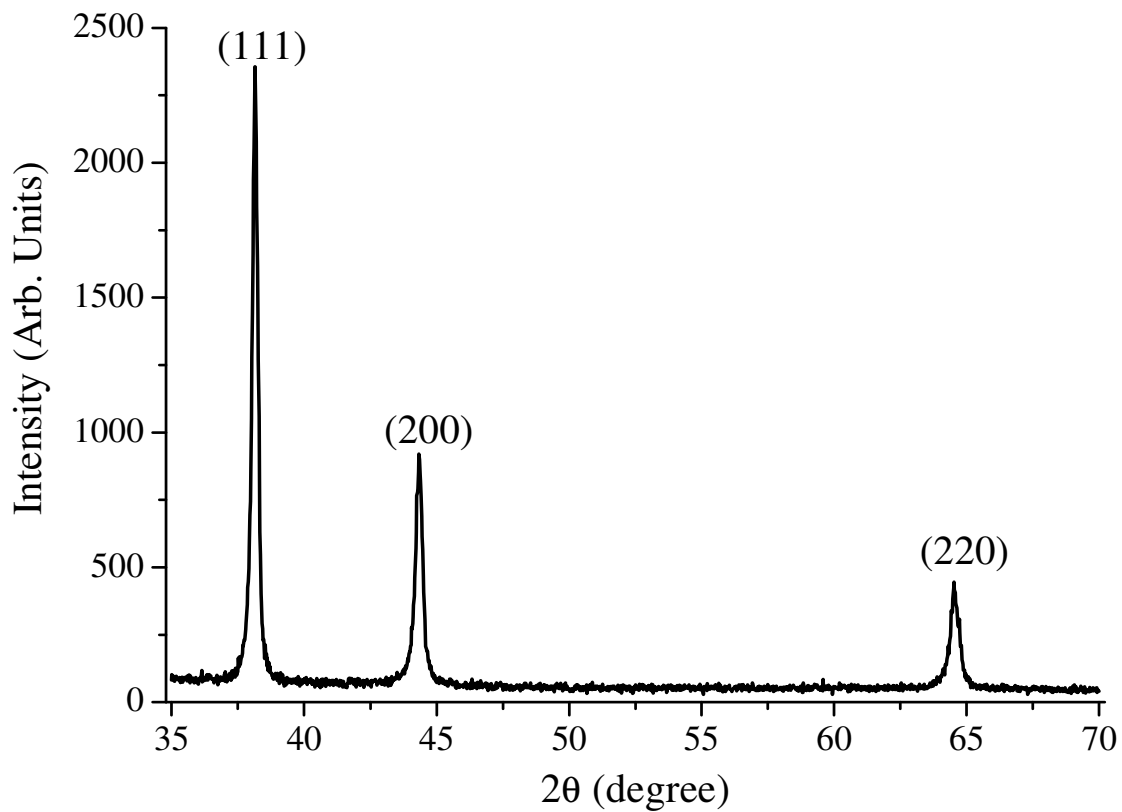


Figure 3.7: XRD pattern of Au-deposited PC membrane prepared by electrochemical deposition

Fig. 3.8 shows the visible absorbance spectrum of the PC membrane after electrochemical deposition of gold in its pores (for both $t_d = 1000$ s and $t_d = 3000$ s). A single red-shifted very broad peak was observed at around 636 nm. The nanostructured gold particles

absorb light in the visible and/or near-infrared region due to the surface plasmon resonance (SPR), and the position of the SPR band(s) depends on particle size, shape, dielectric constant of the local surrounding medium, inter-particle coupling etc. [78-81].

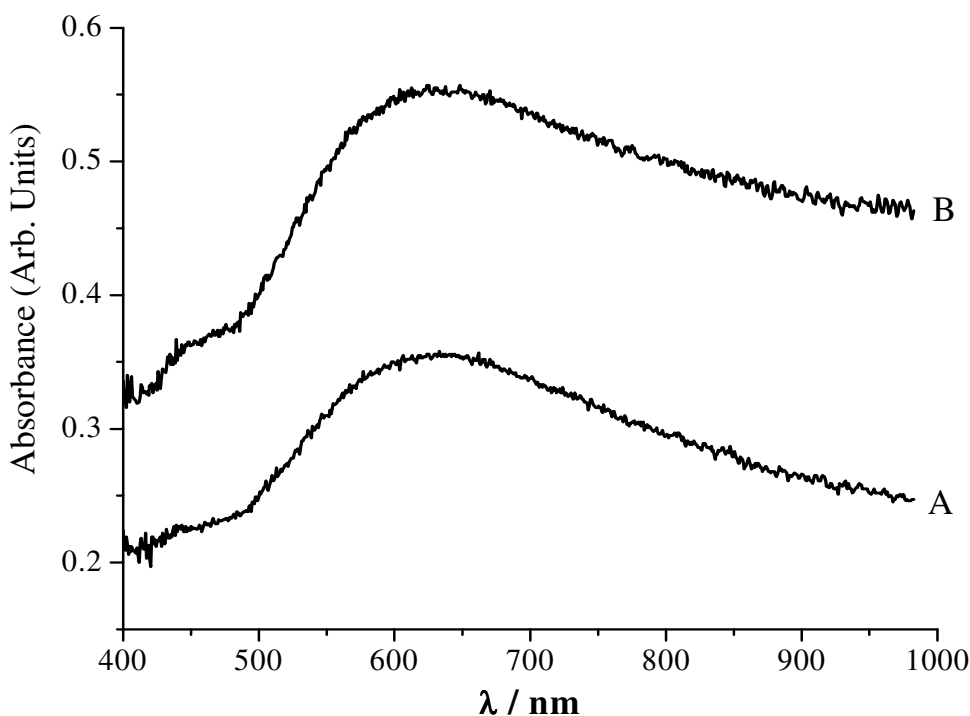


Figure 3.8: Visible absorbance spectrum of Au-deposited PC membrane prepared by electrochemical deposition (A, $t_d = 1000$ s & B, $t_d = 3000$ s)

As is evident from TEM images in Figs. 3.9a and 3.9b, the gold was electrodeposited as nanorods in the pores of the PC membrane. The nanorods were cigar-shaped and their surface was rough. The physical characteristic (diameter, length, surface roughness etc.) of the electrodeposited nanorods depends on the physical properties of the template membrane (pore radius, pore length, internal architecture of the pore etc.) as well as on the parameters used for the electrodeposition (electrodeposition time, electrode potential etc.). The length of the gold nanorods increased on increasing the deposition time (Figs. 3.9a and 3.9b).

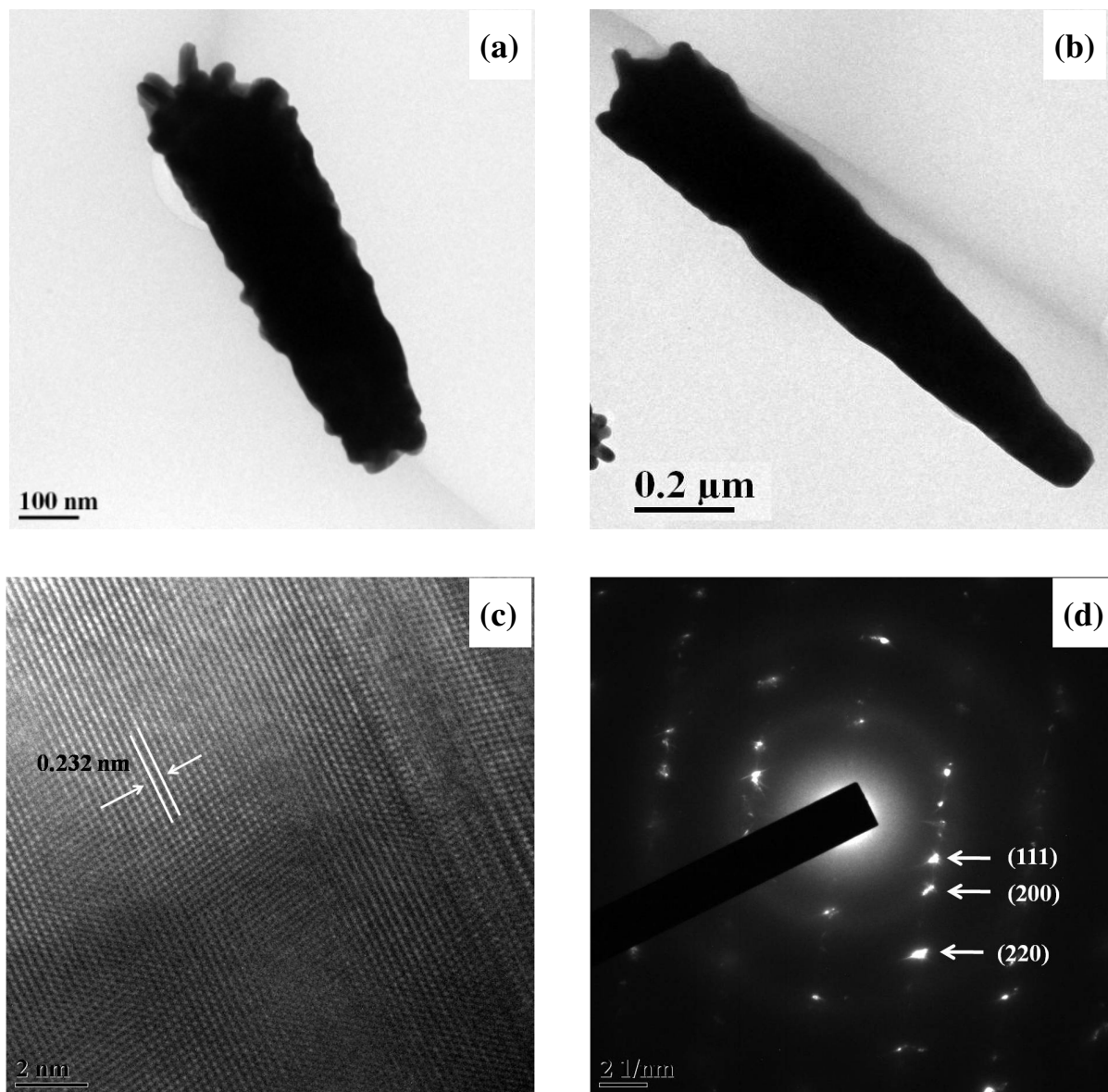


Figure 3.9: FEG-TEM images of the gold nanorods after dissolution of the PC membrane (a) $t_d = 1000$ s (b) $t_d = 3000$ s (c) 2 nm resolution image showing lattice distances (d) SAED pattern

Track-etched polycarbonate membranes are prepared by bombarding the polycarbonate sheets with high energy ions, nuclear particles etc. The latent tracks produced by these ions are subjected to chemical etching in alkaline solution to enlarge the pore size which can be tuned by controlling the process parameters. The damaged sites in polymeric chain are more reactive than

the undamaged sites in the latent tracks, therefore, the etching and the enlargement of the pores along the length of the latent tracks is non-uniform. This leads to the surface roughness of the pore wall and diameter of the circular cross-section is non-uniform along the length of the pore, more often the pores are cigar-shaped. Therefore, the metal nanorods or nanowires synthesized in such pore often have rough surface, which is the replica of the surface roughness of the pore wall. Prior to development of this newly reported approach, we used to synthesize the nanorods or nanowires of noble metals in track-etched polycarbonate membranes by coating one surface of the template membrane by metal film, and we observed the similar rough surface morphology. Therefore, the observed rough surface morphology of gold nanorods in our present work was the replica of surface roughness of the pore wall in PC membrane.

There are reports on modification of pores wall by molecular anchors to synthesize the nanorods with smooth surface [74]. In the TEM experiments, we observed that some of the gold nanorods were branched. The branching of nanorods corroborated the AFM observations that a number of pores were not perpendicular to the surface of membrane, but instead made an angle with respect to the surface plane, and the overlapping of two or more pores occurred in the membrane. Fig. 3.9c shows 2 nm resolution image with lattice distance of about 0.232 nm which is close to lattice distance (d_{hkl}) of (111) plane of face-centered cubic structure of gold. From the selected area electron diffraction (SAED) pattern (Fig. 3.9d), the diffraction spots were indexed to (111), (200) and (220) diffraction planes of the face-centered cubic structure of gold in agreement with the XRD pattern.

AFM analyses of the surface morphology of the PC membranes were done after the electrochemical deposition of gold in the pores of PC membranes. Figs. 3.10 and 3.11 show the

surface morphology of both the sides of the track-etched PC membrane after carrying out the electrodeposition of gold for 1000 s and 3000 s, respectively.

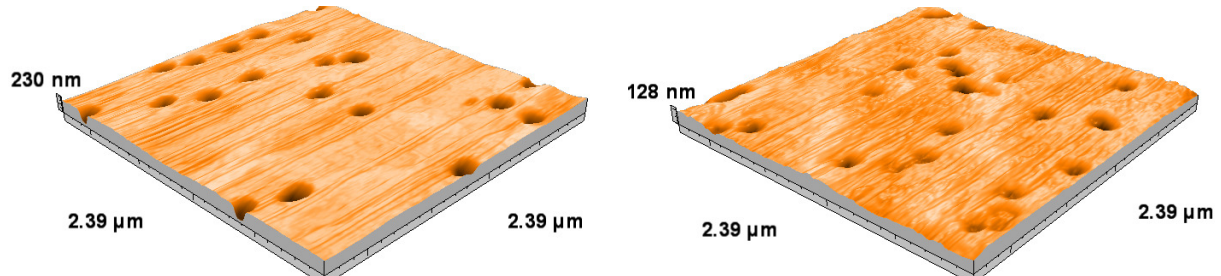


Figure 3.10: AFM images of both the surfaces of the track-etched PC membrane after electrochemical deposition of gold ($t_d = 1000$ s). Side 1: (a) and side 2: (b)

In Fig. 3.10, the randomly distributed pores were observed on both the sides of the membrane with almost the same number density. As evident from the Fig. 3.10, the pores in the PC membrane were not completely filled with the gold because the electrodeposition time of 1000 s might not be sufficient.

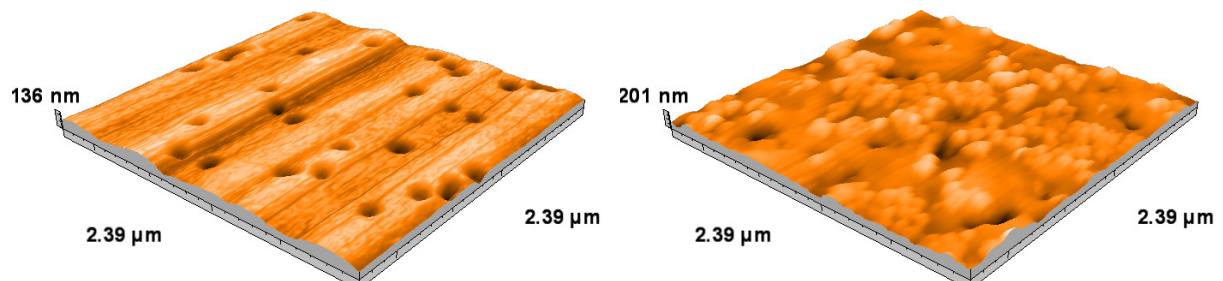


Figure 3.11: AFM images of both the surfaces of the track-etched PC membrane after electrochemical deposition of gold ($t_d = 3000$ s). Side 1: (a) and side 2: (b)

If the cathodic potential was applied for a longer time, the deposition of gold began on the surface of the PC membrane once the pores were completely filled. After increasing the electrodeposition time to 3000 s, the surface morphology of both the sides of the PC membrane was found to be completely different from each other, as shown in Fig. 3.11. The surface morphology of one side, Fig. 3.11a, was almost similar to those in Fig. 3.4 and Fig. 3.10. As

shown in Fig 3.11b, a very small number of pores were visible on the surface of the other side of the PC membrane due to the complete filling of a large number of pores by the gold and the gold deposits were also observed on the surface.

Fig. 3.12 shows a schematic diagram of the growth of gold nanorods in the PC membrane for shorter (a, b) and longer (c, d) deposition times to elucidate the AFM observations in Fig. 3.10 and Fig. 3.11.

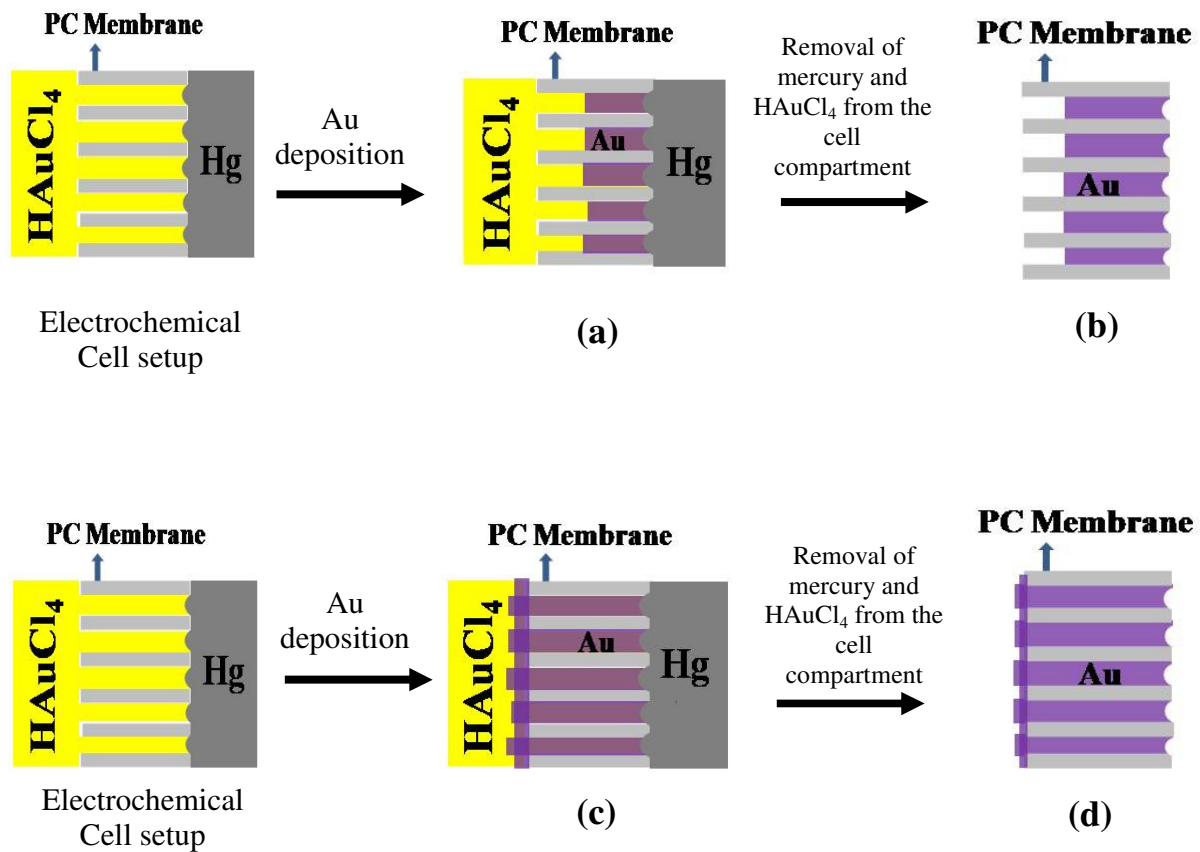
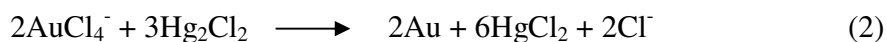


Figure 3.12: Schematic of the growth of gold nanorods in the PC membrane using the removable mercury cathode in two-compartment electrochemical cell for shorter deposition time, $t_d = 1000$ s, (a, b) and longer deposition time, $t_d = 3000$ s, (c, d). Gold-deposited membrane after removing the mercury and HAuCl_4 from the cell compartments and washing it with deionized water: (b, d)

In the absence of applied potential, the galvanic reaction occurred between AuCl_4^- ion and the elemental Hg, leading to the formation of metallic gold, mercurous chloride and mercuric chloride, as shown in the reactions below.



The EDXRF spectrum of the gold-deposited in PC membrane by the galvanic reaction (Fig. 3.13) showed the $L_{\alpha 1}$ and $L_{\beta 1}$ lines of Hg at 10.02 keV and 11.88 keV, respectively along with the $L_{\alpha 1}$ and $L_{\beta 1}$ lines of Au at 9.76 keV and 11.52 keV, respectively.

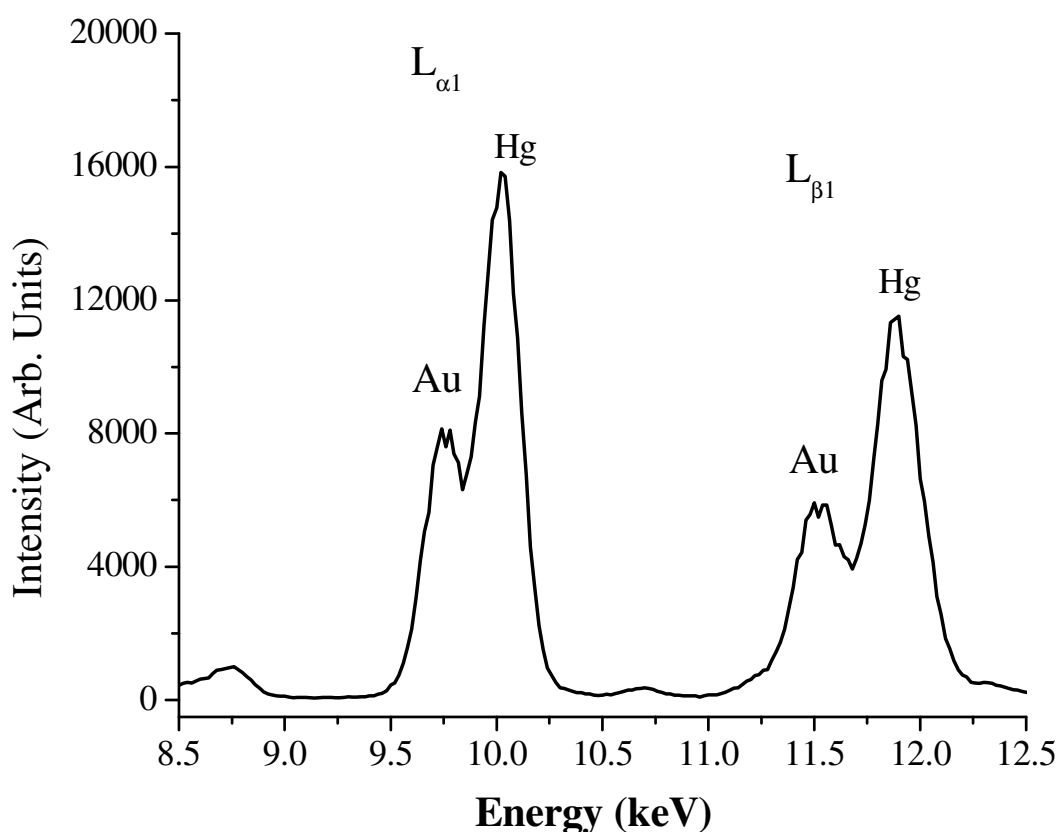


Figure 3.13: EDXRF spectrum of Au-deposited PC membrane prepared by galvanic reaction

There were no lines for Hg in the EDXRF spectrum of the potentiostatically deposited gold nanorods in PC membrane, thus ruling out the possible contamination of electrodeposited Au nanorods by Hg. These observations led to a conclusion that the spontaneous galvanic reaction between HAuCl_4 and Hg was forbidden on applying the cathodic potential on Hg. The visible absorbance spectrum of the gold-deposited in PC membrane by the galvanic reaction showed two peaks with maxima at 456 nm and 571 nm. The peak with maxima at 571 nm was attributed to SPR of gold nanoparticles.

3.4. Conclusion

The gold nanorods were electrochemically synthesized within the pores of the track-etched PC membrane by a simple and cost-effective novel approach based on use of mercury as removable cathode. The novelty of this new approach was that it did not require the coating of a metallic layer on one surface of the template membrane. A malleable track-etched PC membrane with free-standing cigar-shaped gold nanorods in its pore was prepared. The gold-deposited PC membrane having shorter deposition time showed open pores onto surface of both the sides. The gold-deposited PC membrane with longer deposition time showed blockage of pores on surface of one side and the open pores on surface of the other side.

CHAPTER 4

Investigations on Redox Behaviour of Pu(IV)/Pu(III) in H₂SO₄ on Pt Nanoparticles- Modified Glassy Carbon and Pt Electrodes

4.1. Introduction

Analytical chemistry of plutonium is well documented by Metz and Waterbury [82]. Plutonium can exist simultaneously in various ionic species in aqueous solutions—Pu(III), Pu(IV), Pu(V) and Pu(VI). The Pu(IV)/Pu(III) and Pu(VI)/Pu(V) couples both behave reversibly in non-complexing solutions. The electropositive potential of Pu(IV)/Pu(III) and Pu(VI)/Pu(V) redox couples in non-complexing medium, prevents their polarographic investigations at the dropping mercury electrode (DME) due to the oxidation of Hg. However, the complexation of the oxidized form with strong complexing agents like citrate and oxalate shifts the potential of these Pu couples towards the cathodic region, where DME can be used. Cook et al. investigated the reduction of the plutonyl (PuO_2^{2+}) ion in several complexing media with the best results in oxalate medium [83]. A single wave was obtained due to one-electron reduction of Pu(VI) to Pu(V) state. However, the height of this reduction wave was not linear to the plutonium concentration, and this non-linear dependence was attributed to the induced disproportionation of Pu(V) in oxalate solution. Therefore, Milner and Wood investigated the use of a citrate supporting electrolyte to shift the potential of Pu(IV)/Pu(III) couple into the working range of DME and developed a method for the determination of Pu in citrate medium by reducing Pu(IV) [84]. A preliminary report by Jestic et al. described the behaviour of plutonium carbonate complex at HMDE [85].

The use of mercury as a working electrode should be eliminated as far as possible because of its associated toxicity and difficulties encountered while handling radioactive samples inside fumehood and glove box. Solid electrodes are attractive compared to mercury in these circumstances. Harvey et al. used rotating platinum micro-electrode to determine the potential of the Pu(III)/Pu(IV) couple in 1 N sulphuric, hydrochloric and perchloric acids [86]. For a

particular electrode, repetition of the polarograms gave a successive decrease in wave height. This was attributed to the deposition of plutonium oxide on the electrode surface, and heating with aqua regia was found to be necessary to restore the electrode to its original conditions. Koyama studied the reduction of Pu(IV) at stationary Pt electrode in 1 M hydrochloric acid and 2 M nitric acid using square-wave polarography [87]. Yun et al. investigated the electrochemical behaviour of Pu(IV) in 1 to 7 M HNO₃ at platinum electrode [88]. The Pu(IV) complexes reduced quasi-reversibly to Pu(III) species. Plock investigated the determination of plutonium by the oxidation of Pu(III) to Pu(IV) at the glassy carbon electrode and found that Pu(III) can be determined in the concentration range of 0.224 mM to 4.48 mM [89]. Casadio et al. investigated the behaviour of Pu and Np in nitric acid solution at pyrolytic graphite working electrode by cyclic voltammetry (CV) [90]. The results showed that the simultaneous analytical detection of Pu(VI) and Np(VI) is possible using CV by ensuring that only the Pu(VI) is in solution. A number of publications describe the use of controlled-potential coulometry (CPC) on routine basis for precise and accurate determination of Pu [91-94]. The method is based on the fact that Pu(IV)/Pu(III) couple behaves reversibly under suitable electrolytic conditions and that current efficiency of 100% is attainable. Metal wire gauge Pt electrode and carbonaceous electrodes such as graphite [94], glassy carbon have been used as working electrodes for determination of Pu by CPC. Shults reviewed the application of CPC for the determination of plutonium [91]. Pu(VI) is only partially reduced to Pu(III) in HClO₄, HCl and HNO₃ supporting electrolyte solutions leading to inaccurate results when Pu(VI) is present in appreciable amounts. In H₂SO₄, Pu(VI) is quantitatively reduced to Pu(III) and, therefore, H₂SO₄ is commonly used as a supporting electrolyte for Pu determination by CPC.

In our laboratory, controlled potential coulometric determination of Pu is routinely carried out using Pt wire gauze electrode in 1 M H₂SO₄, involving Pu(IV)/Pu(III) redox couple. The sulphate ions are known to stabilize Pu(IV) more than Pu(III) because of the tendency of tetravalent Pu(IV) to form much stronger complexes with sulphate. Therefore, the reduction of Pu(IV) to Pu(III) in 1 M sulphuric acid medium is sluggish and more time consuming than the oxidation of Pu(III) to Pu(IV). The use of graphite working electrode for determination of Pu by CPC was reported from our laboratory [94]. A graphite electrode in the shape of a beaker showed satisfactory performance for the quantitative reduction of Pu(IV) to Pu(III) as well as quantitative oxidation of Pu(III) to Pu(IV), though the time required for the quantitative electrolysis was more with graphite electrode compared to that in the case of Pt electrode. Thus, it was of interest to explore the potential of other carbon-based electrode like glassy carbon (GC) to study the kinetics of Pu(IV) to Pu(III) reduction.

Nanoparticles are finding wide range of electrochemical applications because of their unique physical and chemical properties that are entirely different from the bulk. Nanoparticles of noble metals are utilized by electrochemists to modify the surface of the conventional electrodes to obtain better electrochemical responses [77, 95, 96] due to larger effective surface area, increased mass transport, and better electronic interaction between the analyte and electrode. All these advantages of nanoparticles coated electrodes lead to higher catalytic activity, better sensitivity and selectivity. Electrochemical deposition techniques are promising to synthesis and immobilize the metal nanoparticles onto the electrode surface with easy control of particle shape and size [77, 95]. The modification of conventional electrodes by noble metals' nanoparticles also allows to reduce loading of noble metals.

With an objective of studying the feasibility of nanoparticles deposited solid electrodes to improve the kinetics of electrochemical reduction and oxidation of Pu(IV)/Pu(III) couple in 1 M H₂SO₄, the surfaces of bare GC and Pt electrodes were modified by electrodepositing platinum nanoparticles (PtNPs). In this Chapter, the investigations carried out on the redox behaviour of Pu(IV)/Pu(III) couple in 1 M H₂SO₄ using PtNPs-coated GC and Pt electrodes by voltammetric and impedance techniques are discussed and the results are compared with the corresponding bulk electrodes.

Redox kinetics were observed to improve in both the oxidation and the reduction processes after electrodeposition of PtNPs in contrast to bare electrodes. However, significant improvement was seen for the reduction of Pu(IV) to Pu(III) in PtNPs coated GC electrode compared to bare GC electrode. These studies are of great relevance to develop electroanalytical methodologies for Pu determination using nanoparticles modified electrodes.

4.2. Experiment

Platinum nanoparticles were prepared by potentiostatic method on Pt and GC electrodes in a standard three-electrode cell with CHI 440A potentiostat. Platinum wire and Ag/AgCl/3M KCl were used as counter electrode and reference electrodes, respectively, at room temperature. In a typical procedure, platinum nanoparticles were electrodeposited from 10 mM K₂PtCl₄ in 0.1 M H₂SO₄ at -0.2 V for 10 s. The platinum nanoparticles coated on glassy carbon electrode were characterized by scanning electron microscopy (SEM). Impedance responses were obtained under dc bias with signal amplitude of 10 mV in the frequency range of 200 kHz to 0.05 Hz, using Autolab FRA 2. The different oxidation states of plutonium in the solution were converted into Pu(IV) by controlled potential coulometry.

4.3. Results and Discussion

Fig. 4.1 presents a typical reversible hydrogen adsorption-desorption voltammogram curve for bare Pt and PtNPs coated Pt electrodes to obtain qualitative information of the nature and density of the surface sites on Pt surface [97, 98].

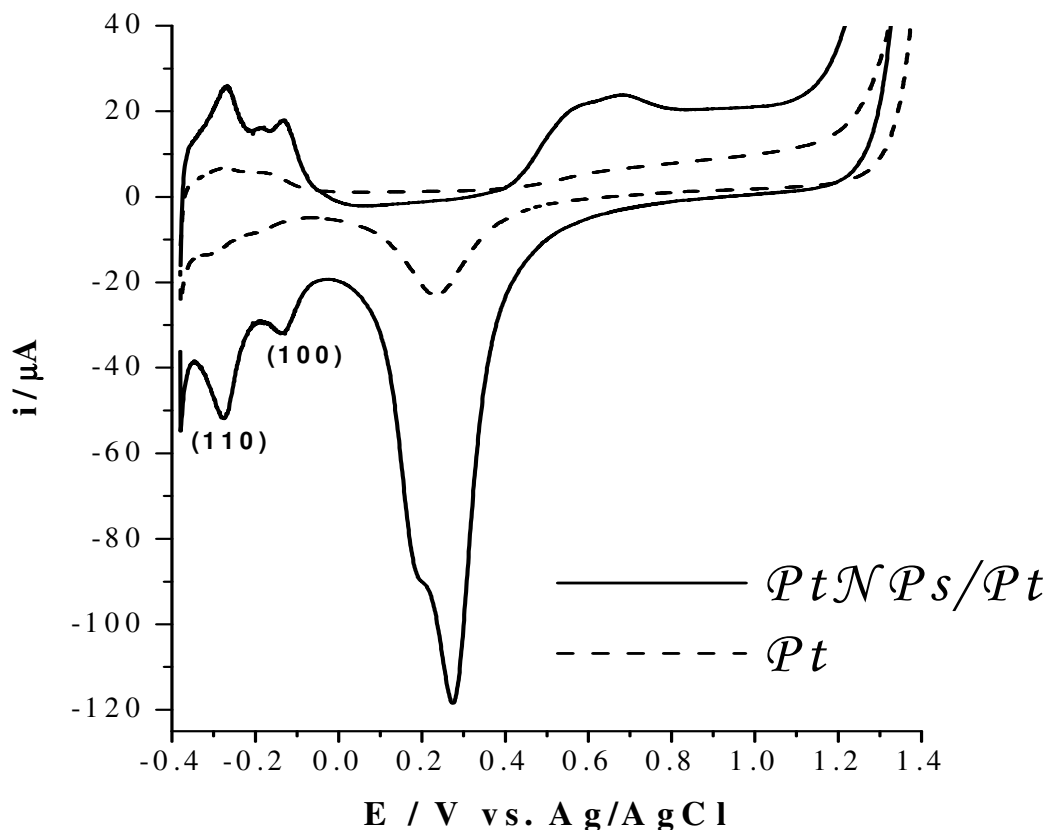


Figure 4.1: Cyclic voltammograms obtained at a scan rate of 100 mV/s in 0.5 M H_2SO_4 for bare Pt and PtNPs coated Pt (PtNPs/Pt) electrodes

The voltammogram showed clearly the presence of adsorption states associated with (110) and (100) sites at -0.28 V and -0.13 V vs. Ag/AgCl electrode, respectively. The electrochemically active surface area of the Pt and PtNPs/Pt were compared from the amount of charged passed for the anodic desorption of the adsorbed hydrogen. The results showed that the electrochemically active surface area of PtNPs/Pt was higher than that of the bare Pt. The double

layer capacitance, measured using CV, was about 10 times higher on PtNPs/Pt than on bare Pt, which corroborated the results of hydrogen adsorption-desorption studies that showed increased active surface area in the case of PtNPs/Pt.

Fig. 4.2 shows the voltammetric behavior of Pt (curve a) and PtNPs/Pt (curve b) electrodes in 0.84 mM Pu(IV) + 1 M H₂SO₄ at 20 mVs⁻¹ scan rate. The bare Pt electrode showed a pair of reduction and oxidation peaks with separation in peak potentials (ΔE_p) of 157 mV. On PtNPs/Pt electrode, the reduction and oxidation peaks were very well defined and ΔE_p was reduced to 79 mV, clearly showing the improved redox kinetics of Pu(IV)/Pu(III) couple on PtNPs/Pt electrode.

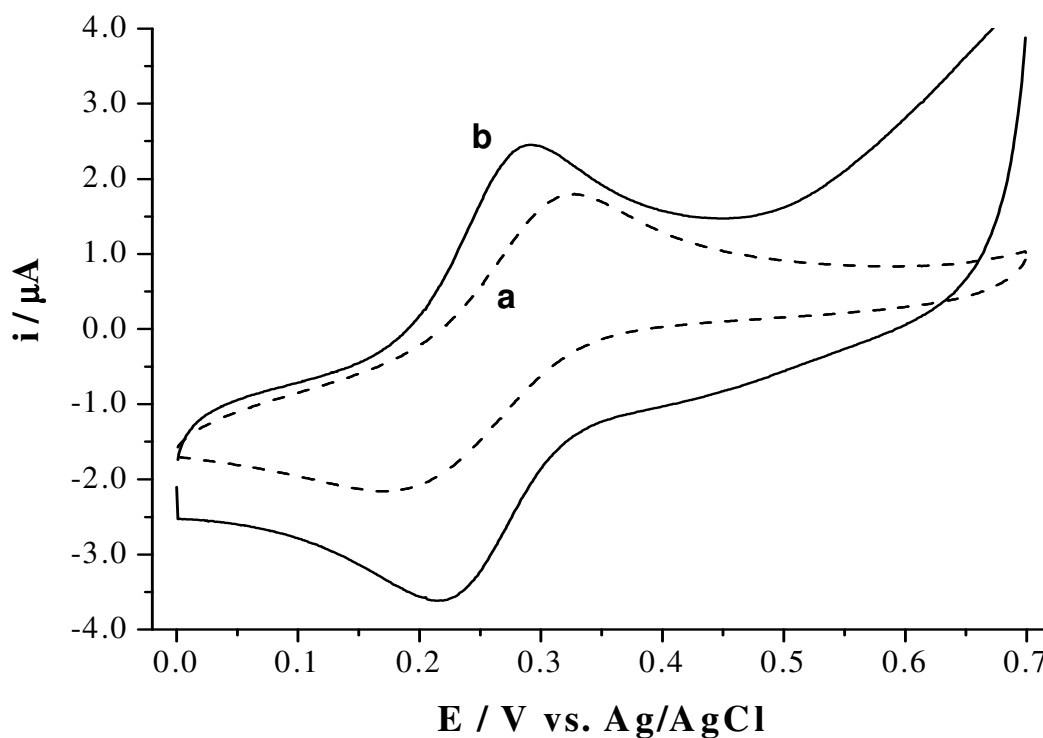


Figure 4.2: Cyclic voltammograms of 0.84 mM Pu(IV) in 1 M H₂SO₄ on (a) Pt and (b) PtNPs/Pt (The potential scanning rate was 20 mV/s)

Differential pulse voltammograms of bare Pt (curve a) and PtNPs/Pt (curve b) electrodes in 0.84 mM Pu(IV) + 1 M H₂SO₄ are shown in Fig. 4.3.

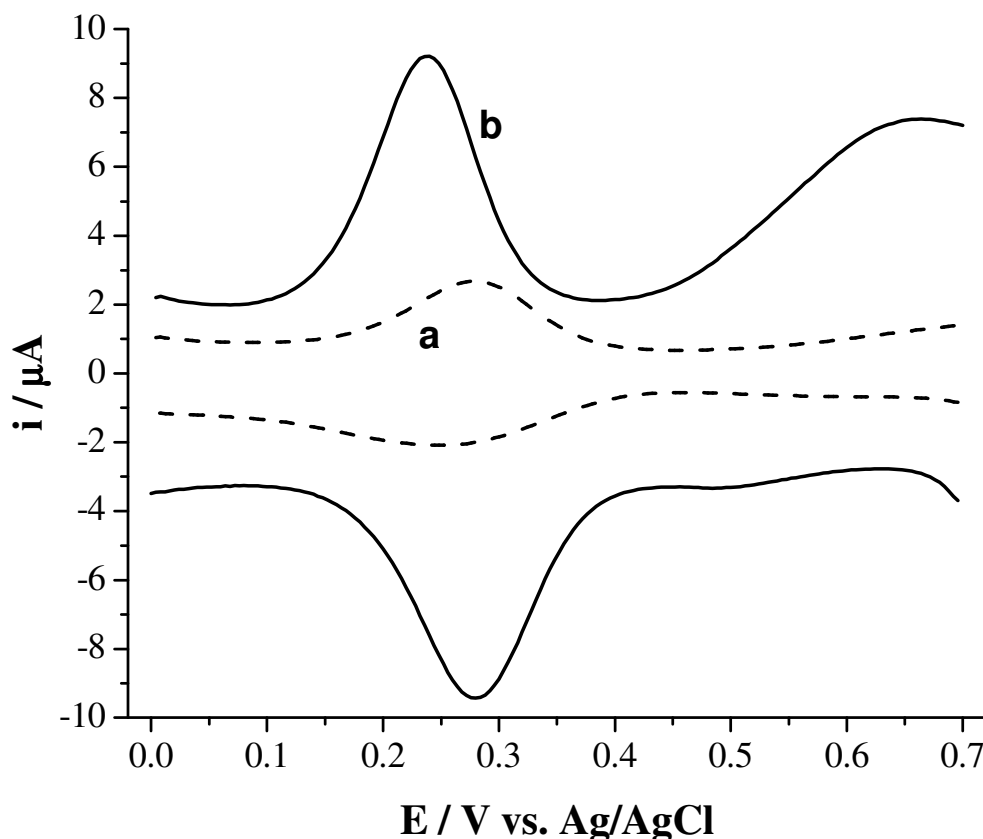


Figure 4.3: DPV of 0.84 mM Pu(IV) in 1 M H₂SO₄ on (a) Pt and (b) PtNPs/Pt

On PtNPs/Pt electrode, the current values corresponding to Pu(IV) reduction and Pu(III) oxidation increased by 5 fold and 4 fold, respectively. The Pu(IV) reduction and Pu(III) oxidation waves were well defined in the case of PtNPs/Pt than the bare Pt electrode. The CV and DPV studies showed that the modification of bare Pt surface with PtNPs results in a better redox behaviour of Pu(IV)/Pu(III) couple.

Figs. 4.4 and 4.5 show the cyclic voltammograms in 0.34 mM Pu(IV) + 1 M H₂SO₄ at various scan rates using Pt and PtNPs/Pt electrodes, respectively. The bare Pt electrode exhibited a larger separation in ΔE_p on increasing the scan rate compared to PtNPs/Pt electrode. These results also corroborated the CV and DPV observations that the Pu(IV)/Pu(III) redox couple in 1 M H₂SO₄ on PtNPs/Pt electrode showed much greater reversibility than the Pt electrode.

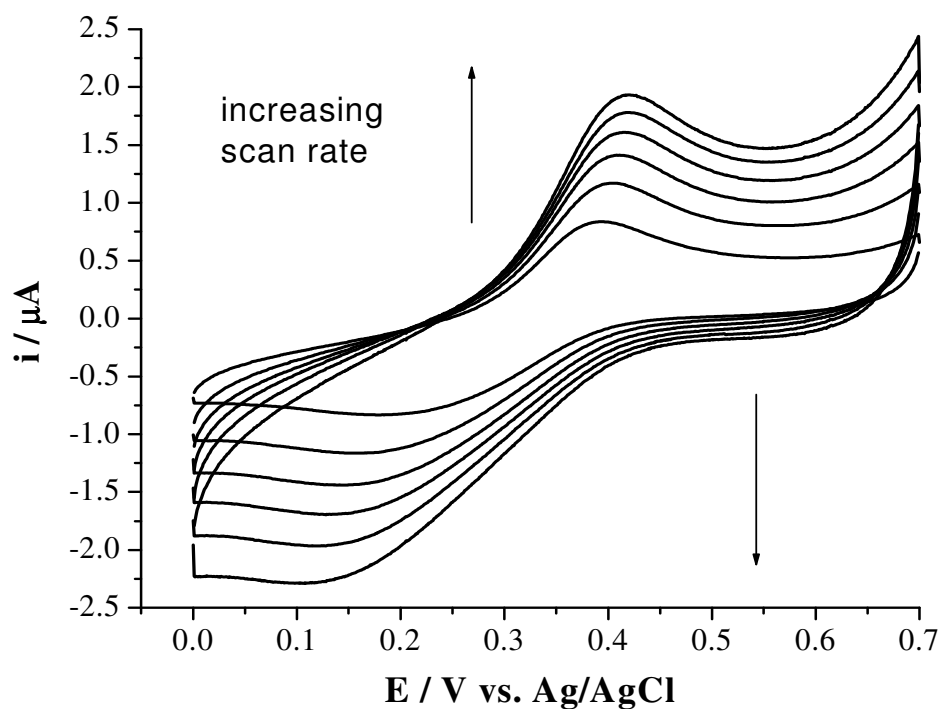


Figure 4.4: Cyclic voltammograms of 0.34 mM Pu(IV) in 1 m H₂SO₄ on Pt electrode at scan rate from 20 to 120 mV/s in intervals of 20 mV/s

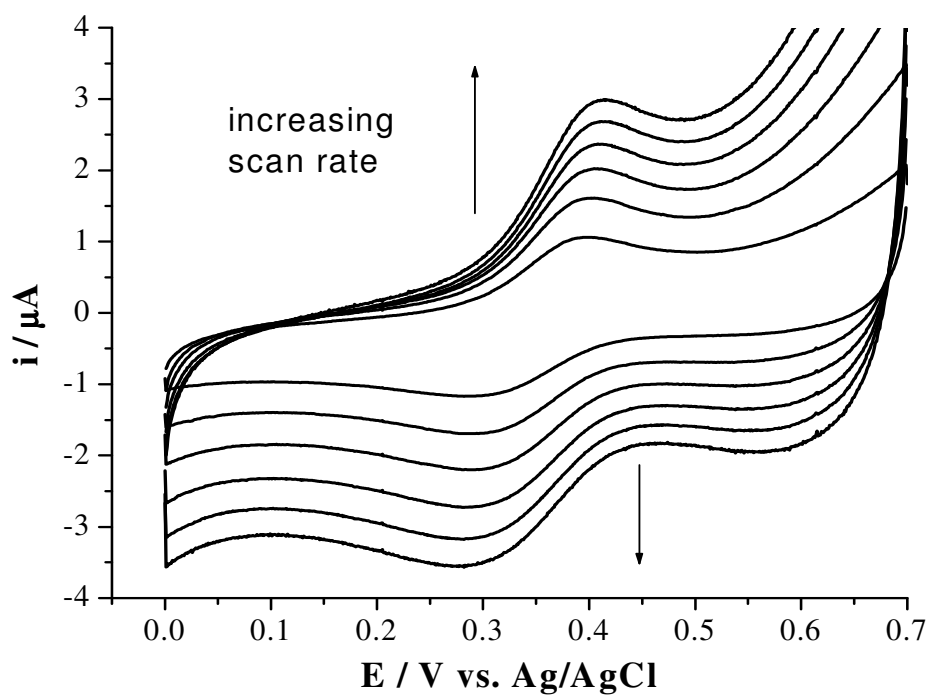


Figure 4.5: Cyclic voltammograms of 0.34 mM Pu(IV) in 1 m H₂SO₄ on PtNPs/Pt electrode at scan rate from 20 to 120 mV/s in intervals of 20 mV/s

Fig. 4.6 shows that redox process was diffusion controlled for both Pt and PtNPs/Pt electrodes, but the slope of peak current (I_p) vs. square root of scan rate for PtNPs/Pt electrode was higher than that with bare Pt.

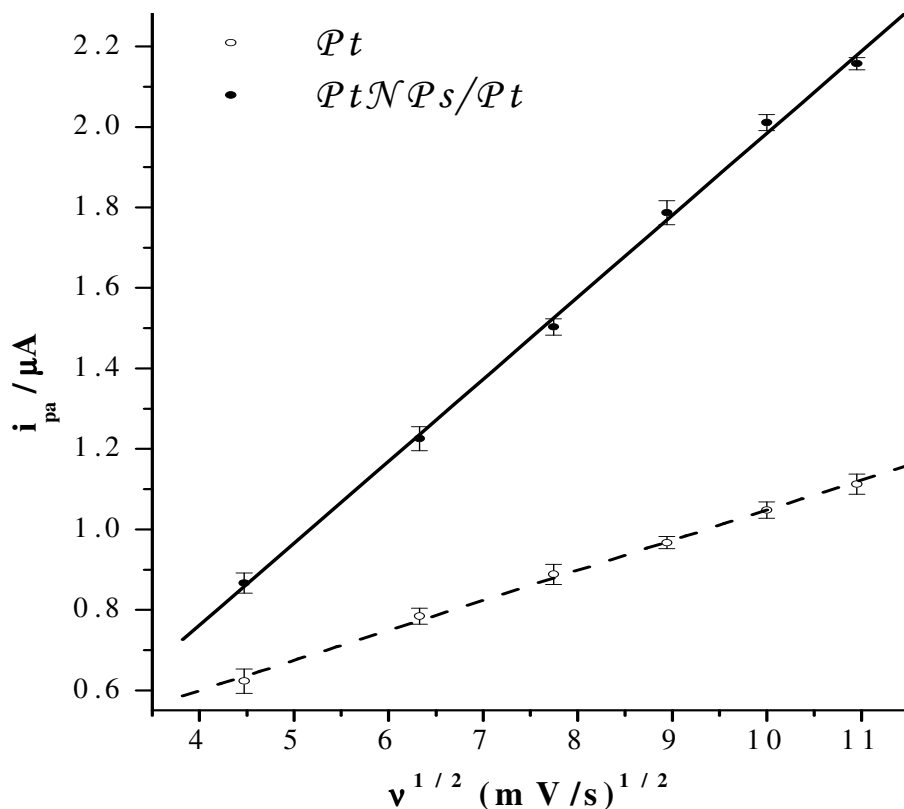


Figure 4.6: Plot of peak current (I_p) vs. square root of scan rate for bare Pt and PtNPs/Pt electrodes

Fig. 4.7 shows the DPV plots for PtNPs/Pt electrode at different Pu concentrations. The peak current (I_p) increased with increase in Pu concentration, showing the potential application of PtNPs/Pt electrode for Pu determination.

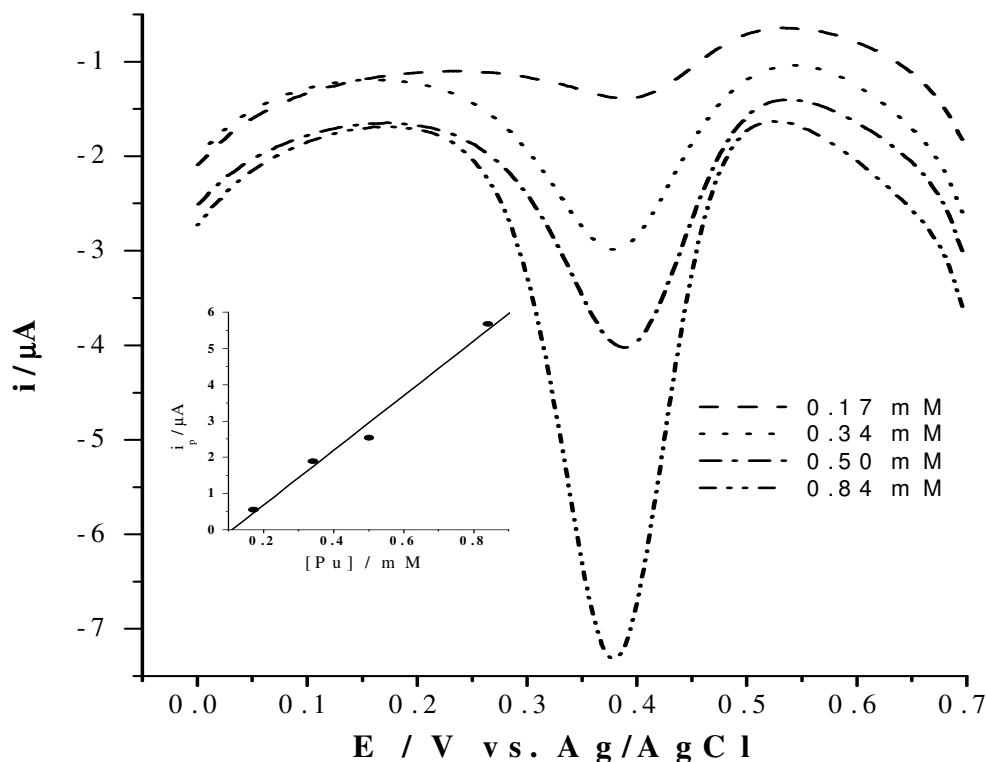


Figure 4.7: DPV of Pu(IV) in 1 M H₂SO₄ at PtNPs/Pt electrode at different concentrations of Pu(IV)

In order to reduce the loading of Pt metal, the electrodeposition of Pt nanoparticles was done on the surface of glassy carbon electrode. The redox response of Pu(IV)/Pu(III) couple in 1 M H₂SO₄ was obtained on the Pt nanoparticles deposited glassy carbon (PtNPs/GC) electrode and the results were compared with those obtained on bare glassy carbon. Fig. 4.8 shows the cyclic voltammogram recorded for PtNPs/GC electrode in 0.5 M H₂SO₄. The appearance of two pairs of redox peaks between 0.0 and -0.4 V, and platinum oxide reduction at 0.2 V clearly showed the electrodeposition of Pt on glassy carbon electrode. Fig. 4.9 shows SEM image of the platinum nanoparticles electrodeposited on the glassy carbon surface. As can be seen, these Pt nanoparticles were well dispersed with a good surface coverage. The particle size ranged from 160 to 200 nm, with narrow size distribution.

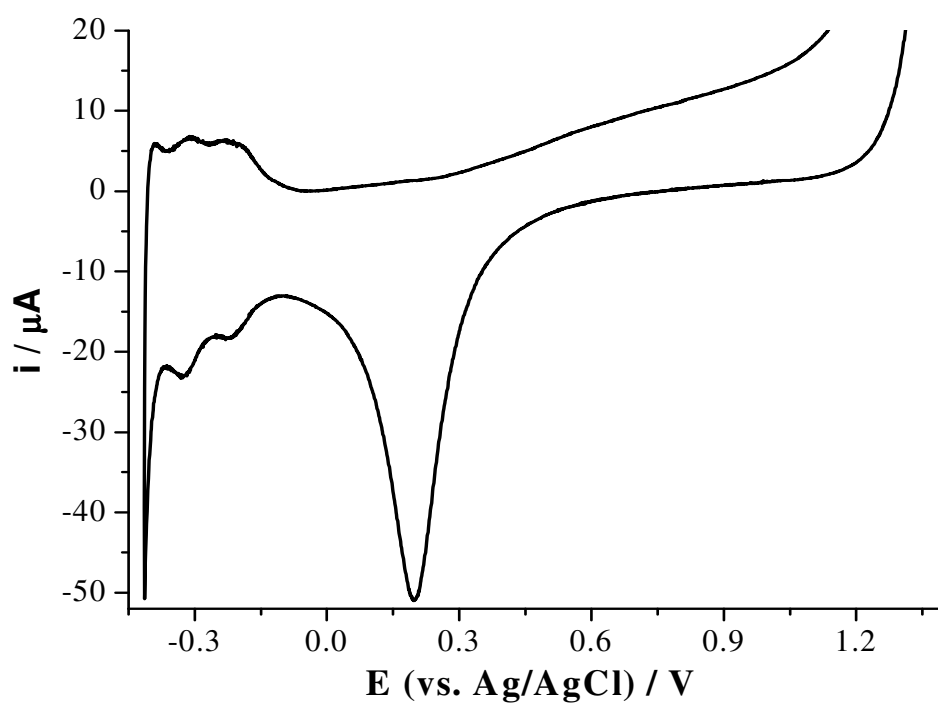


Figure 4.8: Cyclic voltammogram obtained at a scan rate of 100 mV/s in 0.5 M H₂SO₄ for PtNPs coated GC (PtNPs/GC) electrode

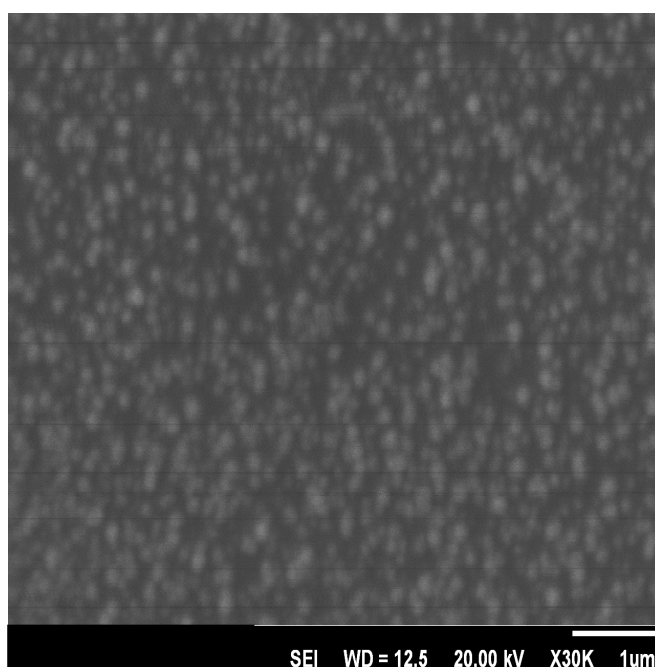


Figure 4.9: SEM image of PtNPs coated GC electrode

Catalytic activity of PtNPs/GC was examined for the reduction of Pu(IV) to Pu(III) in 1 M H₂SO₄ solution by cyclic voltammetry (CV) and differential pulse voltammetry (DPV). Fig. 4.10 compares the cyclic voltammograms recorded in 0.84 mM Pu(IV) + 1 M H₂SO₄ on the glassy carbon electrode before (curve a) and after (curve b) deposition of Pt nanoparticles.

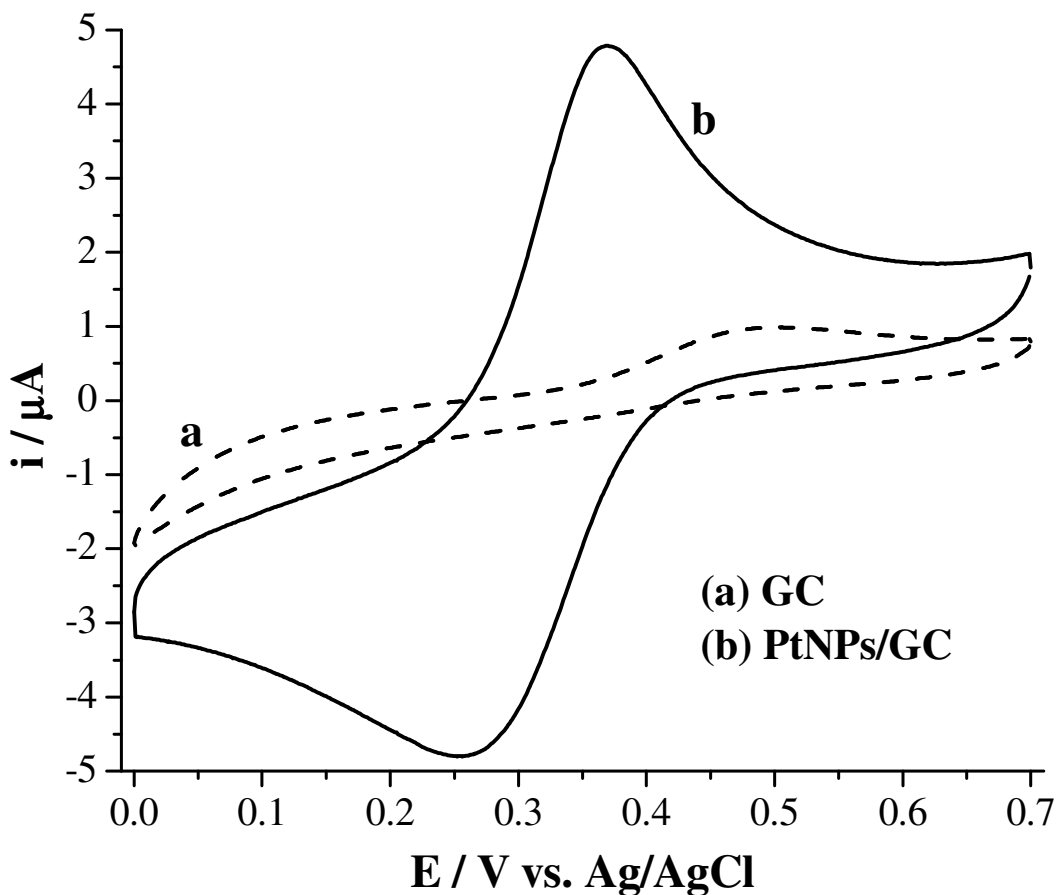


Figure 4.10: Cyclic voltammogram of 0.84 mM Pu(IV) in 1 M H₂SO₄ on (a) GC and (b) PtNPs/GC. The potential scanning rate was 20 mV/s

The electrocatalytic activity of the PtNPs towards Pu(IV)/Pu(III) redox couple was clearly established by the appearance of well-defined cathodic and anodic peaks at 252 mV and 370 mV, respectively. In the potential range of 0 to 0.7 V, a small anodic peak corresponding to the oxidation of Pu(III) to Pu(IV) was observed at 504 mV, but no peak corresponding to reduction of Pu(IV) to Pu(III) was observed on the bare glassy carbon electrode. Fig. 4.11

compares the differential pulse voltammograms on glassy carbon (curve a) and PtNPs/GC (curve b) electrodes. A pair of well-defined reduction and oxidation peaks was observed on the PtNPs/GC electrode at 350 mV and 325 mV, respectively. On the bare glassy carbon electrode, negligibly small Pu(IV) to Pu(III) reduction peak was observed during the cathodic scan, but an oxidation peak was observed at 412 mV during the anodic scan. These results showed that the

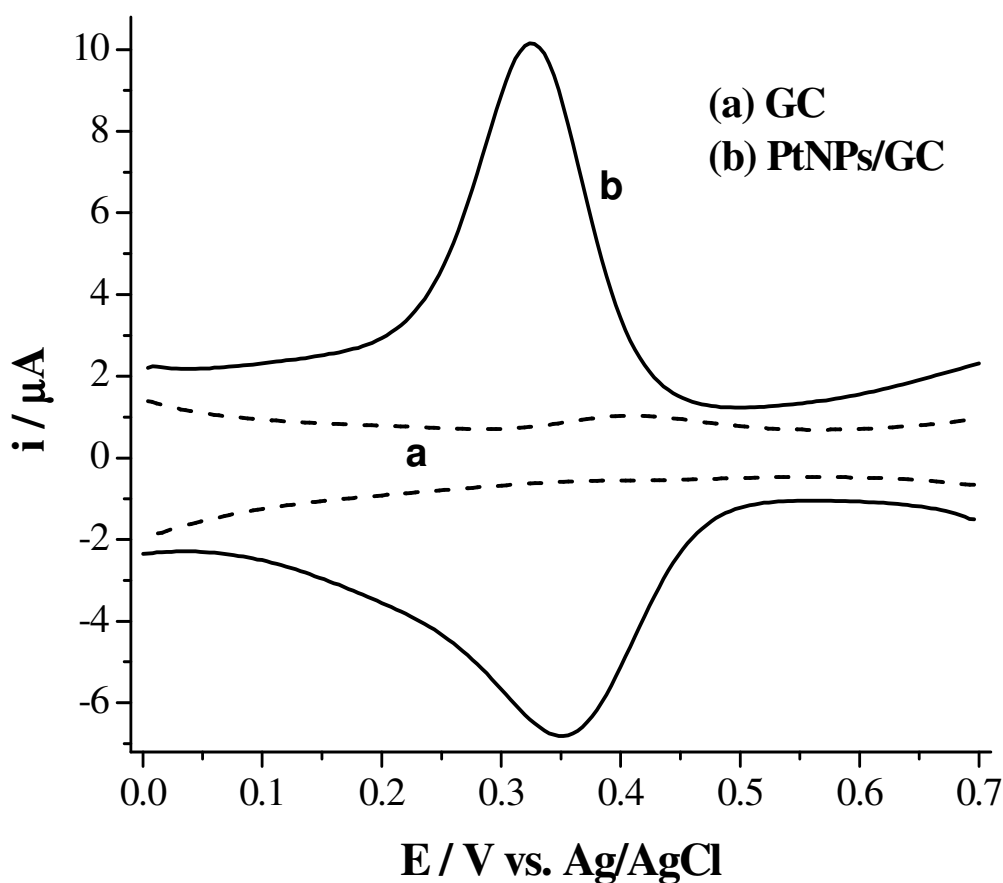


Figure 4.11: DPV of 0.84 mM Pu(IV) in 1 M H₂SO₄ on (a) GC and (b) PtNPs/GC electrodes

presence of the Pt nanoparticles on glassy carbon surface promotes the electron transfer reaction between Pu ions and the GC. The Pu(IV) was observed to be reduced quasi-reversibly to Pu(III) in 1 M H₂SO₄ using the PtNPs/GC electrode.

Fig. 4.12 compares the Nyquist plots of the GC electrode before (curve a) and after (curve b) electrodeposition of the PtNPs. In these experiments, Pu(IV)/Pu(III) was used as a redox couple in solution, and the semicircle diameters on the x-axis of the plot correspond to the interfacial electron transfer resistances at the electrode-solution interfaces. Prior to the

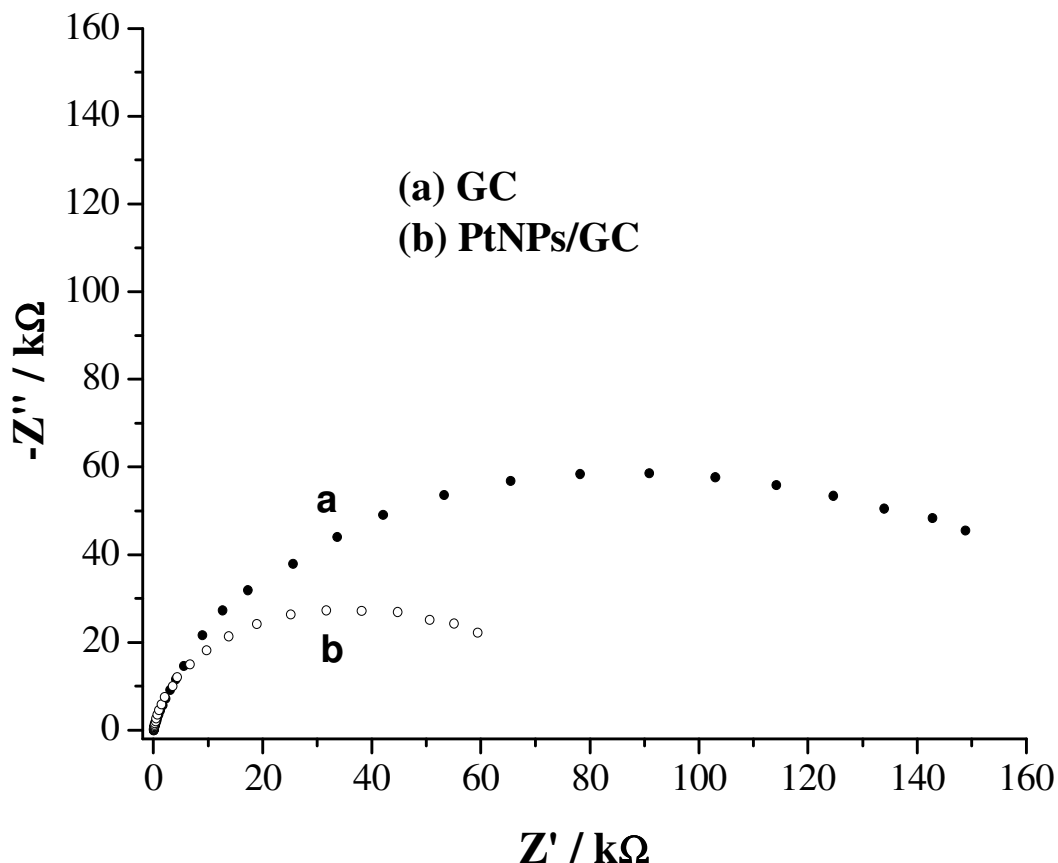


Figure 4.12: Impedance spectra (Nyquist plots) of (a) GC and (b) PtNPs/GC. Data were recorded in the presence of 0.84 mM Pu(IV)/Pu(III) at $E = 0.314$ V with an a.c. potential modulation amplitude of 10 mV and for frequencies ranging between 200 kHz to 0.05 Hz

electrodeposition of PtNPs, the bare glassy carbon electrode resulted in a high electron transfer resistance. The electrodeposition of the PtNPs on the glassy carbon electrode decreased the electron transfer resistance.

4.4. Conclusion

Investigations on the redox behaviour of Pu(IV)/Pu(III) couple in 1 M H₂SO₄ clearly established the improved redox kinetics at the Pt nanoparticles-modified electrodes compared to bare Pt and GC electrodes. The potential peak separation reduced from 157 mV at bare Pt to 79 mV at PtNPs/Pt electrode, indicating faster redox kinetics at PtNPs/Pt electrode. CV and DPV experiments showed that the reduction of Pu(IV) to Pu(III) is more favored at PtNPs/GC electrode, because there was negligibly small peak corresponding to reduction of Pu(IV) to Pu(III) on the bare GC electrode. The redox current on platinum nanoparticles-modified electrode was higher than that using bare electrode for the same concentration of Pu. This would enhance the sensitivity for Pu determination using Pu(IV)/Pu(III) redox couple. The Pu(IV)/Pu(III) redox couple in 1 M H₂SO₄ on PtNPs/GC electrode showed much greater reversibility than the GC electrode. These studies would allow the development of a new and better electrode for quantitative determination of plutonium by coulometry and voltammetry using nanoparticles modified electrode.

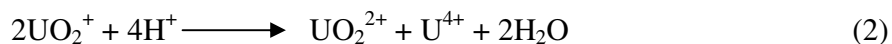
CHAPTER 5

Investigations on Electrochemical Behaviour of U(VI) at Nanomaterials-Modified Electrode Surface

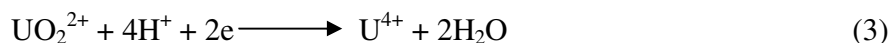
In aqueous solution, uranium can exist in different oxidation states, from +3 to +6 with +6 being the most stable oxidation state. In acidic solution, uranium exists as UO_2^{2+} which undergoes a reversible one-electron reduction at the dropping mercury electrode (at potential approx. equal to -0.18 V vs. SCE) [99, 100]:



The UO_2^+ ions formed at the electrode are unstable and undergo a disproportionation reaction [99-105] yielding UO_2^{2+} and U^{4+} as follows:



The kinetics and mechanism of disproportionation of UO_2^+ were investigated by many researchers. The reaction is second order with respect to the U(V) concentration, first order with respect to the acid concentration, and is dependent on the total ionic strength and nature of the anions present [106, 107]. The rate of this disproportionation reaction is slow, but it increases on increasing the concentration of hydrogen ions [108]. Under strongly acidic conditions, this reaction occurs so quickly that at the potential corresponding to the reaction in equation 1, the U(VI) ions are reduced completely to the tetravalent state [109, 110] according to the reaction:



Electrochemical reactions of uranyl complexes were studied extensively in aqueous [103, 104, 111-115] and non-aqueous [116-123] solutions, and reduction mechanisms were proposed. In the electrochemical processes, electron transfer across the solid-liquid interface is the elementary step. The electrodes merely serve as a source or sink for electrons to transform electroactive species in solution. However, changes in the nature of the electrode surface can alter the efficiency of the electron-transfer process and/or mass-transport regime. Interest in

obtaining the desired electrochemical properties/reaction at the interface between the electrode and the solution has motivated the electrochemists to modify the electrode surface. A number of publications are available where electrochemical studies of UO_2^{2+} ion were carried out on ligand or polymer modified electrodes [124-130]. Bismuth-film electrode was also used for uranium determination [131]. Nanoparticles of noble metals were utilized by electrochemists to modify the surface of the conventional electrodes to obtain better electrochemical response due to the larger effective surface area, increased mass transport, and better electronic interaction between the analyte and the electrode [34, 77, 95]. All these advantages of nanoparticles coated electrodes lead to higher catalytic activity, better sensitivity and selectivity. The electrocatalytic behaviour (faster electrode kinetics) of nanostructured materials is amply documented in the literature and the commonly used diagnostic criteria are the smaller peak separations (or anodic shift in reduction potentials in the case of irreversible processes) and the increased peak current. A few recent reports suggest that the above mentioned diagnostic criteria of electrocatalysis are valid if the mass transport regime for the unmodified and the modified electrodes are the same [132, 133]. In the case of carbon nanotubes modified electrode, porous structures/layers are formed, and the smaller peak separations and the increased peak current in the redox reaction of electroactive species can be described using thin-layer diffusion model. The metal nanoporous film on the bare metal electrode could result in faster electrode kinetics, change in the mass transport regime, or the combined effects leading to higher peak current and a smaller peak separation (or anodic shift in reduction potentials in case of irreversible processes).

There are very less number of publications dealing with the use of nanostructured materials in the electrochemical studies of actinides. In this Chapter, the electrochemical behaviour of UO_2^{2+} ions at the nanostructured gold-modified electrodes is discussed. The

nanostructured gold-modified electrodes were prepared by either physical entrapment of gold nanoparticles (AuNPs) in an anion-exchange membrane or formation of gold nanoporous film (AuNPF) on bare Au electrode.

5.1

Electrochemical Studies of U(VI)/U(V) in Saturated Na₂CO₃ Solution at Gold Nanoparticles Embedded CTA-Modified Electrode

5.1.1. Introduction

In aqueous solution, the known stable complex of UO_2^+ is a carbonate species, $[\text{UO}_2(\text{CO}_3)_3]^{5-}$, which is formed by one-electron reduction of $\text{UO}_2(\text{CO}_3)_3^{4-}$ in basic carbonate aqueous solution ($\text{pH} > 11$) [134-137]. Electrochemical and spectroscopic methods were used by several authors to demonstrate the presence of stable $[\text{UO}_2(\text{CO}_3)_3]^{5-}$ in carbonate solution [108, 135-142]. Uranyl ions (UO_2^{2+} and UO_2^+) are strongly complexed by CO_3^{2-} in aqueous solution [143-145]. In carbonate solutions, the predominant species of UO_2^{2+} is the $[\text{UO}_2(\text{CO}_3)_3]^{4-}$, where the carbonate ions are bidentate. Raman scattering observations showed that the linear dioxo cations UO_2^{2+} retained the $[\text{O-U-O}]^{2+}$ structure in the basic carbonate medium [146]. Cyclic voltammetric studies show that the $\text{UO}_2^{2+}/\text{UO}_2^+$ couple, which is electrochemically reversible in less complexing media, becomes electrochemically irreversible in aqueous CO_3^{2-} solution. Wester et al. observed the irreversible reduction of $\text{UO}_2(\text{CO}_3)_3^{4-}$ to $[\text{UO}_2(\text{CO}_3)_3]^{5-}$ at the mercury electrode in carbonate solution [141]. Mizuguchi et al. showed that a stable $[\text{UO}_2(\text{CO}_3)_3]^{5-}$ complex was formed by the quasireversible reduction of $\text{UO}_2(\text{CO}_3)_3^{4-}$ in carbonate solution at Pt working electrode [136]. The irreversibility of $\text{UO}_2(\text{CO}_3)_3^{4-}/[\text{UO}_2(\text{CO}_3)_3]^{5-}$ couple suggests that a significant conformational change occurs on one electron reduction of $\text{UO}_2(\text{CO}_3)_3^{4-}$. The linear $[\text{O-U-O}]^{2+}$ configuration is retained when there is a one-electron reduction of these ions [147]. EXAFS spectroscopy studies of the reduced species showed that both the axial and the equatorial U-O distance increased, on reduction, from 1.80 to 1.90 Å and from 2.43 to 2.50 Å, respectively. Therefore, the basic geometry of the $\text{UO}_2(\text{CO}_3)_3^{4-}$ complex remains unchanged by reduction, and any conformational change which does occur must be slight [148].

In electrochemical processes, electron transfer across the solid-liquid interface is the elementary step and the interfacial properties such as conductivity, surface area, etc. have

significant influence on electron transfer. Therefore, preparation of well-defined electrochemical interface with highly controllable properties is significant for both the fundamental and the applied studies in electrochemistry. Nanoparticles of noble metals were utilized by electrochemists to modify the surface of conventional electrodes to obtain better electrochemical responses due to larger effective surface area, increased mass transport, and better electronic interaction between the analyte and the electrode [34, 77, 95]. All these advantages of nanoparticles coated electrodes lead to higher catalytic activity, better sensitivity and selectivity. Membranes are promising hosts for a variety of nanoparticles [149] as (a) aggregation and chemical degradation of the nanoparticles is prevented in the polymer matrices, (b) possibility of tailoring the properties of membranes as well as nanoparticles, (c) composite membranes have properties superior to polymer and metal nanoparticles alone, (d) composite membranes find potential applications in tailoring of electrochemical interfaces. Semipermeable membranes embodying nanoparticles are widely prepared and used for the electrode surface modification because of great potential applications in catalysis and interface-electrochemistry [150]. A number of publications were reported where electrochemical studies of UO_2^{2+} ion were carried out on ligand or polymer modified electrodes [124-130]. Bismuth-film electrode was also used for uranium determination [131]. But, there are very less number of publications dealing with the use of nanoparticles in the electrochemical studies of actinides.

In this Chapter, the synthesis of gold nanoparticles (AuNPs) in an anion-exchange membrane, and the redox behaviour of $\text{UO}_2^{2+}/\text{UO}_2^+$ couple in saturated Na_2CO_3 at AuNPs-embedded membrane modified electrode are discussed. The studies were carried out to see the effect of nanoparticles modified electrodes on the partial electrochemical irreversibility of the carbonato-complexes of U(VI)/U(V) . An anion-exchange membrane was used as a host for

stable AuNPs. The host membrane was prepared by physical immobilization of a liquid anion exchanger trioctylmethylammonium chloride (Aliquat 336) in the matrix formed by cellulose triacetate. The membrane was equilibrated with the aqueous solution containing 10 mM AuCl_4^- ions, which were transferred in the membrane matrix by an anion exchange process. These AuCl_4^- ions were subsequently reduced with NaBH_4 to form Au nanoparticles in the membrane matrix. The Au nanoparticles-embedded CTA membrane was characterized by different techniques such as UV-Vis spectrophotometry, X-ray diffraction (XRD), Atomic force microscopy (AFM). The electrochemical properties of AuNPs-CTA modified electrode were evaluated by studying the redox behavior of $\text{UO}_2^{2+}/\text{UO}_2^+$ couple in a saturated Na_2CO_3 solution using voltammetric techniques, and the results were compared with that of the bare Au electrode. Electrochemical studies showed the electrocatalytic reduction of UO_2^{2+} to UO_2^+ in saturated Na_2CO_3 solution at AuNPs-CTA modified electrode with higher current density and faster heterogeneous electron transfer kinetics than that using bare Au electrode. The standard heterogeneous rate constant, k^0 , for the reduction process at AuNPs-CTA modified electrode was about 25 times higher than that of bare Au electrode. Therefore, it was concluded that AuNPs-CTA membrane had improved the interfacial electron-transfer properties of the electrode, resulting in a better electrochemical response than bare Au electrode.

5.1.2. Experimental

Uranyl nitrate, cellulose triacetate (CTA), sodium carbonate, sodium borohydride and dichloromethane used were of analytical reagent grade. All the solutions used in this study were prepared in deionized water purified by the MilliQ water purifier system from Millipore. CTA membrane containing gold nanoparticles was prepared by the following procedure: Cellulose triacetate and Aliquat-336 were dissolved in dichloromethane in the ratio 3:1 (w/w) under

stirring. Then the mixture solution was poured in a petri dish and the solvent was allowed to evaporate slowly over a period of two days. After the complete evaporation of dichloromethane, the transparent membrane was peeled off from the petri dish and was dipped in a solution of HAuCl_4 overnight. It was thoroughly washed with water and HAuCl_4 -loaded CTA was dipped into sodium borohydride solution under stirring to reduce AuCl_4^- ions to gold nanoparticles. AuNPs-CTA modified electrode was prepared by drop-casting 10 μL of dichloromethane solution containing CTA and Aliquat-336 in 3:1 ratio on surface of bare Au electrode. The electrode was rested till the complete volatilization of dichloromethane, and then it was dipped in a solution of HAuCl_4 overnight. It was thoroughly washed with water and HAuCl_4 -loaded CTA modified electrode was dipped into sodium borohydride solution under stirring to reduce AuCl_4^- ions to gold nanoparticles.

Absorbance spectrum of membrane was recorded with a UV-Vis spectrophotometer (QE65000, Ocean Optics Ltd.). The absorbance spectrum was measured in air by placing the membrane in a quartz cell. A CTA membrane without HAuCl_4 was used for background correction. Non-contact mode AFM measurements were performed at ambient temperature conditions using a Nanosurf Easyscan 2 AFM (Nanosurf, Switzerland) with a 10 μm scanner head. The cantilevers in use were NCLR-10 (Nano World) with a resonance frequency of 190 kHz and force constant of 48 N/m. XRD pattern was recorded on a STOE XRD unit using Cu target ($\text{Cu } K_\alpha = 1.5406 \text{ \AA}$) with graphite monochromator. All the voltammetric and the amperometric measurements were carried out on a CHI 440A electrochemical workstation in a three electrode cell. Electrochemical impedance spectroscopy experiments were carried out on Autolab PGSTAT 30 electrochemical workstation. AuNPs-CTA modified electrode and Au electrode ($\Phi = 2 \text{ mm}$) were used as the working electrodes. Platinum wire and Ag/AgCl

electrode were used as counter and reference electrodes, respectively. The saturated sodium carbonate was used as the supporting electrolyte and argon gas was purged through the solution for 10 minutes before each measurement.

5.1.3. Result and Discussion

The AuCl_4^- ions loaded into the cellulose triacetate (CTA) membrane via anion-exchange process were subsequently reduced by 0.1 M NaBH_4 to form Au nanoparticles in the membrane matrix. Fig. 5.1.1 shows the UV-Visible spectrum of the membrane embodying gold nanoparticles. The strong absorption band at 542 nm was attributed to the surface plasmon resonance of Au nanoparticles.

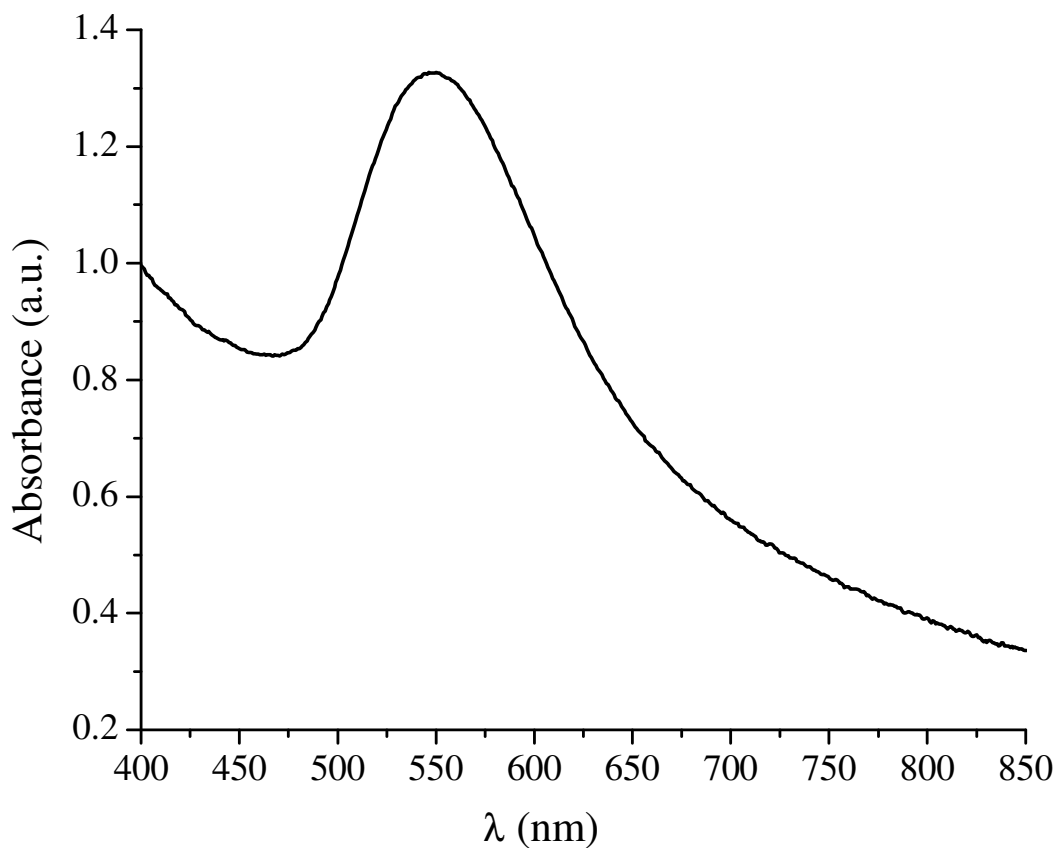


Figure 5.1.1: UV-Visible spectrum of AuNPs-CTA

The crystal phase and crystallite size of Au nanoparticles in the CTA membrane were studied by XRD analysis. As shown in Fig. 5.1.2, the resolvable peaks at 2θ equal to 38.18° and 44.32° were corresponding to the (111), (200)) crystal faces of Au, respectively, indicating the formation of a face-centered cubic phase of Au. The XRD peaks were broadened. This indicated that Au particles formed in the membrane were nanocrystallites. Therefore, broadening of the diffraction peak width of the (111) Bragg reflection was analyzed to estimate the size of Au nanoparticles embedded in the membrane using the Scherrer equation. The size of Au nanoparticles was calculated to be ~ 5 nm.

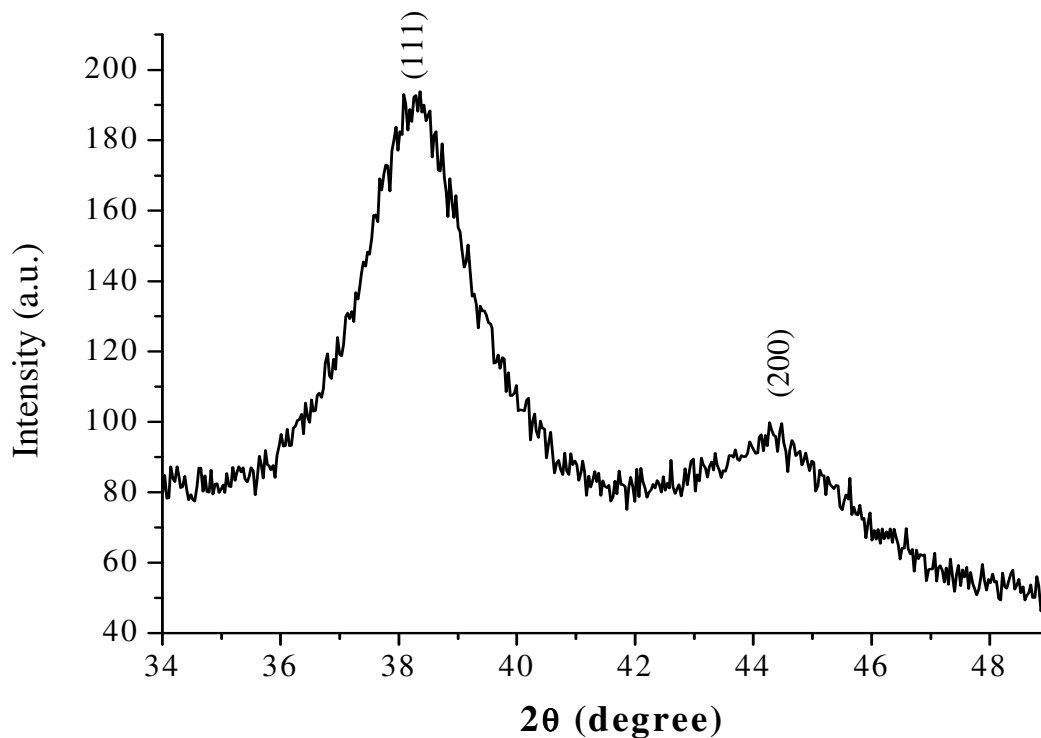


Figure 5.1.2: XRD spectrum of AuNPs-CTA

Fig. 5.1.3 shows the noncontact AFM image of the AuNPs-CTA membrane. Three-dimensional AFM image of AuNPs-CTA membrane indicated a node-grid type structure having egg-basket like external appearance. The gold nanoparticles were embedded in the membrane.

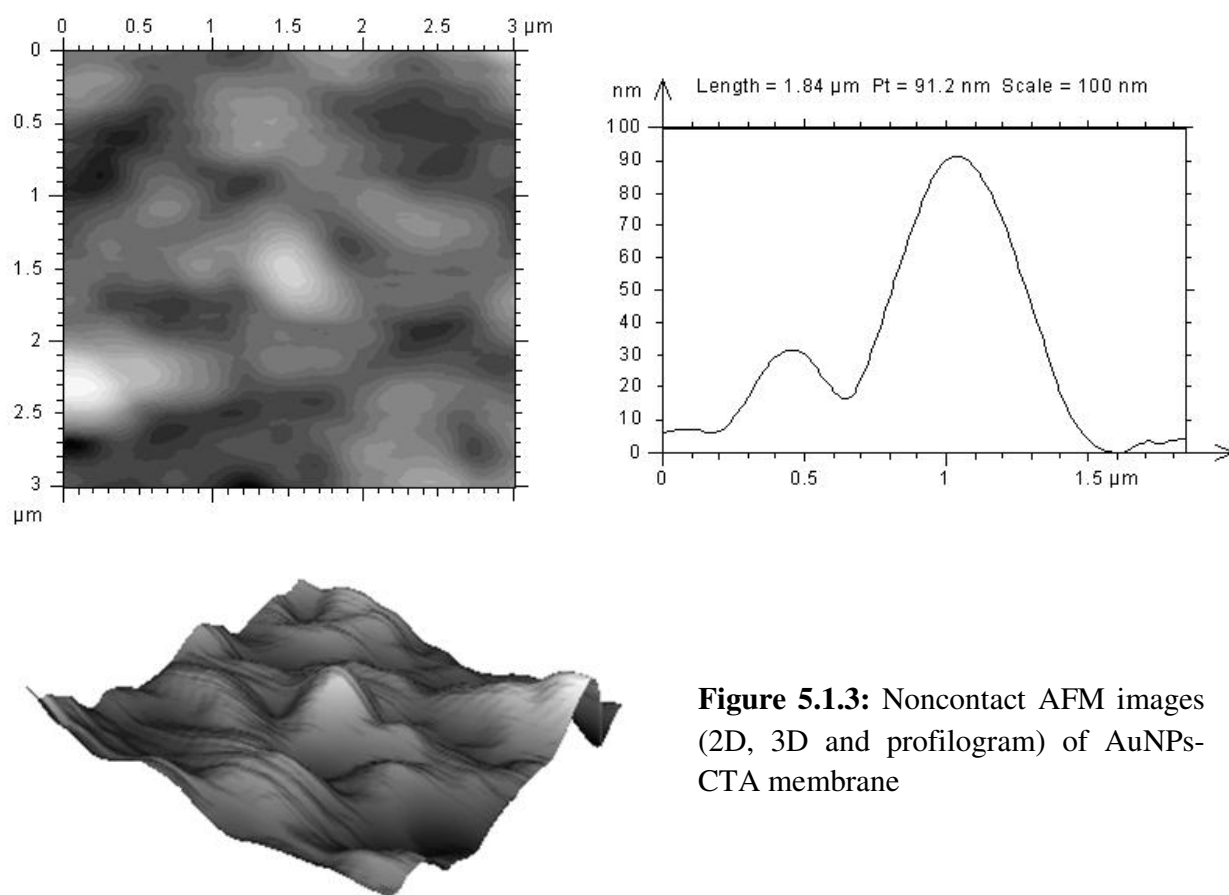


Figure 5.1.3: Noncontact AFM images (2D, 3D and profilogram) of AuNPs-CTA membrane

Fig. 5.1.4 compares the cyclic voltammograms of the AuNPs-CTA modified electrode and bare Au electrode in 1 M H_2SO_4 solution. On AuNPs-CTA modified electrode, the cathodic peak at 0.662 V corresponded to reduction of gold oxide, indicating the formation and immobilization of Au nanoparticles in the CTA membrane. The electrochemically active surface area of the bare Au and AuNPs-CTA modified electrodes was estimated from the charge obtained by integrating the current required for the reduction of gold oxide and a conversion factor of $390 \mu\text{C cm}^{-2}$. The areas calculated for bare Au and AuNPs-CTA modified electrodes were 0.0443 and 0.0037 cm^2 , respectively.

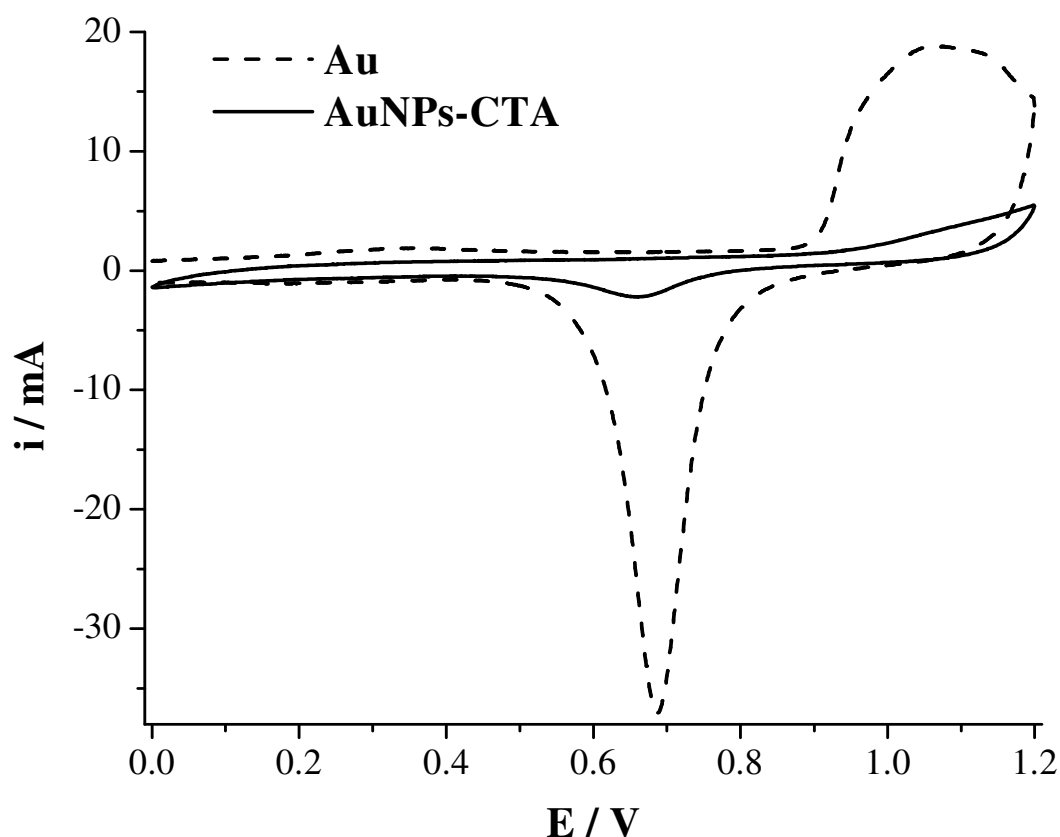


Figure 5.1.4: Cyclic voltammograms of the AuNPs-CTA modified electrode and bare gold electrode in 1 M H_2SO_4 solution. Scan rate = 100 mV/s

The electrocatalytic properties of AuNPs-CTA modified electrode were evaluated by studying the redox behaviour of $\text{UO}_2^{2+}/\text{UO}_2^+$ couple in saturated Na_2CO_3 . The potential was scanned between -0.5 V and -1.2 V at a scan rate of 50 mV/s. Fig. 5.1.5 shows the typical cyclic voltammograms at bare Au and AuNPs-CTA modified electrode in saturated Na_2CO_3 containing 5 mM UO_2^{2+} . On bare Au electrode, a pair of reduction and oxidation peaks were observed at -1.021 V and -0.858 V, respectively with peak potential separation (ΔE_p) of 163 mV. This large ΔE_p value indicated the quasi-reversible nature of the electron transfer process. A pair of reduction and oxidation peaks were observed at -0.959 V and 0.905 V, respectively, on AuNPs-CTA modified electrode with larger redox peak current density and the smaller peak-to-peak separation. The peak potential separation of 54 mV showed increasing reversibility of the redox

process (ΔE_p is 60 mV for reversible one-electron process). Cyclic voltammetric studies indicated an electrocatalytic reduction of UO_2^{2+} to UO_2^+ in saturated Na_2CO_3 solution at AuNPs-CTA-modified electrode with higher current density and faster heterogeneous electron transfer kinetics than that at bare Au electrode. The standard heterogeneous rate constant, k^0 , for the redox reaction was determined by fitting the experimental data using CV simulation software (DigiSim 3, version 3.0, BASi). The k^0 for the reduction process at AuNPs-CTA modified electrode was about 25 times higher than that of bare Au electrode.

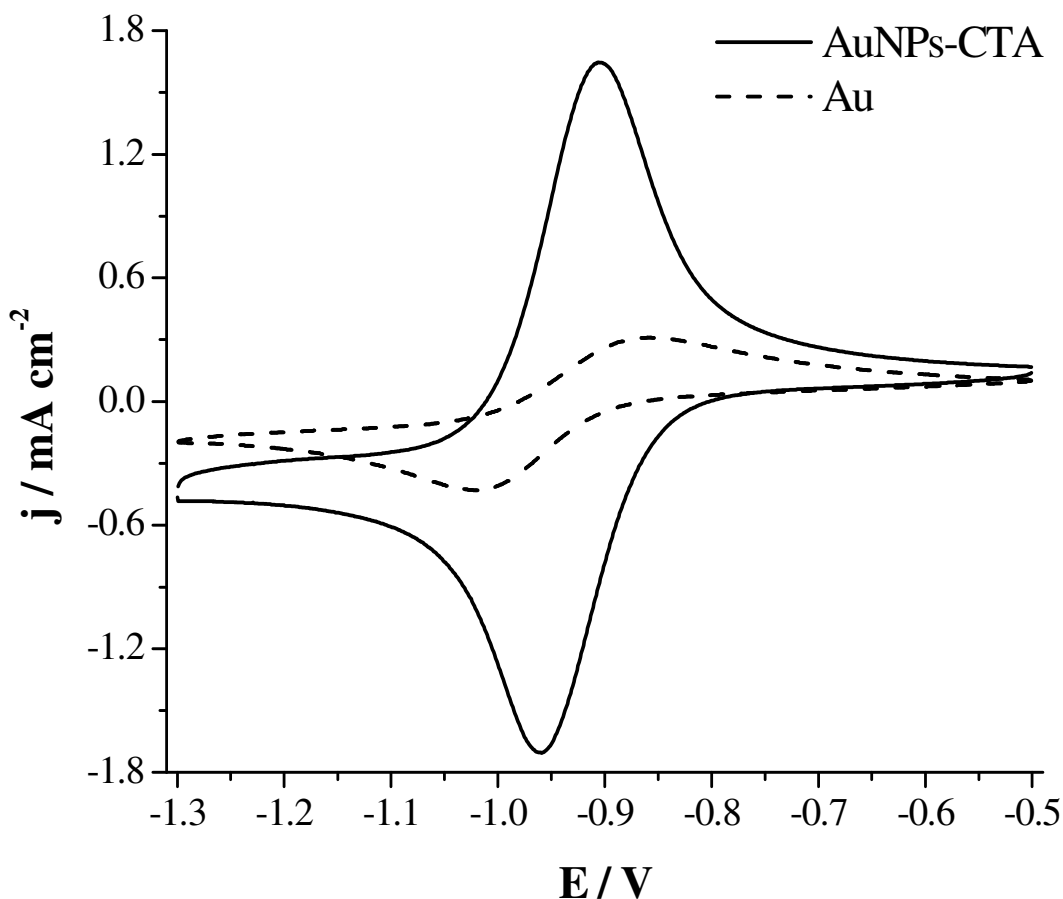


Figure 5.1.5: Cyclic voltammograms of 5 mM UO_2^{2+} in saturated Na_2CO_3 at bare gold and AuNPs-CTA modified electrodes. Scan rate = 50 mV/s

Fig. 5.1.6 shows the chronoamperometric transient of the bare Au and AuNPs-CTA modified electrode upon the application of a reductive potential step from -0.6 V to -1.2 V. The cathodic current transient in AuNPs-CTA modified electrode decayed faster than that of bare Au electrode, indicating a faster electron-transfer process at AuNPs-CTA modified electrode as compared to bare Au electrode.

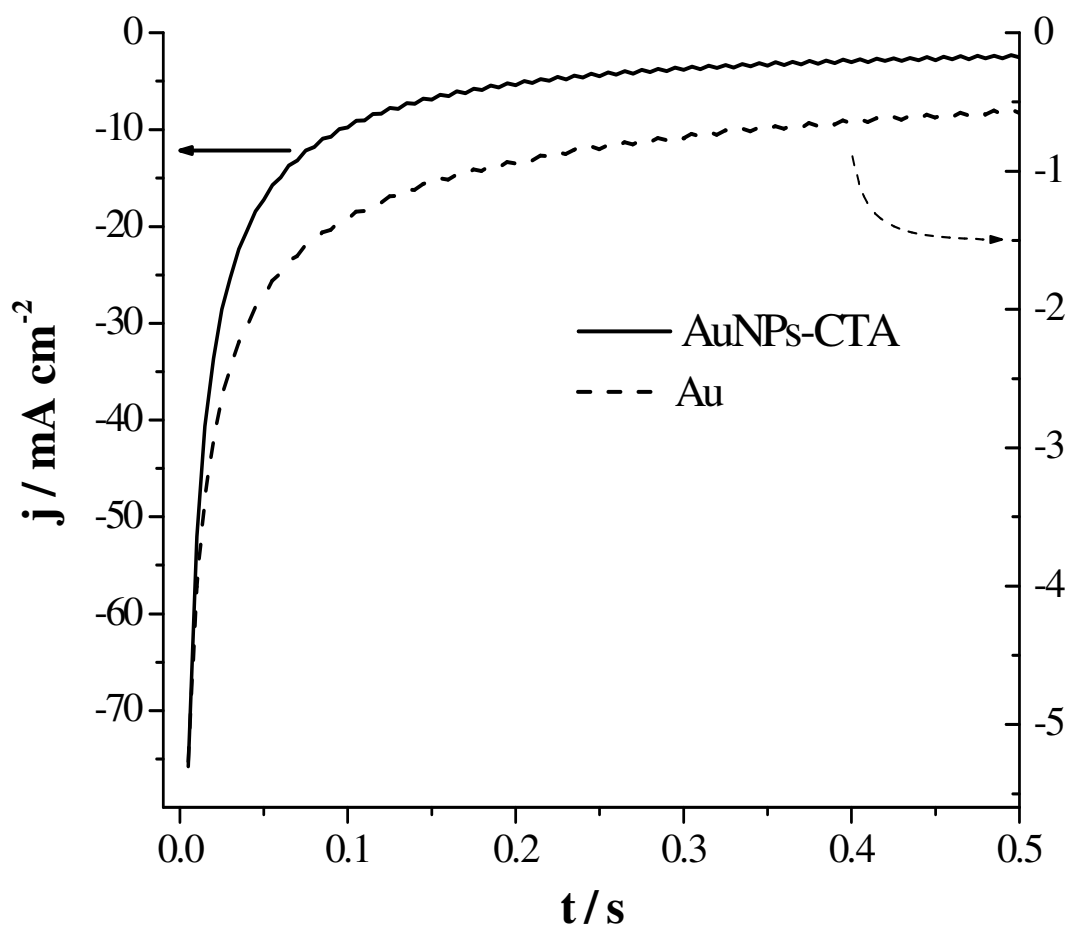
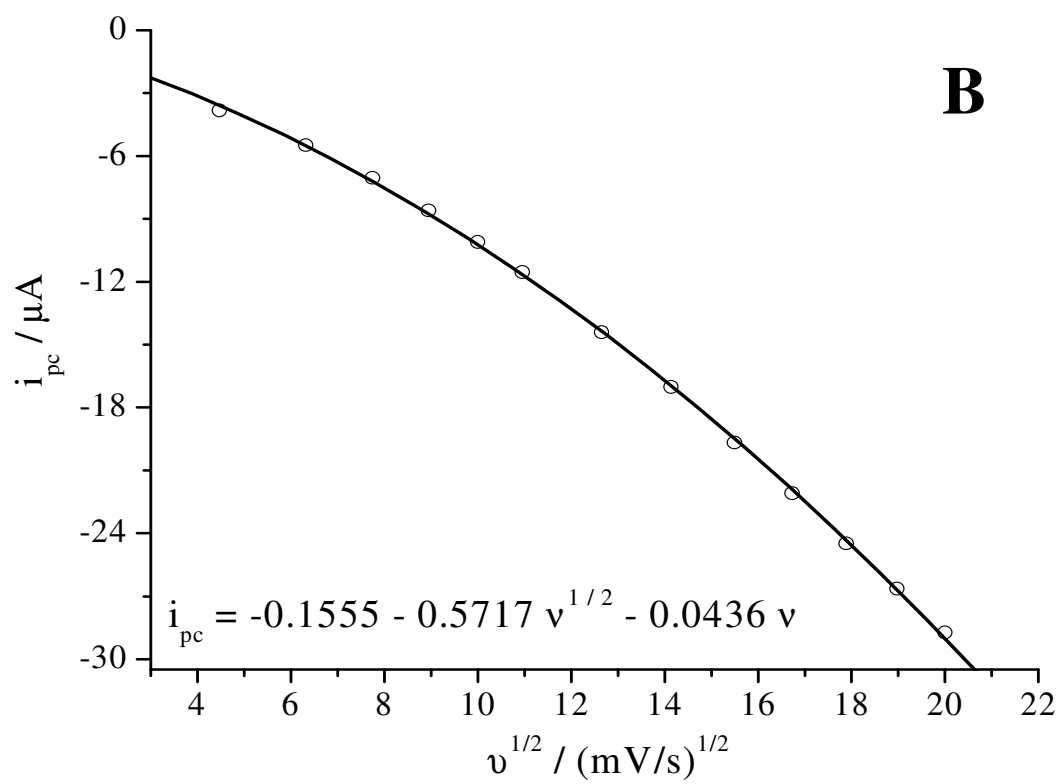
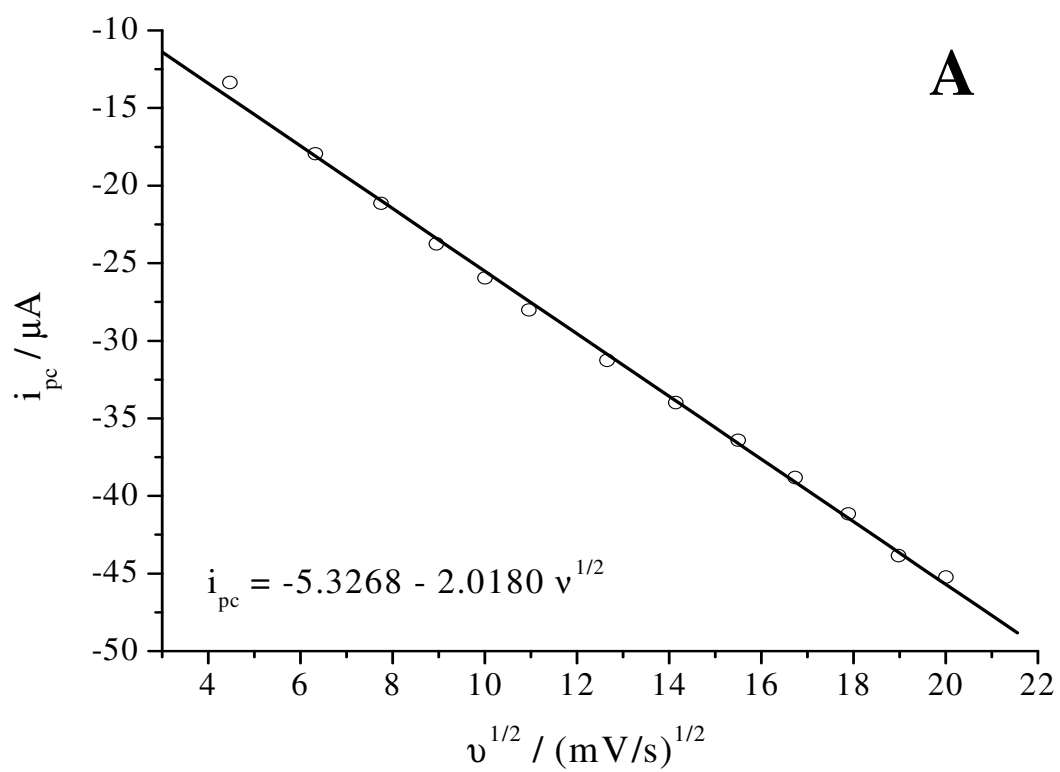


Figure 5.1.6: Chronoamperometric transients of 5 mM UO_2^{2+} in saturated Na_2CO_3 at bare gold and AuNPs-CTA modified electrodes upon the application of a reductive potential step from -0.6 V to -1.2 V



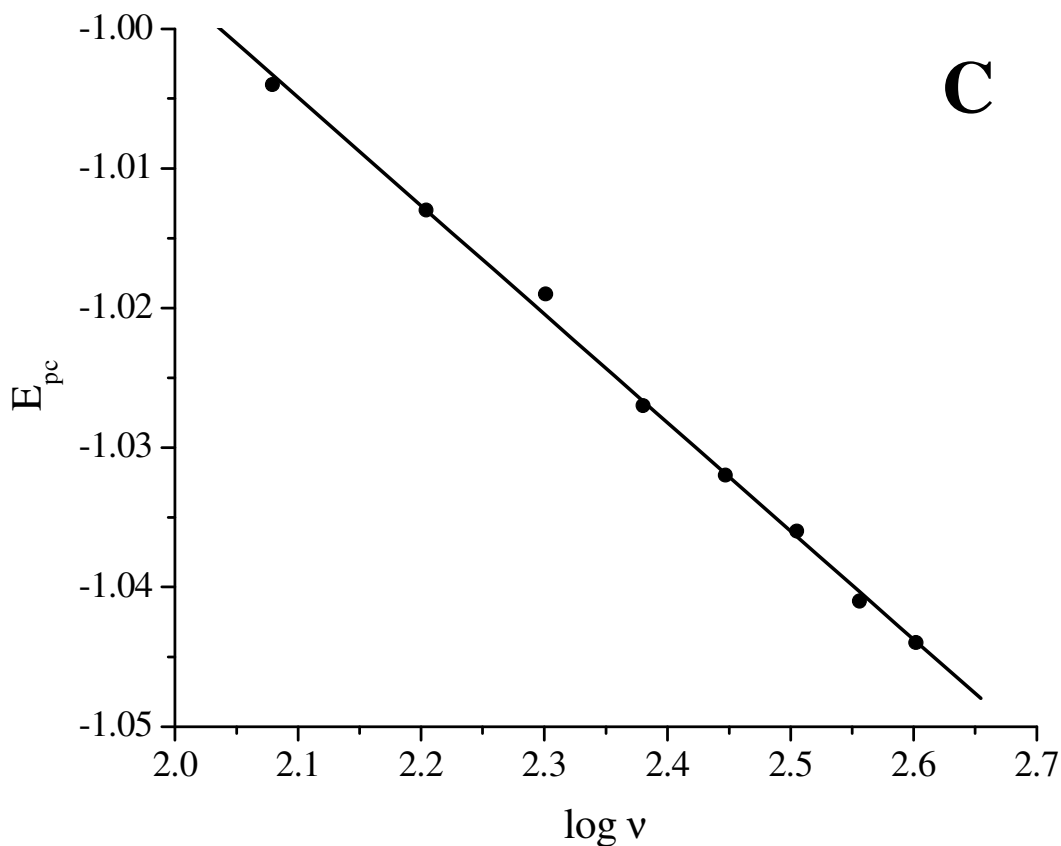


Figure 5.1.7: Plot of i_{pc} vs. $v^{1/2}$ on (A) bare gold and (B) AuNPs-CTA modified electrodes at scan rate from 20 to 400 mV/s in intervals of 20 mV/s. (C) Plot of E_{pc} vs. $\log v$ at higher scan rates. Solution: 5 mM UO_2^{2+} in saturated Na_2CO_3

Fig. 5.1.7A shows the plot of cathodic peak current (i_{pc}) vs. square root of scan rate ($v^{1/2}$) on bare Au in 5 mM UO_2^{2+} in saturated Na_2CO_3 solution. On bare Au, the peak current (i_{pc}) varied linearly with $v^{1/2}$ for scan rates from 20 to 400 mV/s, suggesting diffusion controlled electrochemical process. On AuNPs-CTA modified electrode (Fig. 5.1.7B), the peak current (i_{pc}) was found to follow second order polynomial equation with respect to $v^{1/2}$, $i_{pc} = -0.1555 - 0.5717 v^{1/2} - 0.0436 v$. This equation suggests that at slower scan rate, current due to the diffusion of $UO_2(CO_3)_3^{4-}$ from solution contributes significantly to the total current. But at higher scan rates, current due to the reduction of weakly adsorbed $UO_2(CO_3)_3^{4-}$ starts contributing significantly to the total current along with the diffusion controlled current.

Fig. 5.1.7C shows that the plot of cathodic peak potential (E_{pc}) varied linearly with $\log(v)$ for higher scan rates ($v > 120$ mV/s), thus indicating a possible adsorption of $UO_2(CO_3)_3^{4-}$ on AuNPs-CTA membrane. As the anion-exchange sites of Aliquat-336 in the membrane were readily available after the formation of AuNPs [149], $UO_2(CO_3)_3^{4-}$ in solution could adsorb onto these sites by ion-exchange process.

To further investigate the behaviour of AuNPs-CTA modified electrode, AuNPs-CTA modified electrode was dipped in 1 – 10 mM of $UO_2(CO_3)_3^{4-}$ solution for a long time, and CV was carried out in $UO_2(CO_3)_3^{4-}$ free solution, then very small reduction current was observed which decayed to almost background current after repeated CV cycling (Figure not shown). This suggested that a small number of $UO_2(CO_3)_3^{4-}$ ions got weakly adsorbed at anion-exchange sites of Aliquat-336 in CTA membrane, when dipped in $UO_2(CO_3)_3^{4-}$ solution. Similar studies were also carried out using CTA/Aliquat-336 membrane-modified electrode without AuNPs. It was observed that the redox current in $UO_2(CO_3)_3^{4-}$ solution (1-10 mM) was very less as compared to AuNPs-CTA modified electrode. Therefore, AuNPs incorporated in AuNPs-CTA modified electrode acted as electron-mediator through insulating CTA matrix.

The change in the interfacial electron-transfer properties on modifying the electrode surface with AuNPs-CTA was evaluated by electrochemical impedance spectroscopy (EIS). Fig. 5.1.8 compares the Nyquist plots of the bare Au electrode and the AuNPs-CTA modified electrode employing $[Fe(CN)_6]^{3-/4-}$ redox couple. $[Fe(CN)_6]^{3-/4-}$ is a widely used redox couple in aqueous solution, while comparing the modified and unmodified-electrode using EIS techniques. Therefore, EIS measurements were done using $[Fe(CN)_6]^{3-/4-}$ couple.

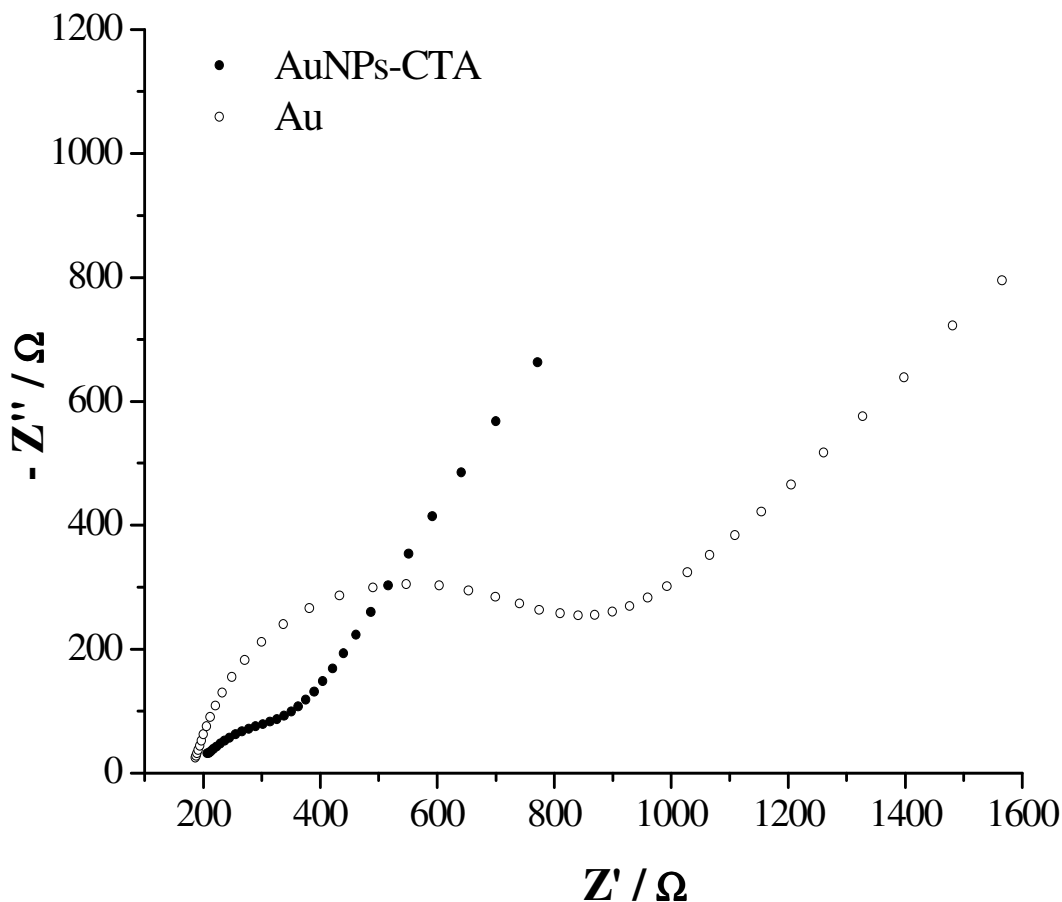


Figure 5.1.8: Impedance spectra (Nyquist plots) of bare gold and AuNPs-CTA modified electrodes. Data were recorded in the presence of 2.5 mM $[\text{Fe}(\text{CN})_6]^{3-/4-}$ with an a.c. potential modulation amplitude of 10 mV and for frequencies ranging between 100 kHz to 0.1 Hz

The diameters of the semicircles on the x-axis of the plot determine the values of the interfacial charge-transfer resistance of the $[\text{Fe}(\text{CN})_6]^{3-/4-}$ redox couple at bare Au and AuNPs-CTA modified electrodes. The AuNPs-CTA modified electrode had smaller interfacial electron-transfer resistance than bare Au.

Aliquat-336 was not only acting as an anion-exchanger in CTA matrix, but acted as a plasticizer also. We tried 1:1 ratio of CTA:Aliquat-336, but found that at higher concentration of Aliquat-336, it slowly leached out of matrix over a period of time. At lower Aliquat-336

concentration, the matrix lost its plasticity and hence the number of solvent/liquid channels available in the CTA matrix was less. Therefore, the diffusion of AuCl_4^- ions inside the membrane was very slow, thus hindering the loading of AuCl_4^- ions in CTA matrix. Thus, 3:1 ratio of CTA: Aliquat-336 was chosen as the optimized ratio keeping both the physical integrity (mechanical strength) and plasticity of the membrane under consideration.

5.1.4. Conclusion

Gold nanoparticles (AuNPs) were prepared in the matrix of cellulose triacetate (CTA) membrane and AuNPs embedded-CTA membrane was coated on the bare Au electrode to tailor the properties of its electrochemical interface. Cyclic voltammetric studies in saturated Na_2CO_3 containing 5 mM UO_2^{2+} showed the larger redox peak current density and smaller peak-to-peak separation at AuNPs-CTA modified electrode compared to bare Au electrode. EIS studies indicated that the faster interfacial electron-transfer kinetics at the AuNPs-CTA electrode compared to bare Au electrode. These studies indicated an electrocatalytic reduction of UO_2^{2+} to UO_2^+ in saturated Na_2CO_3 solution at AuNPs-CTA-modified electrode. The standard heterogeneous rate constant, k^0 , for the reduction process at AuNPs-CTA modified electrode was about 25 times higher than that of bare Au electrode. Therefore, it is concluded that AuNPs-CTA membrane significantly improved the interfacial electron-transfer properties of the electrode surface, resulting in a better electrochemical response than bare Au electrode for the $\text{UO}_2^{2+}/\text{UO}_2^+$ couple in saturated Na_2CO_3 solution.

5.2

Electrochemical Reduction of U(VI) in H₂SO₄ at Gold Nanoporous Film Electrode

5.2.1. Introduction

The electroanalytical method for uranium determination based on the reduction of U(VI) in acidic supporting electrolyte uses mercury as a working electrode because of the higher hydrogen overvoltage on mercury. For the bulk reduction of U(VI), a stirred mercury pool is necessary, and unfortunately this type of electrode is not very convenient to use experimentally. Due to hazards associated with the use of mercury, solid electrodes are preferred for the bulk reduction of U(VI) in acidic medium. The determination of uranium using solid electrodes like graphite [94], silver [151], platinum [152], and gold [153] were reported previously. Carbonaceous electrodes such as graphite, glassy carbon, etc., are known to offer the favorable range of potential required for U(VI) reduction. They do not, however, offer reproducible surface conditions. Also the electrolysis is slow and the background currents are relatively large [94]. Silver dissolves in sulphuric acid electrolyte, and Bi, Cu, Mo and Hg are the main interfering elements. Determination of uranium on a platinum electrode is difficult due to hydrogen evolution reaction (HER) at the potential (-0.35 V vs. SCE) needed for the reduction of U(VI) in acidic medium. However, HER on platinum can be suppressed by dissolving trace amount of Bi(III) or Pb(II) in appropriate electrolyte (4.5 M HCl), but secondary reactions are involved [152]. Rapid reduction of U(VI) on the activated platinum wire gauze electrode for the primary coulometric determination of uranium was reported [154]. Activation of the Pt electrode was achieved by combination of chemical and electrochemical oxidation followed by electrochemical reduction. The enhanced electrochemical activity of the activated Pt electrode was attributed to a significant increase in the catalytic surface area due to the formation of porous surface film which regained its original compact structure on ageing. The time taken for the quantitative reduction of U(VI) on gold was found to be large for routine analysis. Therefore, the

determination of U is routinely carried out by primary coulometry in 1 M sulphuric acid at Hg pool electrode at a potential of -0.35 V vs. SCE.

In classical voltammetry, the electrodes merely serve as a source or sink for electrons, to transform electroactive species in solution. However, changes in the nature of the electrode surface can alter the efficiency of the electron-transfer process and/or mass-transport regime. Interest in obtaining the desired electrochemical properties/reaction at the interface between the electrode and the solution has motivated the electrochemists to modify the electrode surface. Nanostructured-materials – carbon nanotubes, nanoparticles, nanoporous films – have been utilized to modify the surface of the bare electrodes to obtain better electrochemical responses resulting from larger effective surface area, increased mass transport, and better electronic interaction between the analyte and the electrode [34, 155, 156]. The electrocatalytic behaviour (faster electrode kinetics) of nanostructured materials is amply documented in the literature and the commonly used diagnostic criteria are the smaller peak separations (or anodic shift in reduction potentials in the case of irreversible processes) and the increased peak current.

In Chapter 4, we discussed the redox behavior of $\text{Pu}^{4+}/\text{Pu}^{3+}$ couple in 1 M H_2SO_4 on platinum nanoparticles-modified glassy carbon and platinum electrodes [157]. The smaller peak separations and the increased peak currents at platinum nanoparticles-modified electrode indicated the faster electrode kinetics at the modified electrodes compared to bare Pt and GC electrodes. In Chapter 5.1, an electrocatalytic reduction of UO_2^{2+} to UO_2^+ in saturated Na_2CO_3 solution was explained in terms of the smaller peak separation (ΔE_p) and higher current density observed at Au nanoparticles embedded cellulose triacetate-modified electrode. [158].

A few recent reports suggest that the above mentioned diagnostic criteria of electrocatalysis are valid if the mass transport regime for the unmodified and the modified

electrodes are the same [132, 133]. In the case of carbon nanotubes modified electrode, porous structures/layers are formed, and the smaller peak separations and the increased peak current in the redox reaction of electroactive species can be described using thin-layer diffusion model. The metal nanoporous film on the bare metal electrode could result in faster electrode kinetics, a change in the mass transport regime, or the combined effects leading to higher peak current and a smaller peak separation. Therefore, efforts are necessary to understand/determine the mass transport regime while extolling the electrocatalytic behaviour of nanoporous film modified electrode over the unmodified electrode.

In this part of the Chapter, the preparation of gold nanoporous film (AuNPF) electrode and the electrochemical reduction of UO_2^{2+} in 0.5 M H_2SO_4 AuNPF electrode are discussed. Gold nanoporous film (AuNPF) was grown on gold substrate by electrochemical oxidation of the gold electrode at 5 V for 180 s in phosphate buffer (pH 7.4) followed by the reduction of the oxidized gold with ascorbic acid solution. Atomic force microscopy (AFM) showed the porous nature of the prepared film. In cyclic voltammetric (CV) studies, anodic shift of 141 mV in the cathodic peak potential and an increase in the peak current for the reduction of UO_2^{2+} in 0.5 M H_2SO_4 was observed at the AuNPF electrode, showing evidence of its enhanced electrochemical activity as compared to that of the bare Au electrode. The interfacial charge transfer resistance values for the bare Au and the AuNPF electrodes obtained by electrochemical impedance spectroscopy were almost the same indicating similar rates of the heterogeneous electron-transfer kinetics at the bare Au and the AuNPF electrodes. The Cottrell plots obtained from the chronoamperometric experiments showed the Cottrell linearity at the bare Au electrode. In contrast, the Cottrell plot of the AuNPF electrode showed deviation from the linearity at longer times and this was characteristic of the thin-layer diffusion coupled with the electron transfer.

Therefore, the observed anodic shift at the AuNPF electrode for the reduction of UO_2^{2+} was attributed to the contribution from thin-layer diffusion within the gold nanoporous film.

The metal nanoporous film modified electrode demonstrated the possibility of using this electrode for the quantitative reduction of U(VI) at lower cathodic potential with 100 % current efficiency in acidic electrolyte medium. The nanoporosity of the film can be optimized to obtain better electrochemical behaviour by tuning the various chemical and electrochemical parameters involved in its preparation [154, 156].

5.2.2. Experimental

UO_3 , ascorbic acid and sulphuric acid used were of analytical reagent grade. All the solutions used in this study were prepared in deionized water purified by the MilliQ water purifier system from Millipore. Uranyl solution was prepared by dissolving UO_3 microspheres in 1 M sulphuric acid. Reflectance-mode absorbance spectrum of gold nanoporous film was recorded with a UV-Visible spectrophotometer (QE65000, Ocean Optics Ltd.). A bare gold electrode was used for background correction. Non-contact mode AFM measurements were performed at ambient temperature conditions using a Nanosurf EasyScan 2 AFM (Nanosurf, Switzerland) with 10 μm scanner head. The cantilevers used were NCLR-10 (Nano World) with a resonance frequency of 190 kHz and a force constant of 48 N/m. All voltammetric, chronoamperometric and impedance measurements were performed using a CHI 760D electrochemical workstation in a three-electrode cell. Au and AuNPF electrodes ($\Phi = 2 \text{ mm}$) were used as the working electrodes. Platinum wire and Ag/AgCl/3M KCl electrodes were used as the counter and the reference electrodes, respectively. The 0.5 M H_2SO_4 was used as a supporting electrolyte and the argon gas was purged through the solution for 10 min before each measurement. The gold electrode was polished using alumina powder paste of decreasing

particle size from 1.0 to 0.05 μm . The gold electrode was ultrasonically cleaned in water after each polishing step to remove any adhering alumina particles. The cleaned gold electrode was oxidized at 5 V for 180 s in 0.1 M phosphate buffer (pH 7.4). The anodized electrode was dipped in 1 M ascorbic acid solution for 5 minutes to reduce the oxidized gold to Au completely. The color of the electrode surface became black, indicating the formation of nanoporous gold film on gold electrode surface.

5.2.3. Results and Discussion

Fig. 5.2.1 shows the atomic force microscopic images of the bare gold and the gold nanoporous film (AuNPF) electrode surfaces. AFM studies of the AuNPF showed the formation of ensemble of thorns/needle-like structure and porous nature of the prepared film. It seems that thorn-like structures are dispersed perpendicular to the gold surface. The root-mean-square roughness (S_q) value of $10\ \mu\text{m} \times 10\ \mu\text{m}$ surface areas of the AuNPF and the bare Au electrodes were 96.7 nm and 0.81 nm, respectively. The surface area roughness of the AuNPF electrode showed an increase by almost 120 times.

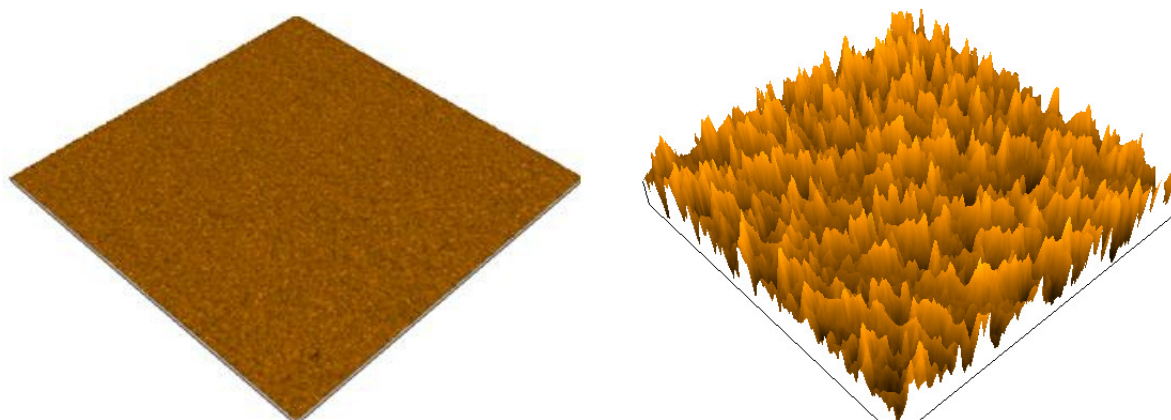


Figure 5.2.1: AFM images of (a) bare gold (b) gold nanoporous film (AuNPF)

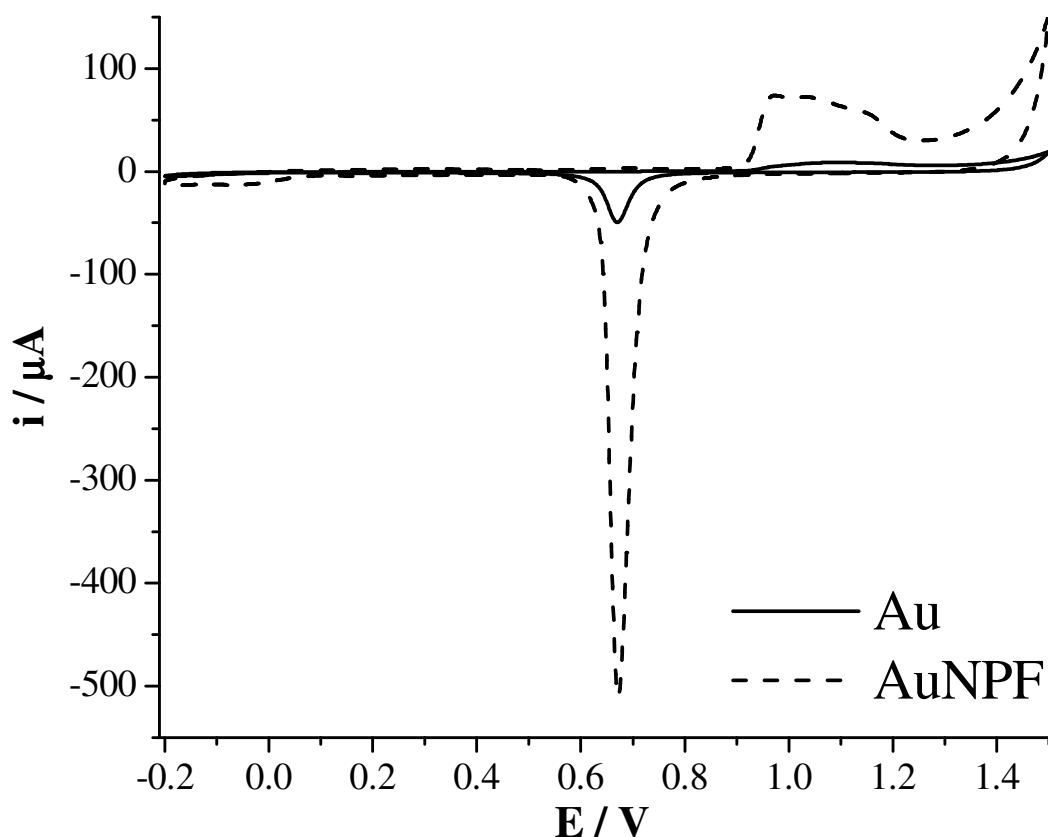


Figure 5.2.2: CVs of a bare gold (Au) and a gold nanoporous film (AuNPF) electrodes in 0.5 M H₂SO₄ at a scan rate of 50 mV/s

Fig. 5.2.2 shows the cyclic voltammograms of the AuNPF and the bare Au electrodes in 0.5 M H₂SO₄. The cathodic peak at 0.670 V corresponds to the reduction of gold oxide. The theoretical charge density for the reduction of gold oxide is 390 $\mu\text{C cm}^{-2}$ [159]. The electrochemically active surface areas of the bare gold and the AuNPF electrodes were estimated from the charge obtained by integrating the current required for the reduction of gold oxide and the conversion factor of 390 $\mu\text{C cm}^{-2}$. The areas calculated for the bare Au and the AuNPF electrodes were 0.075 and 0.916 cm^2 , respectively. The electrochemically active surface area of the AuNPF electrode was 12 times more than that of the bare Au electrode.

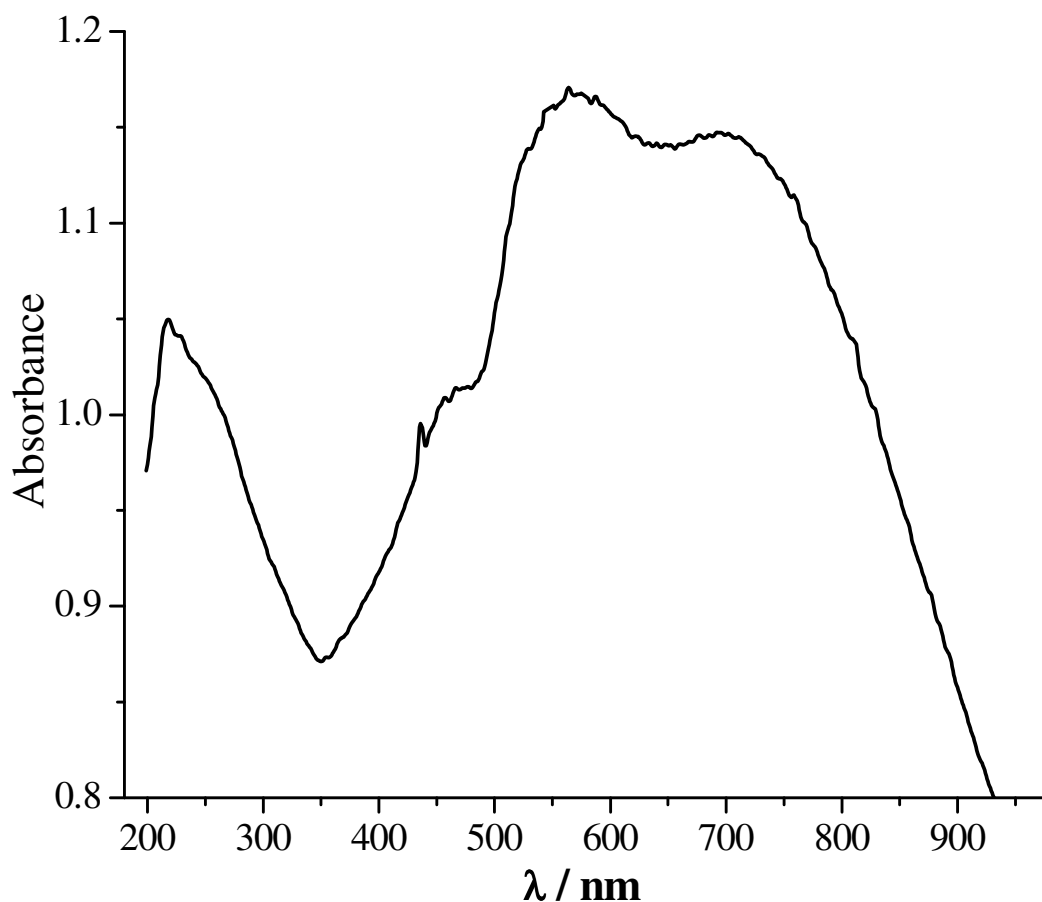


Figure 5.2.3: UV-Visible reflectance spectrum of the gold nanoporous film (AuNPF) electrode

The reflectance-mode UV-Visible absorbance spectrum of the AuNPF showed two peaks maxima at 565 nm and 700 nm (Fig. 5.2.3). The two peaks maxima could originate from the gold nanothorn assemblies, as shown in the AFM image, corresponding to transverse (565 nm) and longitudinal (700 nm) surface plasmon resonances.

The electrochemical properties of the AuNPF electrode were evaluated by studying the reduction of UO_2^{2+} in 0.5 M H_2SO_4 . The potential was scanned between 0.2 V and -0.6 V at a scan rate of 50 mV s^{-1} . Fig. 5.2.4 shows the cyclic voltammograms at the bare Au and the AuNPF electrodes in 0.5 M H_2SO_4 containing 5 mM UO_2^{2+} .

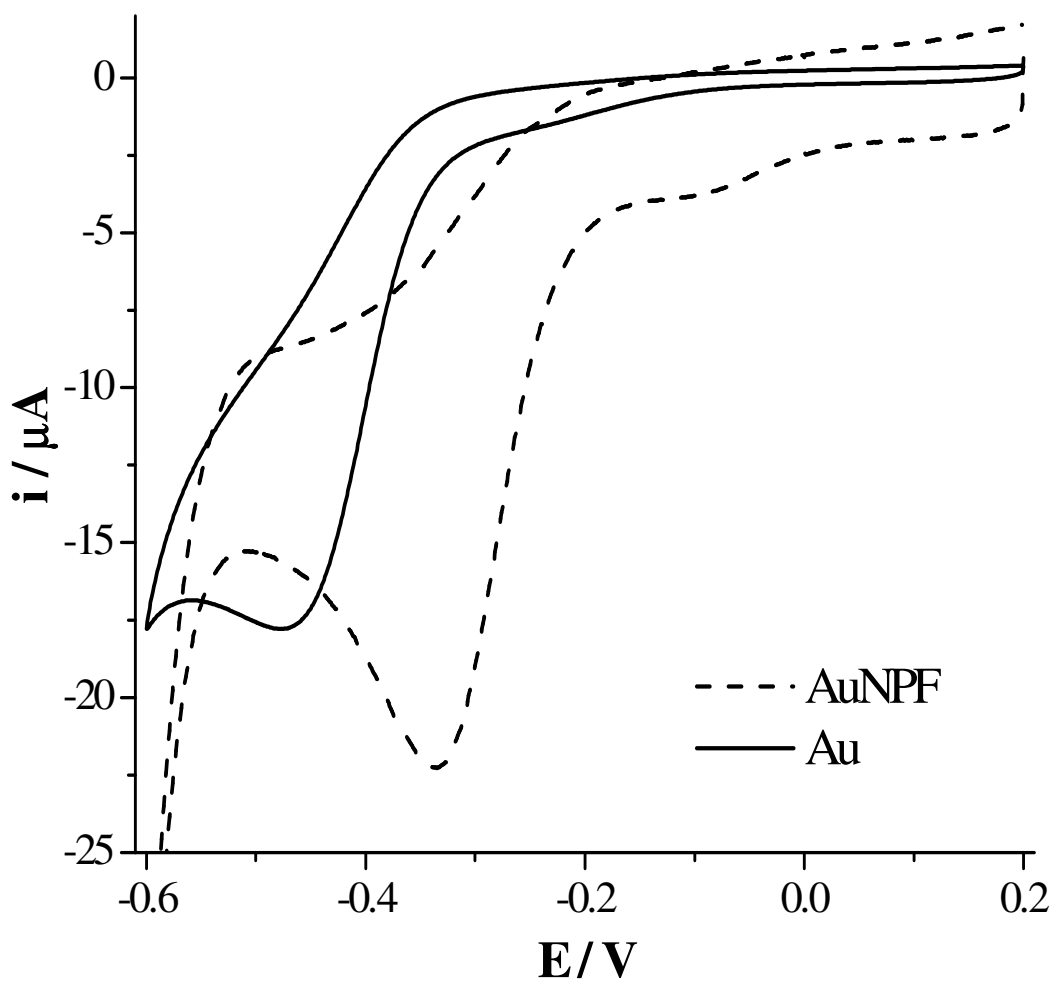


Figure 5.2.4: CVs of a bare gold (Au) and a gold nanoporous film (AuNPF) electrodes in 5 mM UO_2^{2+} in 0.5 M H_2SO_4 at a scan rate of 50 mV/s

At the bare Au electrode, the cathodic peak potential (E_{pc}) for UO_2^{2+} reduction in 0.5 M H_2SO_4 was -0.478 V, which shifted to -0.337 V at the AuNPF electrode. The anodic shift of 0.141 V in the cathodic peak potential showed the evidence of higher electrocatalytic activity of the AuNPF electrode towards the reduction of UO_2^{2+} in 0.5 M H_2SO_4 .

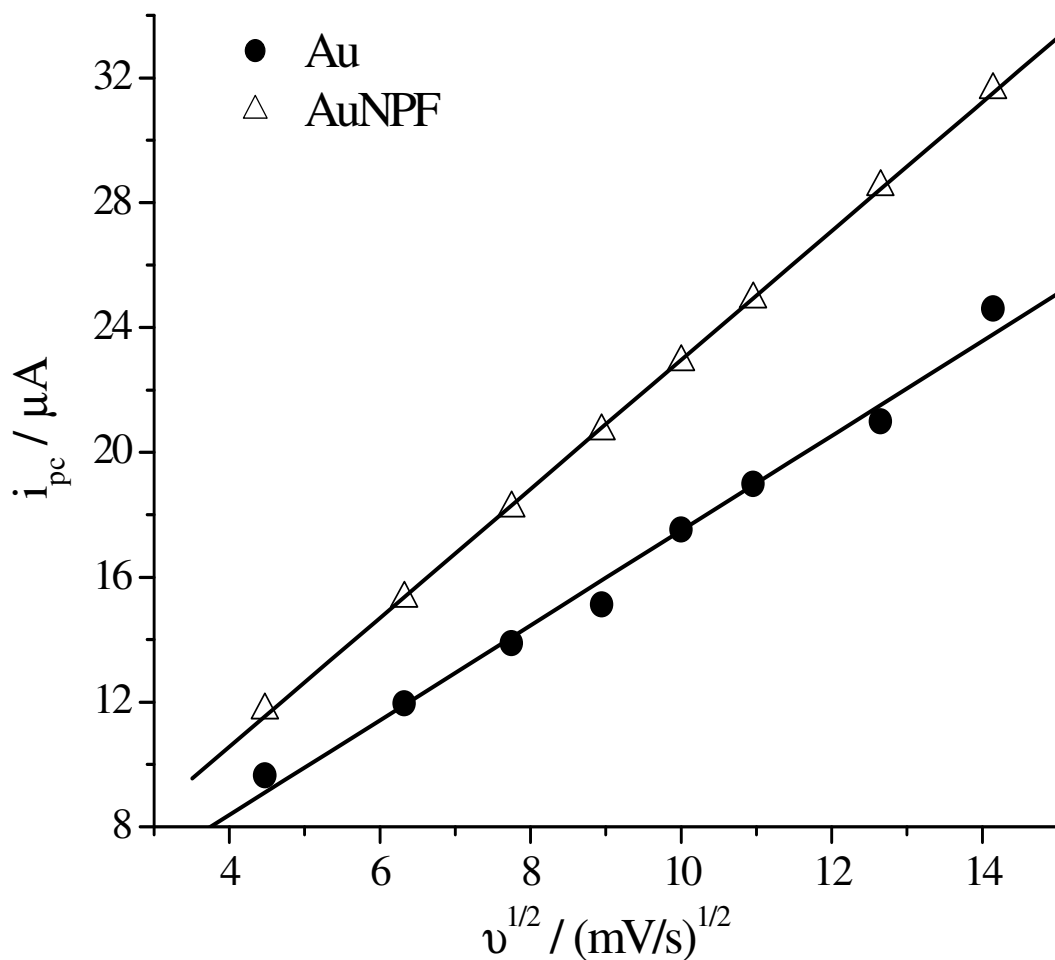


Figure 5.2.5: Cathodic peak current (i_{pc}) vs. $v^{1/2}$ (square root of scan rate) of a bare Au and an AuNPF electrode for the reduction of 5 mM UO_2^{2+} in 0.5 M H_2SO_4

Fig. 5.2.5 shows the plot of cathodic peak current (i_{pc}) vs. square root of scan rate ($v^{1/2}$) at the bare Au and the AuNPF electrodes in 0.5 M H_2SO_4 containing 5 mM UO_2^{2+} . The i_{pc} varied linearly with $v^{1/2}$ for scan rates from 20 to 200 mV s^{-1} , suggesting diffusion controlled process for both the bare Au and the AuNPF electrodes.

Fig. 5.2.6 shows the chronoamperometric transient of the bare Au and the AuNPF electrodes upon the application of potential step from 0.1 V to -0.38 V.

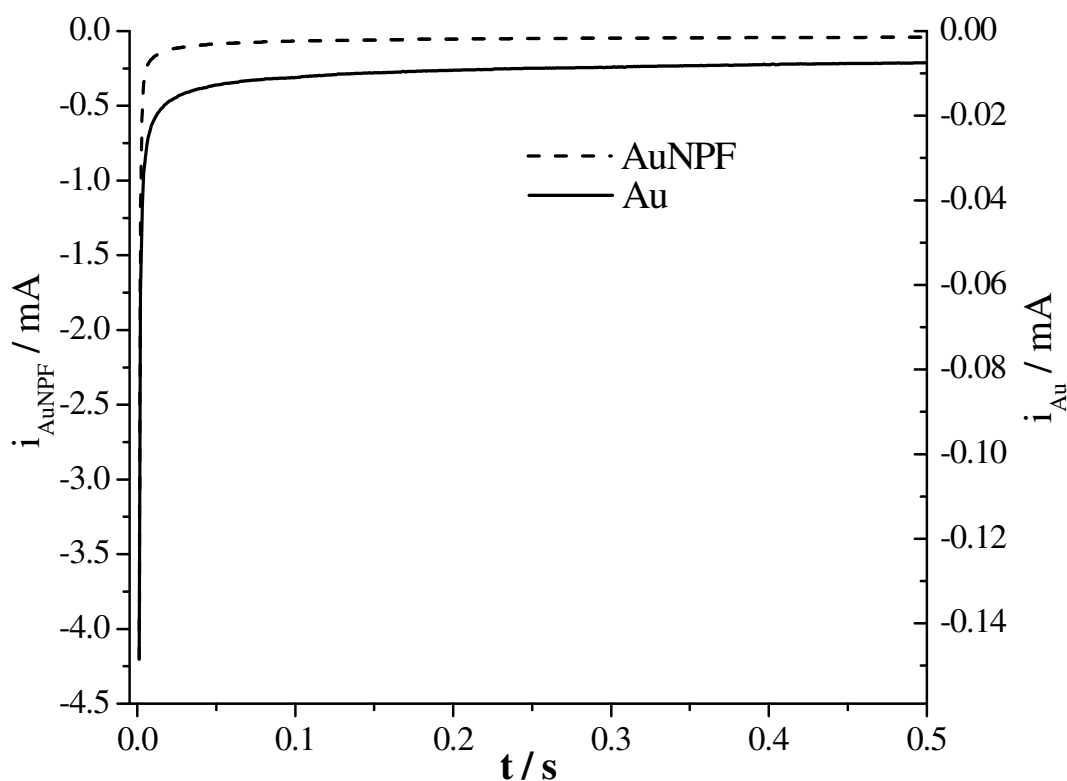


Figure 5.2.6: Chronoamperometric transient of 5 mM UO_2^{2+} in 0.5 M H_2SO_4 at bare Au and AuNPF electrodes to a potential step from 0.1 V to -0.38 V

The currents recorded for the reduction of UO_2^{2+} in 0.5 M H_2SO_4 at the AuNPF electrode were higher than those recorded at the bare Au electrode, as expected due to differences in their surface areas. The cathodic current transient in AuNPF electrode decayed faster than that of the bare Au electrode indicating a faster electron-transfer process for the reduction of UO_2^{2+} in 0.5 M H_2SO_4 at AuNPF electrode as compared to the bare Au electrode.

The interfacial charge-transfer properties of the bare Au and the AuNPF electrodes were evaluated by electrochemical impedance spectroscopy (EIS). EIS measurements were done using $[\text{Fe}(\text{CN})_6]^{3-/4-}$ couple since this couple is commonly used in electrochemistry to compare the modified and the unmodified-electrodes.

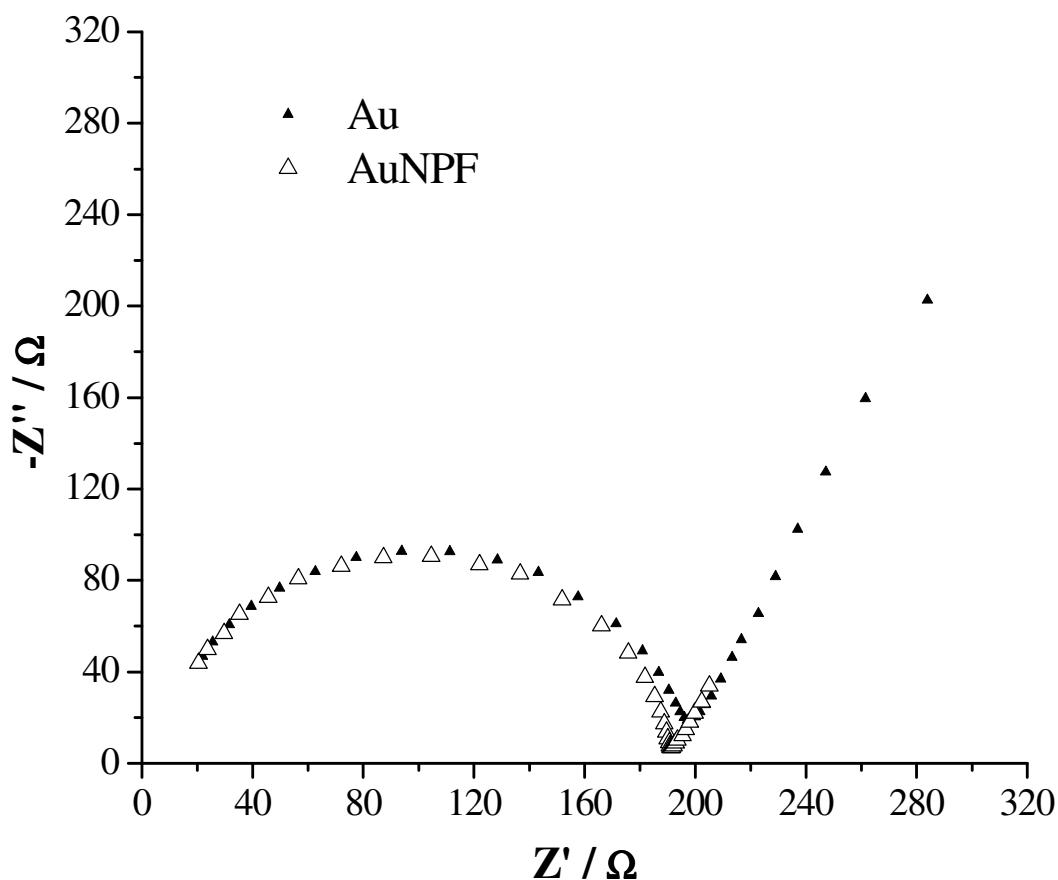


Figure 5.2.7: Impedance spectra (Nyquist plots) of the bare Au and AuNPF electrodes. Data were recorded in the presence of 1 mM $[\text{Fe}(\text{CN})_6]^{3-/4-}$ with an a.c. potential modulation amplitude of 10 mV and for frequency ranging between 100 kHz to 0.5 Hz.

Fig. 5.2.7 compares the Nyquist plots of the bare Au and the AuNPF electrodes. The diameters of the semicircles on the x-axis of the plot determine the values of the interfacial charge-transfer resistance of the $[\text{Fe}(\text{CN})_6]^{3-/4-}$ redox couple at the bare Au and the AuNPF electrodes. The interfacial charge-transfer resistance of the AuNPF electrode was almost the same as that of the bare Au electrode, indicating almost similar rates of heterogeneous electron transfer kinetics at both the bare Au and the AuNPF electrodes. Therefore, the anodic shift of 0.141 V in the cathodic peak potential could not be assigned to the electrocatalytic behaviour of the AuNPF electrode.

Current responses of the bare Au and the AuNPF electrodes were plotted as a function of inverse square root of time (Cottrell plot) for the chronoamperometric experiments shown in Fig. 5.2.6.

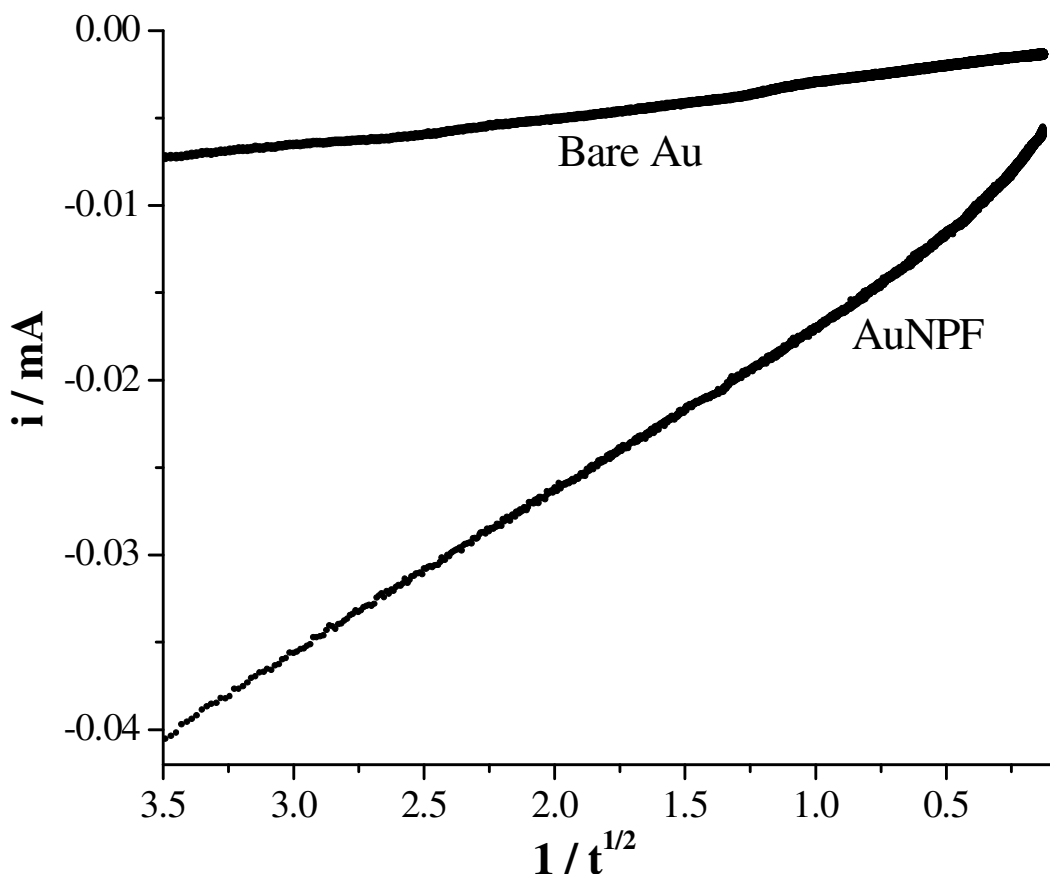


Figure 5.2.8: Cottrell plots for bare Au and AuNPF electrodes

A straight line was observed in the Cottrell plot for a simple redox process where mass transport occurs via semi-infinite diffusion. The Cottrell linearity was observed at the bare Au electrode for the reduction of UO_2^{2+} in 0.5 M H_2SO_4 , as shown in Fig. 5.2.8. However, the current responses of the AuNPF electrode were not directly proportional to the inverse square root of time. The current response of the AuNPF electrode vs. inverse of the square root of time was linear at short times, however, deviation from linearity was observed at longer times. The

Cottrell plot of the AuNPF electrode was characteristic of the thin-layer diffusion coupled with the electron transfer [133].

Therefore, the observed anodic shift at the AuNPF electrode was not due to the electrocatalysis, as expected from the gold nanoporous film, but due to the contribution from thin-layer diffusion within the gold nanoporous film.

5.2.4. Conclusion

Gold nanoporous film (AuNPF) was grown on the gold substrate, and the electrochemical reduction of UO_2^{2+} in 0.5 M H_2SO_4 was shown to occur at lower cathodic potential on AuNPF electrode as compared to the bare Au electrode. The electrochemical impedance spectroscopy studies indicated similar rates of the heterogeneous electron-transfer kinetics at the bare Au and the AuNPF electrodes. The Cottrell plots obtained from the chronoamperometric experiments showed that the Cottrell linearity was observed at the bare Au electrode but at the AuNPF electrode, deviations from the linearity were observed at longer times. The chronoamperometric studies indicated the thin-layer diffusion within the gold nanoporous film. Therefore, the observed anodic shift at the AuNPF electrode was due to the contribution from thin-layer diffusion within the gold nanoporous film. The observed phenomenon of shift in reduction potential to a lesser cathodic potential at metal nanoporous surface due to change in mass transport regime from semi-infinite to thin-layer can be exploited for the quantitative reduction of U(VI) with 100 % current efficiency in acidic electrolyte medium. The nanoporosity of the film can be optimized to obtain better electrochemical behaviour by tuning the various chemical and electrochemical parameters involved in its preparation.

References

1. G. L. Hornyak, J. Dutta and H. F. Tibbals, Introduction to nanoscience, CRC Press (2008).
2. G. A. Mansoori, Principles of nanotechnology: molecular-based study of condensed matter in small system, Hackensack, N.J.: World Scientific (2006).
3. G. Cao and Y. Wang, Nanostructures and nanomaterials: synthesis, properties and applications, New Jersey: World Scientific (2011).
4. G. B. Sergeev, Nanochemistry, Amsterdam, London: Elsevier (2006).
5. G. A. Ozin and A. C. Arsenault, Nanochemistry: a chemical approach to nanomaterials, Cambridge, U.K.: Royal Society of Chemistry (2005).
6. R. Ferrando, Nanoalloys: from theory to applications (vol. 138), Cambridge, U.K.: Royal Society of Chemistry (2008).
7. D. Astruc, Nanoparticles and catalysis, Wiley-VCH Verlag GmbH & Co. KGaA, Weinheim, (2008).
8. K. Kalantar-zadeh and B. Fry, Nanotechnology-enabled sensors, New York: Springer (2007).
9. A. Nabok, Organic and inorganic nanostructures 2nd edition, Artech House (2005).
10. N. A. Kotov, Nanoparticles assemblies and superstructures, CRC Press/Taylor & Francis (2006).
11. J. A. Smith, M. Josowicz and J. Janata, Gold–polyaniline composite. Part I. Moving electrochemical interface, *Phys. Chem. Chem. Phys.* 7 (2005) 3614-3618.
12. J. A. Smith and M. Josowicz, M. Engelhard, D. R. Baer and J. Janata, Gold–polyaniline composites. Part II. Effects of nanometer sized particles, *Phys. Chem. Chem. Phys.* 7 (2005) 3619-3625.

13. S. Jing, S. Xing, L. Yu, Y. Wu and C. Zhao, Synthesis and characterization of Ag/polyaniline core-shell nanocomposites based on silver nanoparticles colloid, *Mater. Lett.* 61 (2007) 2794-2797.
14. R. E. Ward and T.Y. Meyer, O,p-Polyaniline: A new form of a classic conducting polymer, *Macromolecules* 36 (2003) 4368-4373.
15. J. X. Huang, J. A. Moore, J. H. Acquaye and R. B. Kaner, Mechanochemical route to the conducting polymer polyaniline, *Macromolecules* 38 (2005) 317-321.
16. P. Englebienne and A. V. Hoonacker, Gold-conductive polymer nanoparticles: A hybrid material with enhanced photonic reactivity to environmental stimuli, *J. Colloid Interface Sci.* 292 (2005) 445-454.
17. D. Zhang and Y. Wang, Synthesis and applications of one-dimensional nano-structured polyaniline: An overview, *Mater. Sci. Eng. B* 134 (2006) 9-19.
18. S. Bhadra, D. Khastgir, N. K. Singha and J. H. Lee, Progress in preparation, processing and applications of polyaniline, *Prog. Polym. Sci.* 34 (2009) 783-810.
19. T. K. Sarma and A. Chattopadhyay, Reversible encapsulation of nanometer-size polyaniline and polyaniline-gold nanoparticle composite in starch, *Langmuir* 20 (2004) 4733-4737.
20. G. Cui, J. S. Lee, S. J. Kim, H. Nam, G. S. Cha and H. D. Kim, Potentiometric pCO₂ sensor using polyaniline-coated pH-sensitive electrodes, *Analyst* 123 (1998) 1855-1859.
21. A. A. Karyakin, L. V. Lukachora, E. E. Karyakin, A. V. Orlov and G. P. Kappachora, The improved potentiometric pH response of electrodes modified with processible polyaniline. Application to glucose biosensor, *Anal. Commun.* 36 (1999) 153-156.
22. Y. Sun and Y. Xia, Large-scale synthesis of uniform silver nanowires through a soft, self-seeding, polyol process, *Adv. Mater.* 14 (2002) 833-837.

23. M. G. Mason, S. T. Lee and S. Apai, Comparison of electronic structure development in gold clusters formed on amorphous and annealed carbon substrates, *Chem. Phys. Lett.* 76 (1980) 51-53.
24. G. K. Wertheim, S. B. DiCenzo and S. E. Youngquist, Unit charge on supported gold clusters in photoemission final state, *Phys. Rev. Lett.* 51 (1983) 2310-2313.
25. M. Valden, X. Lai and D. W. Goodman, Onset of catalytic activity of gold clusters on titania with the appearance of nonmetallic properties, *Science* 281 (1998) 1647-1650.
26. M. Haruta, N. Yamada, T. Kobayashi and S. Iijima, Gold catalysts prepared by coprecipitation for low-temperature oxidation of hydrogen and of carbon monoxide, *J. Catal.* 115 (1989) 301-309.
27. M. C. Dixon, T. A. Daniel, M. Hieda, D. M. Smilgies, H. W. Chan and D. L. Allara, Preparation, Structure, and Optical Properties of Nanoporous Gold Thin Films, *Langmuir* 23 (2007) 2414-2422.
28. T. F. Jaramillo, S. H. Baeck, B. R. Cuenya and E. W. McFarland, Catalytic Activity of Supported Au Nanoparticles Deposited from Block Copolymer Micelles, *J. Am. Chem. Soc.* 125 (2003) 7148-7149.
29. N. Sakai, Y. Fujiwara, M. Aria, K. Yu and T. Tatsuma, Electrodeposition of gold nanoparticles on ITO: Control of morphology and plasmon resonance-based absorption and scattering, *J. Electroanal. Chem.* 628 (2009) 7-15
30. S. Guo and E. Wang, Synthesis and electrochemical applications of gold nanoparticles, *Anal. Chim. Acta* 598 (2007) 181-192.
31. Y. Y. Yu, S. S. Chang, C. L. Lee and C. R. C. Wang, Gold nanorods: Electrochemical synthesis and optical properties, *J. Phys. Chem. B* 101 (1997) 6661-6664

32. J. M. Pingarron, P. Yanez-Sedeno and A. Gonzalez-Cortes, Gold nanoparticle-based electrochemical biosensors, *Electrochim. Acta* 53 (2008) 5848-5866.
33. M. C. Daniel and D. Astruc, Gold Nanoparticles: Assembly, Supramolecular Chemistry, Quantum-Size-Related Properties, and Applications toward Biology, Catalysis, and Nanotechnology, *Chem. Rev.* 104 (2004) 293-346.
34. W. Cheng, S. Dong and E. Wang, Gold nanoparticles as fine tuners of electrochemical properties of the electrode/solution interface, *Langmuir* 18 (2002) 9947-9952.
35. P. R. Selvakannan, S. Mandal, R. Pasricha and M. Sastry, Hydrophobic, organically dispersible gold nanoparticles of variable shape produced by the spontaneous reduction of aqueous chloroaurate ions by hexadecylaniline molecules, *J. Colloid Interface Sci.* 279 (2004) 124-131.
36. K. Mallick, M. J. Witcomb and M. S. Scurrrell, Polyaniline stabilized highly dispersed gold nanoparticle: an in-situ chemical synthesis route, *J. Mater. Sci.* 41 (2006) 6189-6192.
37. J. A. Smith, M. Josowicz and J. Janata, Polyaniline-Gold Nanocomposite System, *J. Electrochem. Soc.* 150 (2003) E384-E388.
38. A. Saheb, J. A. Smith, M. Josowicz, J. Janata, D. R. Baer and M. H. Engelhard, Controlling size of gold clusters in polyaniline from top-down and from bottom-up, *J. Electroanal. Chem.* 621 (2008) 238-244.
39. E. Granot, E. Katz, B. Basnar and I. Wliiner, Enhanced Bioelectrocatalysis Using Au-Nanoparticle/Polyaniline Hybrid Systems in Thin Films and Microstructured Rods Assembled on Electrodes, *Chem. Mater.* 17 (2005) 4600-4609.
40. D. W. Hatchett, M. Josowicz and J. Janata, Electrochemical Formation of Au Clusters in Polyaniline, *Chem. Mater.* 11 (1999) 2989-2994.

41. K. G. Neoh, T. T. Young, N. T. Looi, E. T. Kang and K. L. Tan, Oxidation-Reduction Interactions between Electroactive Polymer Thin Films and Au(III) Ions in Acid Solutions, *Chem. Mater.* 9 (1997) 2906-2912.
42. E. M. Genies, A. Boyle, M. Lapkowski and C. Tsintavis, Polyaniline: A Historical Survey, *Synthetic Metal* 36 (1990) 139-182.
43. F. Lux, Properties of electronically conductive polyaniline: a comparison between well-known literature data and some recent experimental findings, *Polymer* 35 (1994) 2915-2936.
44. S. T. Selvan and M. Nogami, Novel gold-polypyrrole anisotropic colloids: a TEM investigation, *Mater. Sci. Lett.* 17 (1998) 1385-1388.
45. M. C. Henry, C. C. Hsueh, B. P. Timko and M. S. Freund, Reaction of pyrrole and chlorauric acid. A new route to composite colloids, *J. Electrochem. Soc.* 148 (2001) D155-D162.
46. X. Dai, Y. Tan and J. Xu, Formation of gold nanoparticles in the presence of o-anisidine and the dependence of the structure of poly(o-anisidine) on synthetic conditions, *Langmuir* 18 (2002) 9010-9016.
47. T. S. Sarma, D. Chowdhary, A. Paul and A. Chattopadhyay, Synthesis of gold nanoparticle-conductive polyaniline composite using H_2O_2 as oxidizing as well as reducing agent, *Chem. Commun.* (2002) 1048-1049.
48. J. M. Kinyanjui, D. W. Hatchett, J. A. Smith and M. Josowicz, Chemical synthesis of polyaniline/gold composite using tetrachloroaurate, *Chem. Mater.* 16 (2004) 3390-3398.
49. K. Mallick, M. J. Witcomb, A. Dinsmore and M. S. Scurrall, Polymerization of aniline by auric acid: Formation of gold decorated polyaniline nanoballs, *Macromol. Rapid. Commun.* 26 (2005) 232-235.

50. Y. Wang, Z. Liu, B. Han, Z. Sun, Y. Huang and G. Yang, Facile synthesis of polyaniline nanofibres using chloroaurate acid as the oxidant, *Langmuir* 21 (2005) 833-836.
51. S. K. Pillalamarri, F. D. Blum and Bertino, Synthesis of polyaniline-gold nanocomposites using “grafting from” approach, *Chem. Commun.* (2005) 4584-4585.
52. C. Larosa, E. Stura, R. Eggenhoffner and C. Nicolini, Optimization of optical properties of polycarbonate film with thiol gold nanoparticles, *Materials* 2 (2009) 1193-1204.
53. C. R. Martin, Nanomaterials: A membrane-based synthetic approach, *Science* 266 (1994) 1961-1966
54. C. Schonenberger, B. M. I. Van der Zande, L. G. J. Fokink, M. Henny, C. Schmid, M. Kriiger, A. Bachtold, R. Huber, H. Birk and U. Staufer, Template synthesis of nanowires in porous polycarbonate membranes: Electrochemistry and morphology, *J. Phys. Chem. B* 101 (1997) 5497
55. A. Rahman, M. K. Sanyal, R. Gangopadhyay, A. De and I. Das, Evidence of a ratchet effect in nanowires of a conducting polymer, *Phys. Rev. B* 73 (2006) 125313-125317.
56. R. V. Parthasarathy and C. R. Martin, Template-synthesised polyaniline microtubules, *Chem. Mater.* 6 (1994) 1627-1632.
57. H. S. Nalwa, *Handbook of Nanostructured Materials and Nanotechnology*. Academic Press, New York, USA (2000)
58. G. Hodes, When small is different: Some recent advances in concepts and applications of nanoscale phenomena, *Adv. Mater.* 19 (2007) 639-655
59. M. A. El-Sayed, Small is different: Shape-, size- and composition-dependent properties of some colloidal semiconductor nanocrystals, *Acc. Chem. Res.* 37 (2004) 326-333

60. Y-W. C. Cao , R. Jin and C. A. Mirkin, Nanoparticles with Raman spectroscopic fingerprints for DNA and RNA detection, *Science* 297 (2002) 1536-1540
61. R. Elghanian, J. J. Starhoff, R. C. Mucic, R. L. Letsinger and C. A. Mirkin, Selective colorimetric detection of polynucleotides based on the distance-dependent optical properties of gold nanoparticles, *Science* 277 (1997) 1078-1081
62. J. Couzin, Nanoparticles cut tumor's supply lines, *Science* 296 (2002) 2314-2315
63. M. Schmidt, R. Kusche, B. von Issendorff and H. Haberland, Irregular variations in the melting point of size-selected atomic clusters, *Nature* 393 (1998) 238-240
64. O. S. Ivanova and F. P. Zamborini, Size-dependent electrochemical oxidation of silver nanoparticles, *J. Am. Chem. Soc.* 132 (2010) 70-72
65. R. S. Berry, Size is everything, *Nature* 393 (1998) 212-213
66. C. M. Sanchez-Sanchez, J. Solla-Gullon, F. J. Vidal-Iglesias, A. Aldaz, V. Montiel and E. Herrero, Imaging structure sensitive catalysis on different shape-controlled platinum nanoparticles, *J. Am. Chem. Soc.* 132 (2010) 5622- 5624
67. M. T. Reetz and W. Helbig, Size-selective synthesis of nanostructured transition metal clusters, *J. Am. Chem. Soc.* 116 (1994) 7401-7402
68. S. S. Bale, P. Asuri, S. S. Karajanagi, J. S. Dordick and R. S. Kane, Protein-directed formation of silver nanoparticles on carbon nanotubes, *Adv. Mater.* 19 (2007) 3167-3170
69. Y. Xia, P. Yang, Y. Sun, Y. Wu, B. Mayers, B. Gates, Y. Yin, F. Kim and H. Yan, One-dimensional nanostructures: Synthesis, characterisation, and applications, *Adv. Mater.* 15 (2003) 353-389
70. Y. Xiong and Y. Xia, Shape-controlled synthesis of metal nanostructures: The case of palladium, *Adv. Mater.* 19 (2007) 3385-3391

71. M. H. Huang, A. Choudrey and P. Yang, Ag nanowire formation within mesoporous silica, *Chem. Commun.* (2000) 1063-1064
72. T. S. Ahmadi, Z. L. Wang, T. C. Green, A. Henglein and M. A. El-Sayed, Shape-controlled synthesis of colloidal platinum nanoparticles, *Science* 272 (1996) 1924-1926
73. Y. Sun and Y. Xia, Shape-controlled synthesis of gold and silver nanoparticles, *Science* 298 (2002) 2176-2179
74. S. C. Hernandez, D. Chaudhuri, W. Chen, N. V. Myung and A. Mulchandani, Single polypyrrole nanowire ammonia gas sensor, *Electroanalysis* 19 (2007) 2125-2130
75. D. J. Pena, J. K. N. Mbindyo, A. J. Carado, T. E. Mallouk, C. D. Keating, B. Razavi and T. S. Mayer, Template growth of photoconductive metal-CdSe-metal nanowires, *J. Phys. Chem.* 106 (2002) 7458-7462
76. C. Ruan, W. Luo, W. Wang and B. Gu, Surface-enhanced Raman spectroscopy for uranium detection and analysis in environmental samples, *Anal. Chim. Acta* 605 (2007) 80-86
77. Y. Tian, H. Liu, G. Zhao and T. Tatsuma, Shape-controlled electrodeposition of gold nanostructures, *J. Phys. Chem. B* 110 (2006) 23478-23481
78. K. M. Mayer and J. H. Hafner, Localized surface plasmon resonance sensors, *Chem. Rev.* 111 (2011) 3828-3857
79. N. J. Halas, S. Lal, W-S. Chang, S. Link and P. Nordlander, Plasmons in strongly coupled metallic nanostructures, *Chem. Rev.* 111(2011) 3913-3961
80. S. Eustis and M. A. El-Sayed, Why gold nanoparticles are more precious than pretty gold: Noble metal surface plasmon resonance and its enhancement of the radiative and nonradiative properties of nanocrystals of different shapes, *Chem. Soc. Rev.* 35 (2006) 209-217

81. S. K. Ghosh and T. Pal, Interparticle coupling effect on the surface plasmon resonance of gold nanoparticles: From theory to applications, *Chem. Rev.* 107 (2007) 4797-4862
82. C. F. Metz and G. R. Waterbury: I. M. Kolthoff and P. J. Elving (eds.): In: *Treatise on Analytical Chemistry*. vol. 9, Part II., Interscience, New York (1962), pp. 189.e
83. G. P. Cook, J. K. Foreman and E. F. Kemp, Some experiments on the polarography of Pu(VI) in complexing media, *Anal. Chim. Acta.* 19 (1958) 174-179.
84. G. W. C. Milner and A. J. Wood, The determination of plutonium by A.C. polarography, *J. Electroanal. Chem.* 7 (1964) 190-205.
85. L. J. Jeftic, J. Caza and M. Branica, A preliminary electrochemical study of plutonium in carbonate solutions on HMDE, *Croat. Chem. Acta* 39 (1967) 225-228.
86. B. G. Harvey, H. G. Heal, A. G. Maddock and E. L. Rowley, The chemistry of plutonium, *J. Chem. Soc.* (1947) 1010-1021.
87. K. Koyama, Square-wave polarography of plutonium, *Anal. Chem.* 32 (1960) 523-524.
88. K. S. Yun, A. Toshihide and M. Yasuji, Electrochemical studies of Pu(IV) complexes in aqueous nitrate solution, *Nippon Genshiryoku Kenkyujo JAERI* (2005) 341-344.
89. C. E. Plock, Anodic voltammetric determination of plutonium – Diffusion coefficients of plutonium(III) in mineral acids, *Anal. Chim. Acta* 49 (1970) 83-87.
90. S. Casadio and F. Orlandini, Cyclic voltammetry of Pu and Np in nitric acid media, *J. Electroanal. Chem.* 33 (1971) 212-215.
91. W. D. Shults, Applications of controlled-potential coulometry to the determination of Pu, *Talanta* 10 (1963) 833-849.

92. H. S. Sharma, N. B. Khedekar, S. G. Marathe and H. C. Jain, Controlled potential coulometric determination of Pu in mixed (U,Pu) carbide fuels, Nucl. Technol. 89 (1990) 399-404.
93. I. S. Sklyarenko, V. V. Andriets and T. M. Chubukova, Analysis of plutonium dioxide by coulometry, Radiochemistry 37 (1995) 343-345.
94. H. S. Sharma, R. B. Manolkar, J. V. Kamat and S. G. Marathe, Studies on the coulometric determination of uranium and plutonium employing a graphite electrode, Fresenius' J. Anal. Chem. 347 (1993) 486-490.
95. S. Cavaliere, F. Raynal, A. Etcheberry, M. Heerlem and H. Perez, Direct electrocatalytic activity of capped platinum nanoparticles toward oxygen reduction, Electrochemical and Solid-State Letters 7 (2004) A358-A360.
96. N. Tian, S. Zhou, S. Sun, L. Cui, B. Ren and Z. Tian, Electrochemical preparation of platinum nanothorn assemblies with high SERS activity. Chem. Commun. (2006) 4090-4092.
97. J. Clavilier and A. Wieckowski (ed.): In: *Interfacial Electrochemistry, Theory, Experiments and Applications*. Marcel Dekker, New York (1999), pp. 231.
98. F. J. Vidal-Iglesias, J. Solla-Gullon, P. Rodriguez, E. Herrero, V. Montiel, J. M. Feliu and A. Aldaz, Shape-dependent electrocatalysis: ammonia oxidation on platinum nanoparticles with preferential (1 0 0) surfaces, Electrochem. Commun. 6 (2004) 1080-1084.
99. W. E. Harris, and I. M. Kolthoff, The polarography of uranium. I. Reduction in moderately acid solution. Polarographic determination of uranium, J. Am. Chem. Soc. 67 (1945) 1484.
100. H. G. Heal, Electrochemistry of uranium. Nature 157 (1946) 225-225.
101. P. Herasymenko, Electroreduction of uranyl salts by means of the mercury dropping cathode, Trans. Faraday Soc. 24 (1928) 272-279.

102. I. M. Kolthoff and W. E. Harris, The polarography of uranium. II. Polarography in strongly acid solution, J. Am. Chem. Soc. 68 (1946) 1175-1179.
103. M. Mastragostino and L. M. Saveant, Disproportionation and ECE mechanisms-II. Reduction of the uranyl cation in perchloric acid, Electrochim. Acta 13 (1968) 751-762.
104. K. U. Din, J. Kuta and L. Pospisil, Polarographic and voltammetric measurements of disproportionation of uranium (V) in sulphate and other complexing media on mercury electrode, Electrochim. Acta 22 (1977) 1109-1112.
105. D. M. H. Kern and E. F. Orlemann, The potential of the uranium(V), uranium(VI) couple and the kinetics of uranium disproportionation in perchlorate media, J. Am. Chem. Soc. 71 (1949) 2102-2106.
106. I. M. Kolthoff and P. J. Elving (Eds): In: *Treatise on Analytical chemistry*. vol. 9, Part II, Interscience, New York (1962), pp. 115.
107. I. M. Kolthoff and J. J. Lingane (Eds): In: *Polarography*. vol. 2, Interscience, New York (1952), pp. 462.
108. K. A. Kraus, F. Nelson and G. L. Johnson, Chemistry of aqueous Uranium (V) solutions .I. Preparation and properties. Analogy between Uranium (V), Neptunium (V) and Plutonium (V), J. Am. Chem. Soc. 71 (1949) 2510-2517.
109. J. Kuta and E. Yeager, Regeneration of a substance undergoing an electrode reaction by disproportionation at a rotating electrode II. Disproportionation of uranium(V) at a gold electrode, Electroanal. Chem. Interfacial Electrochem. 46 (1963) 233-241.
110. P. J. Elving and A. F. Krivis, Polarographic reduction of uranium(VI) under complexing and non-complexing conditions nature of the uranium(V) sulphate complex, J. Inorg. Nucl. Chem. 11 (1959) 234-241.

111. B. McDuffie and C. N. Reilley, Twin electrode thin layer electrochemistry: kinetics of second order disproportion of uranium (V) by decay of steady state current, *Anal. Chem.* 38 (1966) 1881-1887.
112. J. Kuta and E. Yeager, The study of the charge transfer reaction of U(VI)-U(V) couple on the rotating gold disc electrode, *J. Electroanal. Chem.* 31 (1971) 119-127.
113. L. Sipos, L. J. Jetic, M. Branica and J. Galus, Electrochemical redox mechanism of uranium in acidic perchlorate solutions, *J. Electroanal. Chem.* 32 (1971) 35-47.
114. D. W. Wester and J. C. Sullivan, Electrochemical and spectroscopic studies of U(VI), (V), (IV) in carbonate –bicarbonate buffers, *Inorg. Chem.* 9 (1980) 2838-2840.
115. D. Hodko and V. Pravdic, Kinetics parameters for reduction of U (VI) in carbonate solutions from measurements at thin mercury film electrodes, *Electrochim. Acta* 30 (1985) 1341-1344.
116. H. Bildstein, H. Fleischer and V. Gutmann, The polarographic behavior of uranium compounds in propanediol-1,2 carbonate and N,N-dimethylacetamide, *Inorg. Chim. Acta* 2 (1968) 343-346.
117. P. Zanello, A. Cinquantini and G. A. Mazzocchin, Voltammetric behavior of uranyl-diethyldithiocarbamate complexes in aprotic medium, *Inorg. Chim. Acta* 21 (1977) 195-199.
118. P. Zanello, A. Cinquantini, P. D. Bernardo and L. Magon, Polarographic investigations on uranyl(VI) complexes in dimethylsulfoxide.1. Monocarboxylic ligands, *Inorg. Chim. Acta* 24 (1977) 131-137.

119. P. Zanello, A. Cinquantini, G. A. Mazzocchin and O. Travarso, Polarographic investigations on uranyl(VI) complexes in dimethylsulfoxide.III. Halides and pseudohalides, *Inorg. Chim. Acta* 27 (1978) 157-161.
120. P. Zanello, A. Cinquantini and G. A. Mazzocchin, Electrochemical behavior of uranyl (VI) ion in different non-aqueous solvents. *J. Electroanal. Chem.* 131 (1982) 215-227.
121. R. Seeber and P. Zanello, Solvent Effects on the Redox Potential of the Uranium(VI)-Uranium(V) Couple, *J. Chem. Soc. Dalton Trans.* (1985) 601-603.
122. S. Marouani and A. L. M. Gross, Influence du solvant sur la reduction electrochimique du nitrate et de l'acetate d'uranyle, *Electrochim. Acta* 33 (1988) 147-155.
123. L. Bahadur and J. P. Pandey, Voltammetric studies of some oxo-uranium (VI) complexes of dithio ligands at thin film semiconducting ZnO/Acetonitrile interface for photosensitizer applications, *J. Electrochem. Soc.* 137 (1990) 3755-3760.
124. K. H. Lubert, M. Schnurrbusch and A. Thomas, Preconcentration and determination of uranyl ions on electrodes modified by tri-n-octylphosphine oxide, *Anal. Chim. Acta* 144 (1982) 123-136.
125. K. Izutsu, T. Nakamura, R. Takizawa and H. Hanawa, Voltammetry at a trioctylphosphine oxide-coated glassy carbon electrode and its use for the determination of trace uranyl ions after preconcentration, *Anal. Chim. Acta* 149 (1983) 147-155.
126. K. Izutsu, T. Nakamura and T. Ando, Voltammetric determination of uranium in sea water after Preconcentration on the trioctylphosphine oxide-coated glassy carbon electrode, *Anal. Chim. Acta* 152 (1983) 285-288.

127. K. H. Lubert and M. Schnurrbusch, The mechanisms of preconcentration and voltammetric behaviour of Uranium(VI) at glassy carbon electrodes modified by trioctylphosphine oxide, *Anal. Chim. Acta* 186 (1986) 57-69.
128. D. Leroy, L. Martinot, M. Debecker, D. Strivay, G. Weber, C. Jerome and R. Jerome, New system for complexation of uranyl ions from liquid wastes of low-level activity: polypyrrole doped with complexing polyanions, *J. Applied Polymer Science* 77 (2000) 1230-1239.
129. A. Becker, H. Tobias, Z. Porat and D. Mandler, Detection of uranium(VI) in aqueous solution by a calix[6]arene modified electrode, *J. Electroanal. Chem.* 621 (2008) 214-222.
130. R. K. Shervedani and S. A. Mozaffari, Impedimetric sensing of uranyl ion based on phosphate functionalized cysteamine self-assembled monolayers, *Anal. Chim. Acta* 562 (2006) 223-228.
131. L. Lin, S. Thongngamdee, J. Wang, Y. Lin, O. A. Sadik and S. Y. Ly, Adsorptive stripping voltammetric measurements of trace uranium at the bismuth film electrode, *Anal. Chim. Acta* 535 (2005) 9-13.
132. I. Streeter, G. G. Wildgoose, L. Shao and R. G. Compton, Cyclic Voltammetry on Electrode Surfaces Covered with Porous Layers: An Analysis of Electron Transfer Kinetics at SWCNTs Modified Electrodes, *Sens. Actuators B* 133 (2008) 462-466.
133. G. P. Keeley and M. E. G. Lyons, The effect of thin layer diffusion at glassy carbon electrodes modified with porous films of single-walled carbon nanotubes, *Int. J. Electrochem. Sci.* 4 (2009) 794-809.
134. E. D. Marshall, Polarographic study of the reaction between uranium(VI) and uranium(IV) in carbonate media, *AECD* 3289, 1951.

135. R. D. Saini, P. K. Bhattacharyya and R. M. Iyer, Formation and isolation of uranium (V) in the photochemical reduction of uranyl ion in aqueous carbonate medium, *J. Photochem. Photobiol. A* 47 (1989) 181-189.
136. K. Mizuguchi, Y. Y. Park, H. Tomiyasu and Y. Ikeda, Electrochemical and spectrochemical studies on uranyl carbonate and aquo complexes, *J. Nucl. Sci. Technol.* 30 (1993) 542-548.
137. D. Cohen, The preparation and spectrum of uranium (V) ions in aqueous solutions, *J. Inorg. Nucl. Chem.* 32 (1970) 3525-3530.
138. D. Wester and J. C. Sullivan, Electrochemical and spectroscopic studies of neptunium (VI), (V) and (IV) in carbonate-bicarbonate buffers, *J. Inorg. Nucl. Chem.* 43 (1981) 2919-2923.
139. P. G. Varlashkin, D. E. Hobart, G. M. Begun and J. R. Peterson, Electrochemical and spectroscopic studies of plutonium in concentrated aqueous carbonate and carbonate-hydroxide solutions, *Radiochim. Acta* 35 (1984) 211-218.
140. P. G. Varlashkin, D. E. Hobart, G. M. Begun and J. R. Peterson, Electrochemical and spectroscopic studies of neptunium in concentrated aqueous carbonate and carbonate-hydroxide solutions, *Radiochim. Acta* 35 (1984) 91-96.
141. D. W. Wester and J. C. Sullivan, The absorption spectra of Pu(VI), (V) and (IV) produced electrochemically in carbonate-bicarbonate media, *Radiochem. Radioanal. Lett.* 57 (1983) 35-42.
142. K. A. Kraus and F. Nelson, Chemistry of aqueous uranium(V) solutions. 11. Reaction of Uranium Pentachloride with water. Thermodynamic stability of UO_2^+ . Potential of U(IV)/(V), U(IV)/(VI) and U(V)/(VI) Couples, *J. Am. Chem. Soc.* 71 (1949) 2517-2522.

143. U. Kramerschnabel, H. Bischoff, R. H. Xi and G. Marx, Solubility products and complex formation equilibria in the systems uranyl hydroxide and uranyl carbonate at 25 °C and I = 0.1 M, *Radiochim. Acta* 56 (1992) 183-188.
144. G. Meinrath and T. Kimura, Carbonate complexation of Uranyl (VI) ion, *J. Alloys Compd.* 202 (1993) 89-93.
145. I. Pashalidis, K. R. Czerwinski, T. Fangahanel and J. I. Kim, A study of Solid-liquid phase equilibria of Pu(IV) and U(VI) in aqueous carbonate systems. Determination of stability constants, *Radiochim. Acta* 76 (1997) 55-62.
146. L. J. Basile, J. R. Ferraro, M. L. Mitchell and J. C. Sullivan, The Raman scattering of actinide (VI) ions in carbonate media, *Appl. Spectrosc.* 32 (1978) 535-537.
147. J. P. Nigon, R. A. Penneman, E. Starsky and L. B. Asprey, Alkali carbonates of Np(V), Pu(V) and Am(V), *J. Phys. Chem.* 58 (1954) 403-404.
148. T. I. Docrat, J. F. W. Mosselmans, J. M. Charnock, M. W. Whiteley, D. Collison, F. R. Livens, C. Jones and M. J. Edmiston, X-ray absorption spectroscopy of tricarbonatodioxouranate(V), $[\text{UO}_2(\text{CO}_3)_3]^{5-}$, in aqueous solution, *Inorg. Chem.* 38 (1999) 1879-1882.
149. R. Kumar, A. K. Pandey, A. K. Tyagi, G. K. Dey, S. V. Ramagiri, J. R. Bellare and A. Goswami, In situ formation of stable gold nanoparticles in polymer inclusion membranes, *J. Colloid Interface Sci.* 337 (2009) 523-530.
150. Y. Huang, Di Li, P. He, C. Sun, M. Wang and J. Li, Semipermeable membrane embodying noble metal nanoparticles and its electrochemical behaviors, *J. Electroanal. Chem.* 579 (2005) 277-282.

151. G. W. C. Milner and J. W. Edwards, The controlled-potential coulometric determination of uranium using silver gauge working electrode, Report AERE-R 3951, U. K. Atomic Energy Authority, (1962).
152. W. Davies, W. Gray and K. C. McLeod, Coulometric determination of uranium with a platinum working electrode, *Talanta* 17 (1970) 937-944.
153. J. B. Fardon and I. R. McGowan, Controlled-potential coulometry: The application of a secondary reaction to the determination of plutonium and uranium at a solid electrode, *Talanta* 19 (1972) 1321-1334.
154. N. Gopinath, N. N. Mirashi, K. Chander and S. K. Aggarwal, Rapid reduction of U(VI) on activated platinum wire gauge electrode for the primary coulometric determination of uranium, *J. Appl. Electrochem.* 34 (2004) 617-622.
155. J. Wang, Carbon-nanotube based electrochemical biosensors: A review, *Electroanalysis* 17 (2005) 7-14.
156. J. Jia, L. Cao and Z. Wang, Platinum-coated gold nanoporous film surface: Electrodeposition and enhanced electrocatalytic activity for methanol oxidation, *Langmuir* 24 (2008) 5932-5936.
157. M. K. Sharma, A. S. Ambollikar and S. K. Aggarwal, Investigations on redox behaviour of Pu(IV)/Pu(III) in H_2SO_4 on Pt nanoparticles-modified glassy carbon and platinum electrodes, *Radiochim. Acta* 99 (2011) 17-21.
158. M. K. Sharma, A. S. Ambollikar and S. K. Aggarwal, Electrochemical studies of U(VI)/U(V) in saturated Na_2CO_3 solution at gold nanoparticles embedded CTA-modified electrode, *Radiochim. Acta* 99 (2011) 555-561.

159. S. Trasatti and O. A. Petrii, Real surface measurements in electrochemistry, *Pure Appl. Chem.* 63 (1991) 711-734.

List of Publications

Refereed Journals

1. In-situ synthesis of gold-polyaniline composite in nanopores of polycarbonate membrane
Manoj K. Sharma, Arvind S. Ambolika and Suresh K. Aggarwal
Journal of Material Science, 46 (2011) 5715-5722.
2. Electrochemical synthesis of gold nanorods in track-etched polycarbonate membrane using removable mercury cathode
Manoj K. Sharma, Arvind S. Ambolika and Suresh K. Aggarwal
Journal of Nanoparticle Research, 14 (2012).
DOI 10.1007/s11051-012-1094-z
3. Investigation on redox behaviour of Pu(IV)/Pu(III) in H₂SO₄ on platinum nanoparticles-modified glassy carbon and platinum electrode
Manoj K. Sharma, Arvind S. Ambolika and Suresh K. Aggarwal
Radiochimica Acta, 99 (2011) 17-21.
4. Electrochemical studies of U(VI)/U(V) in saturated Na₂CO₃ solution at gold nanoparticles embedded CTA-modified electrode
Manoj K. Sharma, Arvind S. Ambolika and Suresh K. Aggarwal
Radiochimica Acta, 99 (2011) 555-561.
5. Electrochemical Reduction of U(VI) in H₂SO₄ at Gold Nanoporous Film Electrode
Manoj K. Sharma and Suresh K. Aggarwal
Radiochimica Acta, DOI 10.1524/ract.2013.2021